An Investigation in to the Effects of Recycling of Ti-6Al-4V Powders Used Within Selective Laser Melting

Richard O'Leary – 0932242

MPhil

December 2015

Abstract:

This report details a systematic study into the effects of recycling of Ti-6Al-4V powders used within Selective Laser Melting. Five identical test builds were produced with a variety of test pieces in order to ascertain any effect of changes in powder characteristics observed on mechanical, chemical and metallurgical properties of laser melted parts. Testing included tensile testing, fatigue testing, chemical composition testing and porosity testing.

A quantity of Grade 23 Ti-6Al-4V powder was taken from a single manufacturing batch and run through the SLM process five times. Powder samples were taken from the initial manufacture's batch, and from within the build chamber at the end of each build, as well as post sieving of the powder from each build. The powders were subjected to Particle Size Distribution analysis, chemical composition analysis and imaged under Scanning Electron Microscope. The purpose of this was to determine the effect of repeated recycling on their PSD range, chemical composition and morphology.

The effect of recycling on powder characteristics was shown to be an increase in the number of larger particles contained within the population, and a reduction in the number of fine particles. Repeated recycling was shown to have a statistically significant effect on values of Dx(10), Dx(50) and Dx(90), which all increased.

These changes in powder characteristics within the powder population were shown to have no statistically significant effect on the mechanical properties of parts produced. There was no effect observed on UTS, Yield Strength, Percentage Elongation or Fatigue Strength for parts produced in the five builds. It was not possible to say that this trend would continue with indefinite recycling. The effect of position within the build chamber in which the parts were built was shown to be strongly significant, with large variation in mechanical properties of parts produced in different positions. Porosity analysis showed an increase in porosity for parts which exhibited the worst mechanical performance when compared to that of those with the best mechanical performance.

Through chemical composition testing, there was shown to be a large increase in the percentage by weight of oxygen contained within laser melted parts when compared to the powder that was used to manufacture them. These parts contained a percentage by mass of oxygen that was outside the allowable limit stipulated for Grade 23 Ti-6Al-4V parts. It was not possible to say whether the level of oxygen absorption varied with build position.

Acknowledgements:

The author would like to express his extreme gratitude to the following people for their support during the completion of this project:

- To Paul Prickett and Rossi Setchi, for their continued advice, support and encouragement throughout the project.
- Andrew Rankmore and all the staff within the Mechanical Workshop for their advice on machining and design of parts, and work in machining of parts for testing.
- Sam Evans for advice and assistance in performing tensile and fatigue testing.
- Shwe Soe for his help and advice.
- Emmanuel Brousseau for his assistance in obtaining SEM images.
- Harry Lane and the staff in the ACE labs for their assistance in conducting tensile and fatigue tests.
- Paul Malpas and Julian Steer for their assistance in running PSD analysis.
- Nick Jones, Matthew Parkes, David Beeby, Ravi Aswathanarayanaswamy and Hossein Sheykh-Poor for all their help and support.

DECLARATION AND STATEMENTS

DECLARATION

This work has not previously been accepted in substance for any degree and is not being concurrently submitted in candidature for any degree.

Signed..... (candidate) Date .....

STATEMENT 1

This thesis is being submitted in partial fulfilment of the requirements for the degree of PhD.

Signed ..... (candidate) Date .....

STATEMENT 2

This thesis is the result of my own investigation, except where otherwise stated. Other sources are acknowledged by giving explicit reference.

Signed ..... (candidate) Date .....

STATEMENT 3

I hereby give consent for my thesis, if accepted, to be available for photocopying and for inter-library loan, and for the title and summary to be made available to outside organizations.

Signed ..... (candidate) Date .....

STATEMENT 4

I hereby give consent for my thesis, if accepted, to be available for photocopying and for inter-library loan, after expiry of a bar on access approved by the Graduate Development Committee.

Signed..... (candidate) Date .....

Contents

Table of Figures

1.0. Introduction

Increasing the use of Selective Laser Melting (SLM) to produce production parts necessitates both a more thorough understanding and better control of the process. At present the necessary levels of understanding and control of the process have not been fully attained. Currently, the process is operated largely in an unregulated manner. With parts being produced through laser melting looking to gain acceptance for operational use in some of the most highly regulated industries, such as the aerospace industry, the properties of produced components must be fully understood.

One of the key parameters in bringing the process under control is the powder used within SLM. The powdered material used within the process is incredibly expensive when compared to that used within traditional subtractive technologies, owing to the high level of reactivity of Ti-6Al-4V and the powder manufacturing process used.

As a result, there are both strong economic and environmental requirements to recycle any un-melted powder that remains following the SLM process. Industrial recognition of the requirement to recycle powder used within the SLM process, and the problem with current understanding of recycling control systems, has led to the requirement for the development of methodologies for both recycling and determining the level of recycling possible for differing powders.

This report focuses entirely on the recycling of Ti-6Al-4V powders and aims to define the steps taken in the development of a methodology for determining the changes in powder characteristics through repeated recycling. Powder was recycled five times within the SLM process with the aim of determining the end of life for the powder. An appreciation of the way in which powder changes through repeated recycling was seen as essential for the SLM process as a whole to be considered under control and for it to gain acceptance in the production of Ti-6Al-4V parts.

Section two of this report provides a review of the literature currently available and concerned with this topic. There are a variety of tests that are suitable for powder characterisation. Section three of

this report details the techniques and methodologies used in the sampling and characterisation of powders and provides a basis for future characterisation work. Within this study Particle Size Distribution (PSD) analysis was used to determine the distribution of particle sizes. Powders were imaged using a Scanning Electron Microscope (SEM) to both determine changes in particle morphology and confirm the results obtained through PSD analysis. Chemical composition analysis was performed to determine any changes in chemical composition through repeated recycling.

This analysis was performed to quantify any changes in powder characteristics through repeated recycling. Powder samples were taken at a variety of points within testing for this very reason. Analysis of Variance (ANOVA) was then used to show any differences in the measurements obtained for powder samples collected at different points within the process and between powders that had been recycled at each stage. Additionally, a powder collection box was designed with the aim of establishing an in-process powder sampling method.

Upon completion of the characterisation of powders, and gaining an appreciation of the way in which they changed through repeated recycling, it was important to understand the effect that changes in powder characteristics would have on laser melted parts. Section five of this report details the work completed in mechanical characterisation of test pieces built with each of the five builds. Tensile and fatigue test pieces were laser melted in each of the five builds produced. Tensile tests were performed on twelve samples per build with Ultimate Tensile Strength (UTS), Yield strength, Young's Modulus and Elongation being the measured variables. This work used ANOVA to quantify any effect that variation in powder characteristics had on both tensile and fatigue strength properties of laser melted parts.

In addition to the mechanical characterisation work, an understanding of the effect of changes in powder characteristics effect on the chemical composition and metallographic structure was deemed essential. Section six details the testing conducted to attempt to determine this effect. The final chapter of this repost provides the conclusions determined as a result of testing and analysis, and makes recommendations for any future work to be completed.

2.0. Literature Review

There have been very few papers published which consider the effects of recycling of metal powders used within SLM to date. One study of interest was that conducted by Axelsson (2012). This study attempted to investigate the change in oxide layer thickness and composition of Ti-6Al-4V powders used within Electron Beam Melting. This study used both X-ray Photoelectron Spectroscopy (XPS) to characterise the thickness and chemical composition of the oxide later. It was concluded that the oxide layer was comprised mainly of TiO_2 and Al_2O_3. The surface was said to be impoverished of vanadium for virgin powder, but this increased through repeated recycling. The study also concluded that the oxide layer thickness increased through repeated recycling and that the powder surface became roughened. This study made no mention of the methodology for recycling the powder, or the point within the process at which it was obtained. Crucially, the study makes no mention of the number of times that the powder was recycled.

Seyda et al (2012) conducted an investigation of the ageing processes of Ti-6Al-4V power material used in laser melting. Within this study, powder was recycled 12 times over the course of several months. This study concluded that there was a significant change in powder in terms of its Particle Size Distribution (PSD), as illustrated in Figure 1. They also noted that powder particles coarsened and their flowability increased with an overall increase in PSD. The study showed that there was an effect of increasing density of laser melted parts, a reduction in porosity, an increase in surface roughness of laser melted parts and an increase in UTS of laser melted parts through repeated recycling. The reduction in porosity was attributed to higher powder bed density and flowability of the powder.

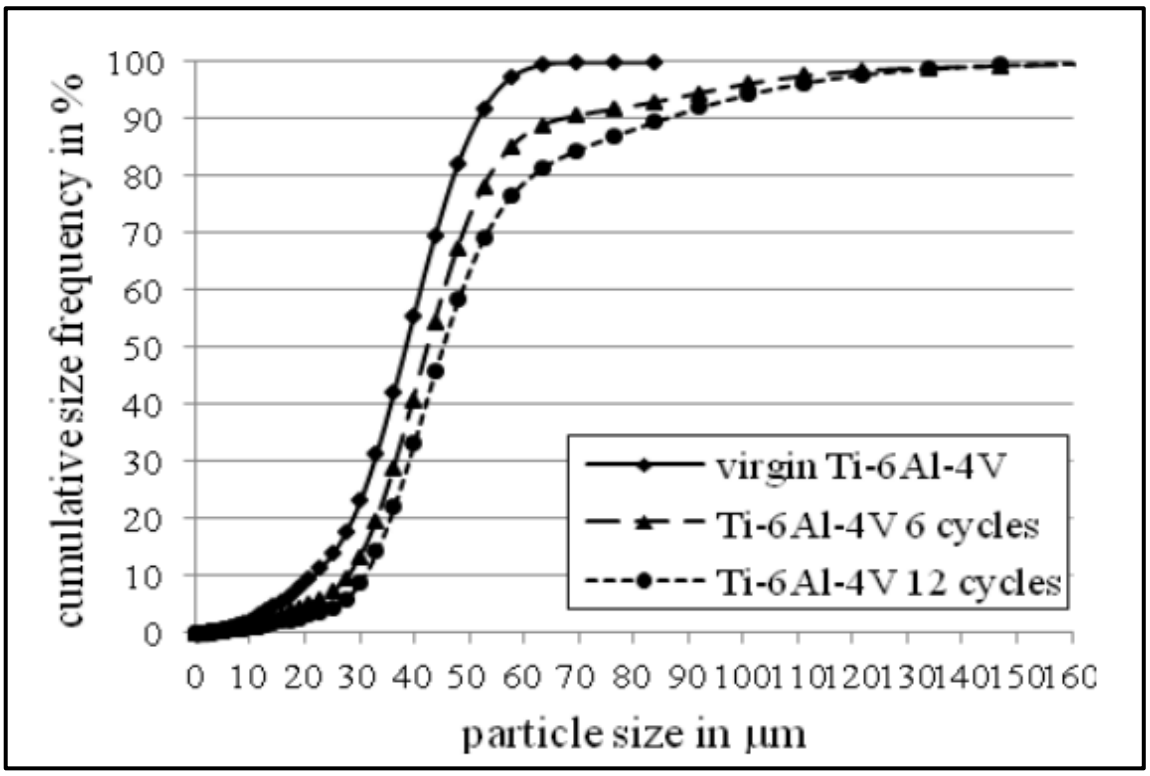

Figure 1 - Graph Showing Change in PSD for Ti-6Al-4V Powder. Figure Reproduced from Seyda et al (2012).

An investigation in to the effect of PSD on processing parameters conducted by Liu et al. (2011) compared two powders of differing size ranges. Both powders were 316L stainless steel, with the first possessing a size range of 15 – 45 µm, and the second possessing a range of 0 – 45 µm. The study concluded that there was a significant difference in the performance of laser melted parts produced from the powders with differing size ranges. The second powder produced parts with higher density, but lower UTS and Elongations results when compared to the first powder. This study used a Malvern Mastersier 2000, which used laser diffraction to determine size ranges. This study highlighted the differences in packing density on the powder bed as a result of the differing size distributions of particles and the effect on part density as a result. The second powder, with the wider particle size range was also less susceptible to a fall in density for varying machine process parameters. The prior work indicates that PSD is a key characteristic of powders and that analysis should be conducted as per the guidance defined in BS ISO 13320 Particle size analysis; Laser diffraction methods (2009).

When considering the literature concerned with metallic powder characterisation, there is little mention of the methodologies used to sample and analyse powders. As such, an attempt shall be

made within this study to derive a suitable methodology for full characterisation of powders used within SLM. ASTM F3001-14 is the Standard Specification for Additive Manufacturing Titanium-6 Aluminum-4 Vanadium Extra Low Interstitial (ELI) with Powder Bed Fusion. This standard stipulates chemical composition requirements for Ti-6Al-4V powders used within powder bed fusion. The author could find no literature concerned with the full chemical analysis of powders used within SLM and this therefore requires investigation. Chemical composition testing in terms of the oxygen and nitrogen content is defined within ASTM E1409-13; Standard Test Method for Determination of Oxygen and Nitrogen in Titanium and Titanium Alloys by Inert Gas Fusion.

Upon completion of such characterisation, the effect on mechanical, metallurgical and chemical properties of laser melted parts must be determined. Facchini et al. (2010) investigated the ductility of laser melted parts produced with Ti-6Al-4V. They determined that parts possessed a martensitic microstructure as a result of laser melting and showed higher tensile strength than parts produced through hot working as a result of this microstructure. Ductility however was found to be lower in comparison. They concluded that ductility could be improved by manipulation of the material microstructure through a suitable heat treatment. It is clear then that in order for Ti-6Al-4V parts to satisfy requirements in terms of mechanical properties such as elongation a suitable heat treatment processes must be applied. The microstructure of laser melted parts is thus something that requires investigation.

Ferrar et al. (2012) considered the effect of gas flow within the build chamber on parts produced through SLM. They noted that parts produced in different positions within the build chamber showed varying mechanical properties. This led the author to consider investigating any difference in mechanical properties of parts produced at different positions in the build chamber within this study.

There are a number of standard specification that define methodologies for a variety of testing for determination of mechanical and metallurgical properties of laser melted parts. The standards to be used are:

- ASTM E8/E8M-15a. Standard Test Methods for Tension Testing of Metallic Materials (2015).

- ASTM E466-07. Standard Practice for Conducting Force Controlled Constant Amplitude Axial Fatigue Tests of Metallic Materials (2007).
- ASTM E3-11. Standard Guide for Preparation of Metallographic Specimens (2011).
- ASTM E407-07e1. Standard Practice for Microetching Metals and Alloys (2007).

3.0. Powder Characterisation: Results and Discussion

3.1. Powder Characterisation Overview

For the SLM process to be considered to be under effective control, a thorough understanding of the effects of powder recycling was required. As such, the author set out to define a methodology that would allow for the controlled recycling of Ti-6Al-4V powders used within the SLM process. Additionally, an understanding of the effect of changes in powder composition through repeated recycling, on mechanical, metallurgical and chemical properties of laser sintered parts was required. The methodology described within this section was decided upon, with the aim of the determination of any correlation between powder characteristics and characteristics of the laser sintered parts.

A test build was created with the following parts to be laser melted, as shown in Figure 2:

- 12 X tensile test specimen (Figure 35 & Figure 33).
- 12 X fatigue test specimens (Figure 49 & Figure 33).
- 12 X test pyramids for porosity, hardness and microstructure evaluation (Figure 33).
- 12 X chemical composition test cubes (Figure 33).
- 1 X powder collection test piece (Figure 5 & Figure 33).

The build shown in Figure 2 allowed for the calculation of the volume of powder required for one complete build. The yellow outline shows the entire region to be filled with powder during the build. In order to assess the effect of repeated recycling of Ti-6Al-4V powder, five identical repeat builds were to be completed. This meant that careful calculations were required to estimate the total volume of powder required to complete all five builds, accounting for the removal of powder lost to create the laser melted parts, powder lost to in process filtering and powder lost to post build sieving. The total volume required to complete the five builds was loaded into the material hopper at the top of the AM250. The feed stock powder was Extra Low Interstitial (ELI) Ti-6Al-4V Grade 23 (ASTM F3001-14).

Following the completion of build 1, all the remaining powder within the hopper was dosed into the machine in a layer by layer fashion to ensure that the powder experienced the same mechanical and thermal history as the bulk of the remaining powder.

In order to fully consider the changes to the properties arising by this process the author investigated the type of testing required. This was determined by the nature of the changes anticipated and the availability of test equipment. Following the completion of the five builds, the powder was analysed using the following techniques:

- Particle Size Distribution (PSD) analysis using laser diffraction.
- Chemical composition analysis.
- Scanning Electron Microscopy (SEM) analysis for surface microstructure and morphology characterisation.

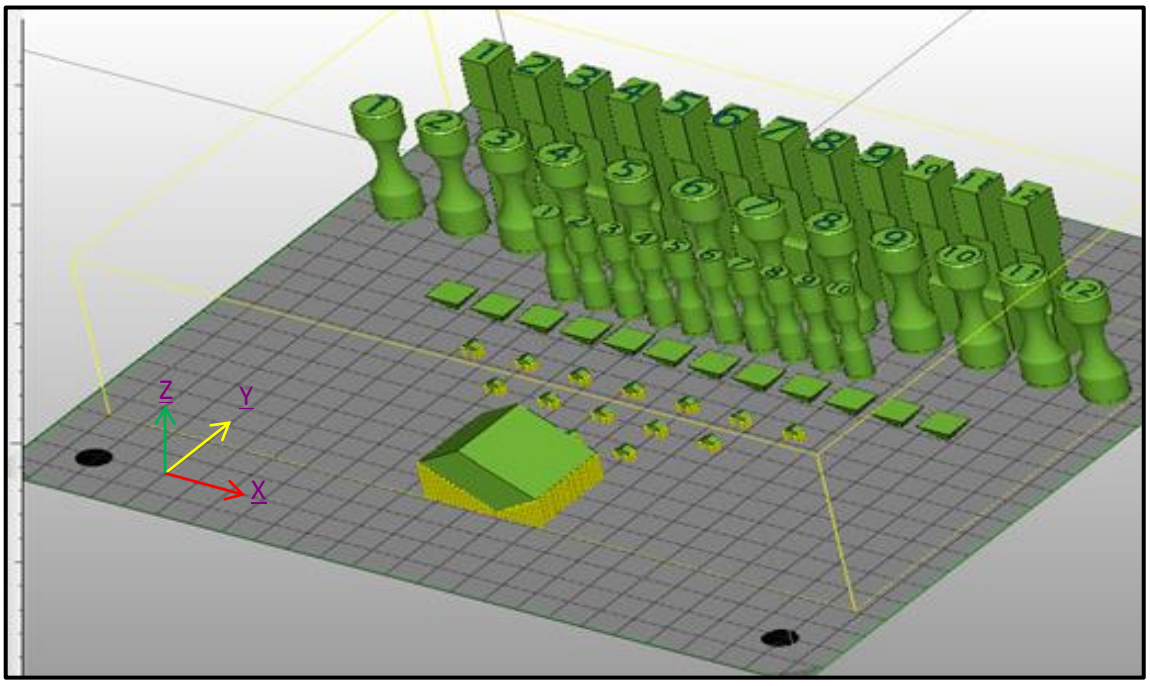

Figure 2 - Test Build Image Showing Parts to be Laser Melted

3.2. Powder Sampling Locations

Powder was sampled at various sections of testing. A sample of the feed stock powder was taken for analysis, as described within the following sections of this dissertation. A powder sample was taken

from within the build chamber, close to the substrate plate and site of laser melting. The remaining un-melted powder was then swept in to the machine overflow containers. This powder was then sieved, and another sample taken for powder characterisation. The entire amount of sieved powder was re-introduced into the powder hopper, and the second build was completed using powder that had been recycled once. This process was repeated until five identical builds had been completed with powder that had been recycled once additionally from the previous build.

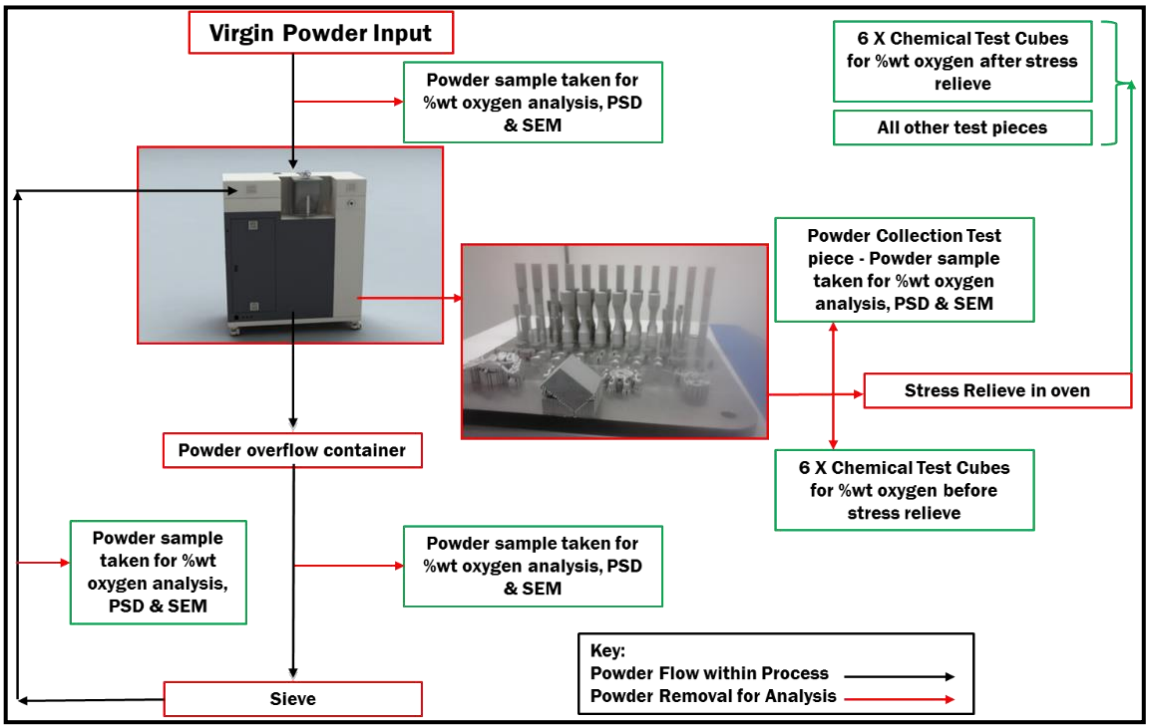

Figure 3 - Powder Flow and Sampling through Testing

Figure 4 - Images Showing Completed Build and Powder to be swept to Overflow

Overall, 26 powder samples were collected and labelled using the naming convention shown in Table 1.

Table 1 - Naming Convention for Powder Samples

Sample Name	Description
Feed Stock	Feed stock powder for Build 1.
Build 1 Chamber.	Sample taken from close to substrate plate following build 1.
Build 1 PCB Small	Sample taken from PCB Small Chamber.
Build 1 PCB Medium	Sample taken from PCB Medium Chamber.
Build 1 PCB Large	Sample taken from PCB Large Chamber.
Build 1 Post Sieve.	Sample taken from sieved powder used for build 1. This was the feed powder for build 2.
Build 2 Chamber.	Sample taken from close to substrate plate following build 2.
Build 2 PCB Small	Sample taken from PCB Small Chamber.
Build 2 PCB Medium	Sample taken from PCB Medium Chamber.
Build 2 PCB Large	Sample taken from PCB Large Chamber.
Build 2 Post Sieve.	Sample taken from sieved powder used for build 2. This was the feed powder for build 3.
Build 3 Chamber.	Sample taken from close to substrate plate following build 3.
Build 3 PCB Small	Sample taken from PCB Small Chamber.
Build 3 PCB Medium	Sample taken from PCB Medium Chamber.
Build 3 PCB Large	Sample taken from PCB Large Chamber.
Build 3 Post Sieve.	Sample taken from sieved powder used for build 3. This was the feed powder for build 4.
Build 4 Chamber.	Sample taken from close to substrate plate following build 4.
Build 4 PCB Small	Sample taken from PCB Small Chamber.
Build 4 PCB Medium	Sample taken from PCB Medium Chamber.
Build 4 PCB Large	Sample taken from PCB Large Chamber.
Build 4 Post Sieve.	Sample taken from sieved powder used for build 4. This was the feed powder for build 5.
Build 5 Chamber.	Sample taken from close to substrate plate following build 5.
Build 5 PCB Small	Sample taken from PCB Small Chamber.
Build 5 PCB Medium	Sample taken from PCB Medium Chamber.
Build 5 PCB Large	Sample taken from PCB Large Chamber.
Build 5 Post Sieve.	Final powder condition after 5 builds.

Within each of the five builds, a Powder Collection Box (PCB) was built as shown in Figure 5. This box was designed by the author to explore how the material collection process could be simplified. This was seen as being of great potential for future process capability assurance. The PCS was built to contain three separate chambers of increasing size and filled with powder. The purpose of this box was to investigate whether collection of powder in such a box would be representative of the powder remaining in process. If the box was then there would be no requirement for manual powder sampling from within the build chamber for determining the suitability of the remaining powder for production.

Additionally samples within the box were to allow for investigation of the effect of proximity of the powder to the site of laser melting on powder characteristics.

The box contained one small chamber, one medium sized chamber and one large chamber, providing a test volume of 6000 mm^3. The different locations within the box were to allow for investigation of the effect of proximity of the powder to the site of laser melting on powder characteristics. These boxes were completely sealed during laser melting by the inclusion of a walls and a roof surrounding each chamber. Following the completion of each build, each chamber had a small hole of 2mm diameter drilled in the top for the powder to be collected and analysed.

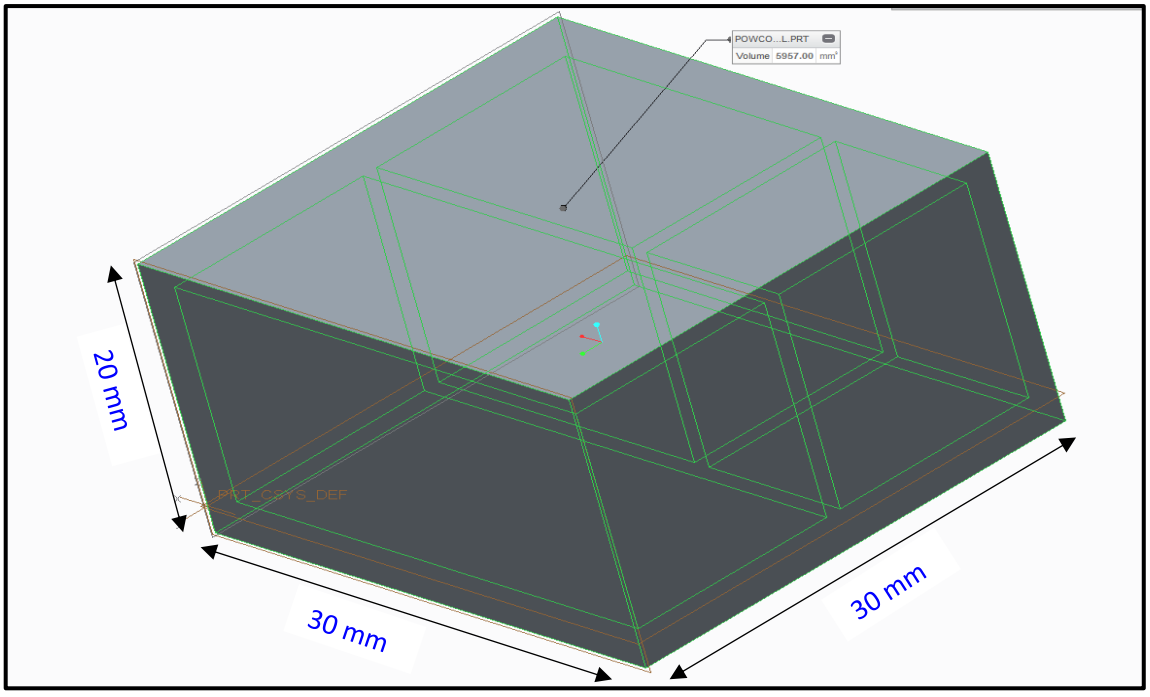

Figure 5 - Powder Collection Box with 3 Chambers of Increasing Size

3.3. Particle Size Distribution Analysis (PSD)

One of the significant pieces of information in the characterisation of powders is the particle size distribution. Particle size is known to have an effect on the flowability of powders, which in turn will affect the way in which powders are distributed to the build plate within SLM. Packing density of the powders on to the build plate will affect the density of laser melted parts. Powders that do not flow sufficiently to attain a suitable powder packing density on to the build plate will produce laser melted parts with higher than desirable or acceptable levels of porosity. This could be detrimental to the

strength and fatigue resistance of laser melted components. The way in which PSD was measured was through the use of laser diffraction; a Malvern Mastersizer 3000 was used for analysis.

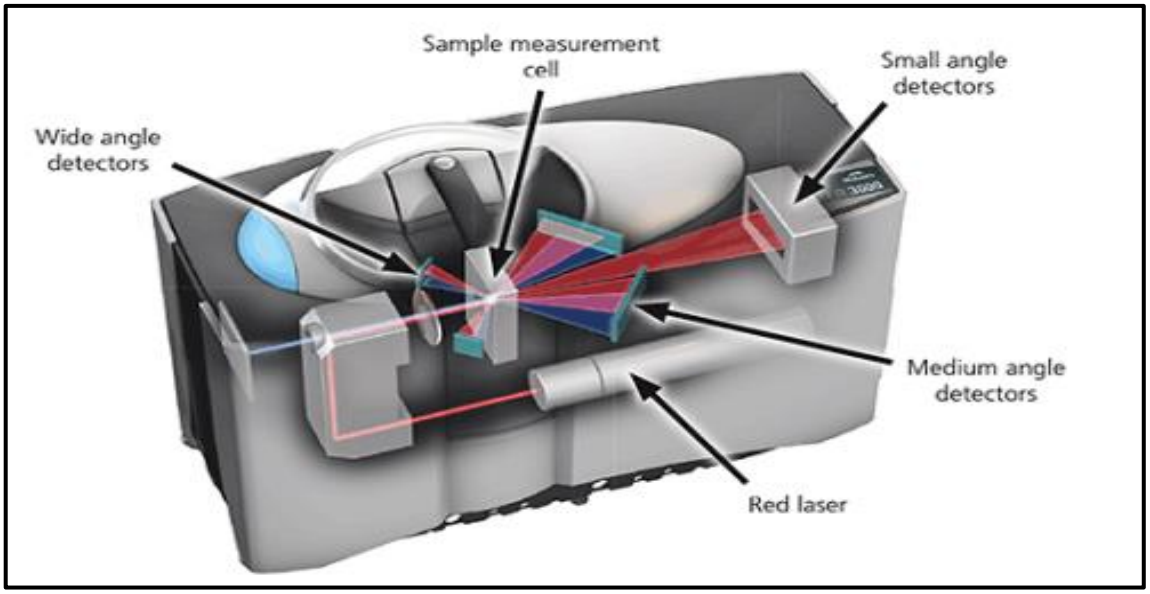

Figure 6 - Optical layout of Malvern Mastersizer 3000 (Malvern, 2015)

The application of this test is specified by BS ISO 13320-2009, which states:

> "A sample, dispersed at an adequate concentration in a suitable liquid or gas, is passed through the beam of a monochromatic light source, usually a laser. The light scattered by the particles, at various angles, is measured by multi-element detectors, and numerical values relating to the scattering pattern are recorded for subsequent analysis. These numerical scattering values are then transformed, using an appropriate optical model and mathematical procedure, to yield the proportion of the total volume of particles to a discrete number of size classes forming a volumetric PSD. "

The laser diffraction technique for the determination of PSDs is based on the phenomenon that particles scatter light in all directions with an intensity pattern that is dependent on particle size. Figure 7 illustrates this dependency in the scattering patterns for two sizes of spherical particles.

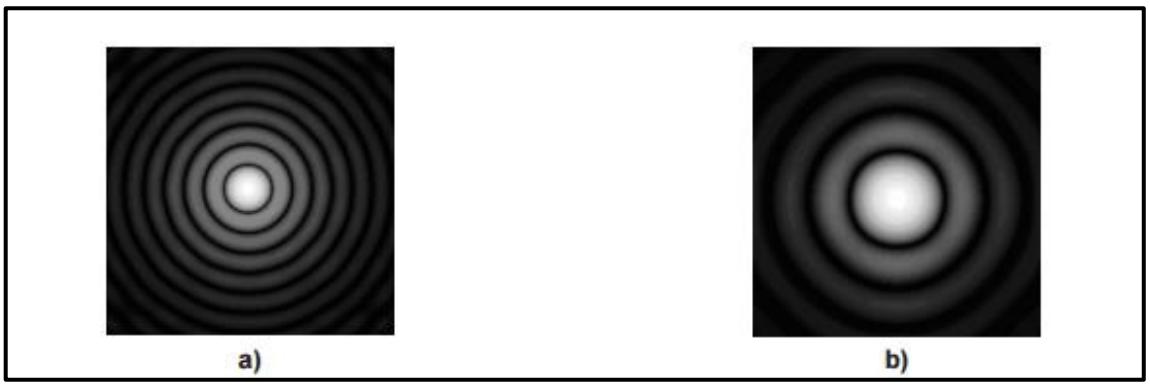

Figure 7 - Scattering Pattern for Two Spherical Particles: The Particle Generating Pattern a) is Twice as Large as the One Generating Pattern b) (BS ISO 13320 2009).

Particle size distributions measured by laser diffraction rely on measurement of variation in the angular intensity of scattered light in response to a dispersed particulate sample passing through a laser beam. The difference in angle of light scattering for large and small particles is illustrated in Figure 8, where large particles scatter light at small angles relative to the laser beam and small particles scatter light at large angles relative to the laser beam. Angular scattering intensity data is measured by small, medium and wide angle detectors as shown in Figure 6. This data is then analysed using the Mie theory of light scattering, to determine the size of the particles that were responsible for creating the scattering pattern. Particle size is reported as a volume equivalent sphere diameter (Malvern 2015).

Within this analysis, the dispersant used was distilled water. The powder sample was added to the dispersant slowly to create a dispersed particulate sample, until the point that there were sufficient particles held within the suspension to provide enough laser obscuration for calculation of the PSD within the overall population. The dispersant was contained within the centrifugal pump and stirrer unit shown in Figure 9, which pumped the dispersed particulate sample to the Malvern Mastersizer 3000 measurement cell, in which laser diffraction occurred and is shown in Figure 6.

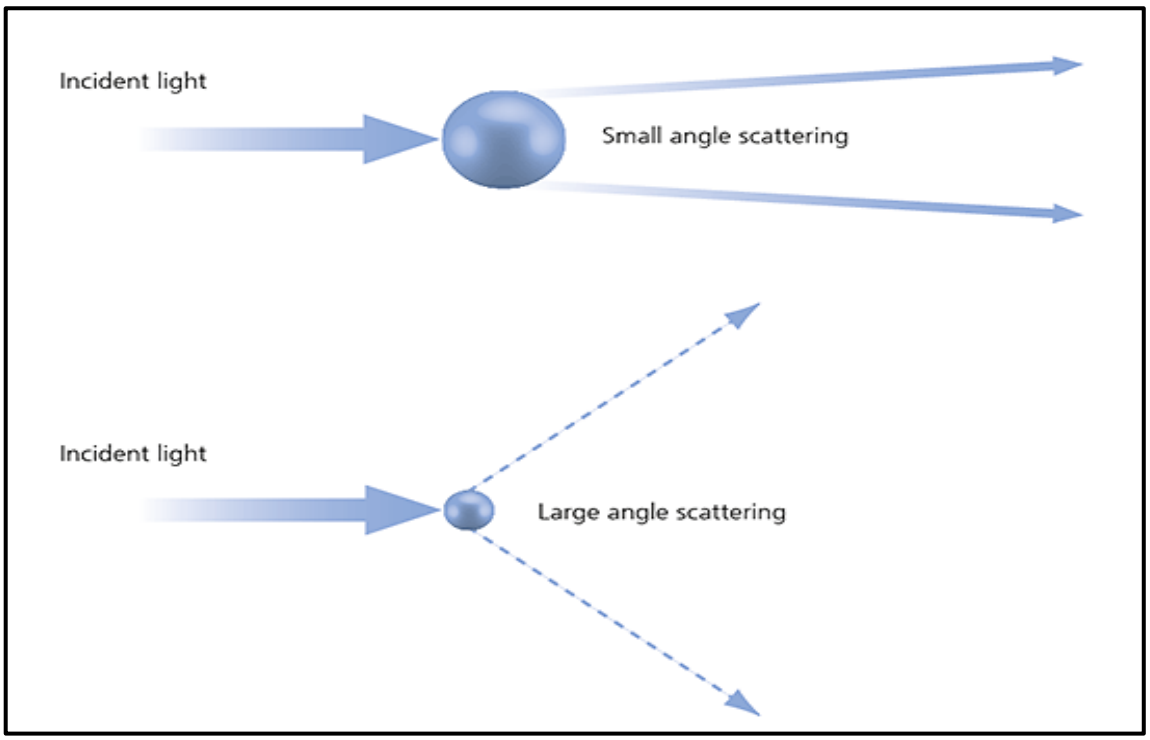

Figure 8 - Scattering of Light from Small and Large Particles (Malvern, 2015).

Figure 9 - Image Showing Malvern Mastersizer 3000 with Centrifugal Pump and Stirrer Unit (Malvern, 2015).

For each powder sample, five repeat measurements were taken and an average determined. The data output shows the percentage of the population of particles that are determined to have a diameter within pre-specified ranges. An example of the data output for the Feed Stock sample is shown in Table 2, where outputs included:

- Φ Dx(10) µm

- Φ Dx(50) µm
- Φ Dx(90) µm
- % Result In Range (14.5 – 45.6 µm)
- % Result Below (14.5 µm)
- % Result Above (45.6 µm)

Additional data collected shows the percentage of the powder population analysed that was contained within discrete particle size ranges. These data sets are too large to be displayed within this report and are contained within the raw data section of the CD supplied, appended to the report. This data was, however, used to produce graphs showing the range of particle sizes contained within each powder sample. The five repeat PSD measurements for the Feed Stock powder sample analysed are shown in Figure 10, with the average of the five runs shown in Figure 11.

Table 2 - Data Recorded for PSD Measurement of Feed Stock Powder Sample

Sample Name	Feed Stock Ti-6Al-4V	Feed Stock Ti-6Al-4V	Feed Stock Ti-6Al-4V	Feed Stock Ti-6Al-4V	Feed Stock Ti-6Al-4V	Average Ti-6Al-4V
Measurement Date & Time	08/09/2014 15:14	08/09/2014 15:14	08/09/2014 15:14	08/09/2014 15:15	08/09/2014 15:15	08/09/2014
Dx (10)	17.5	17.6	18.0	17.8	17.5	17.7
Dx (50)	27.4	27.4	28.0	27.3	26.8	27.4
Dx (90)	41.2	41.2	41.9	40.6	39.9	41.0
Particle Density	4.4	4.4	4.4	4.4	4.4	4.4
Result Below (14.5 µm)	2.7	2.6	2.2	2.3	2.6	2.5
Result In Range (14.5 -45.6 µm)	92.9	93.1	92.8	94.0	94.2	93.4
Result Above (45.6 µm)	4.3	4.3	4.6	3.7	3.1	4.1

The powder supplied by the manufacturer (Feed Stock powder) was intended to be within the range of 15 - 45 µm. This was the reason for defining the percentage of the population both within this range, and outside as an output of the analysis. These outputs show the change in PSD of powder through repeated recycling by highlighting the change in the relative percentage of the population being made up of fine and course particles. Fine particles in this instance were considered to be particles of less than 14.5 µm in diameter and course particles were considered to be those of greater than 45 µm in diameter. The remainder of the graphs showing individual PSD measurements and average measurements for samples are shown in Appendix 1 as Figure 66 - Figure 85.

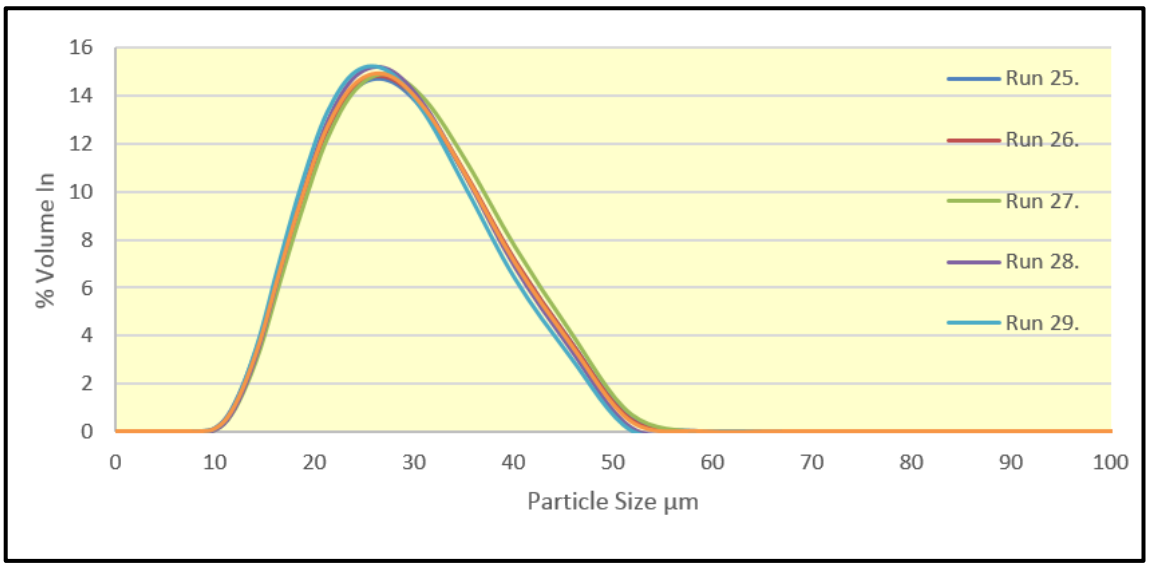

Figure 10 - Graph Showing PSD Results for Feed Stock Powder Sample

Figure 11 - Graph Showing Average PSD for Feed Stock Powder Sample

Consideration of the data displayed in Figure 11 and Table 2 affords a picture of the PSD of the Feed Stock powder supplied by the manufacturer. The powder was shown to be normally distributed and well controlled in terms of the percentage of the powder sample population that was in fact within the stated range of 15 – 45 µm. In fact, 93.39 % of the powder particles within the sample analysed were within the desired range, with 2.51 % of the particles being of a diameter less 14.5 µm and 4.09 % of the particles being of a diameter greater than 45.6 µm.

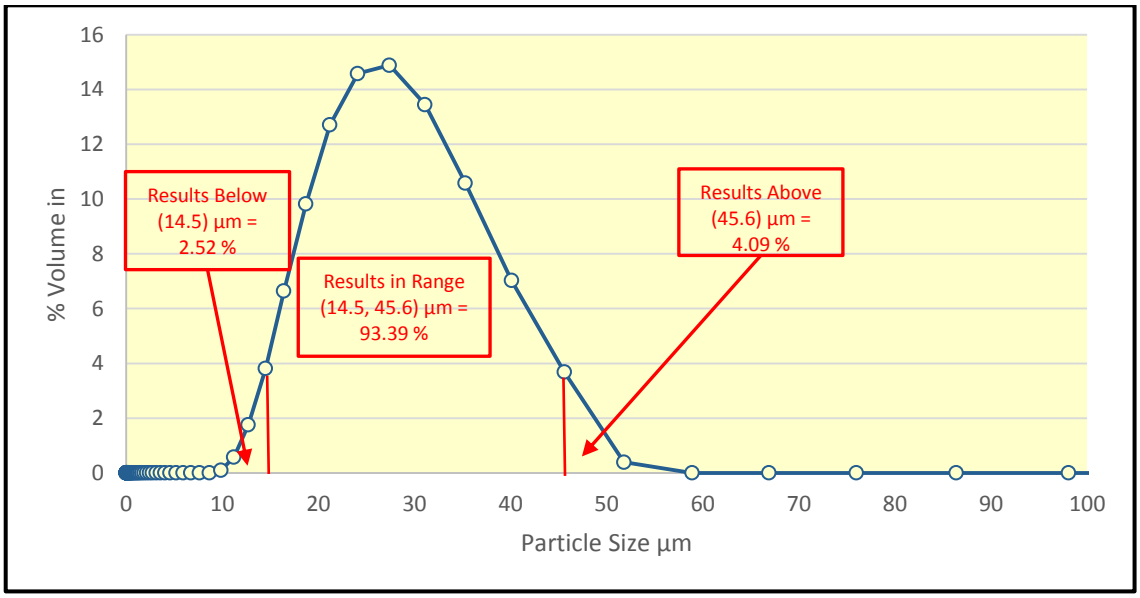

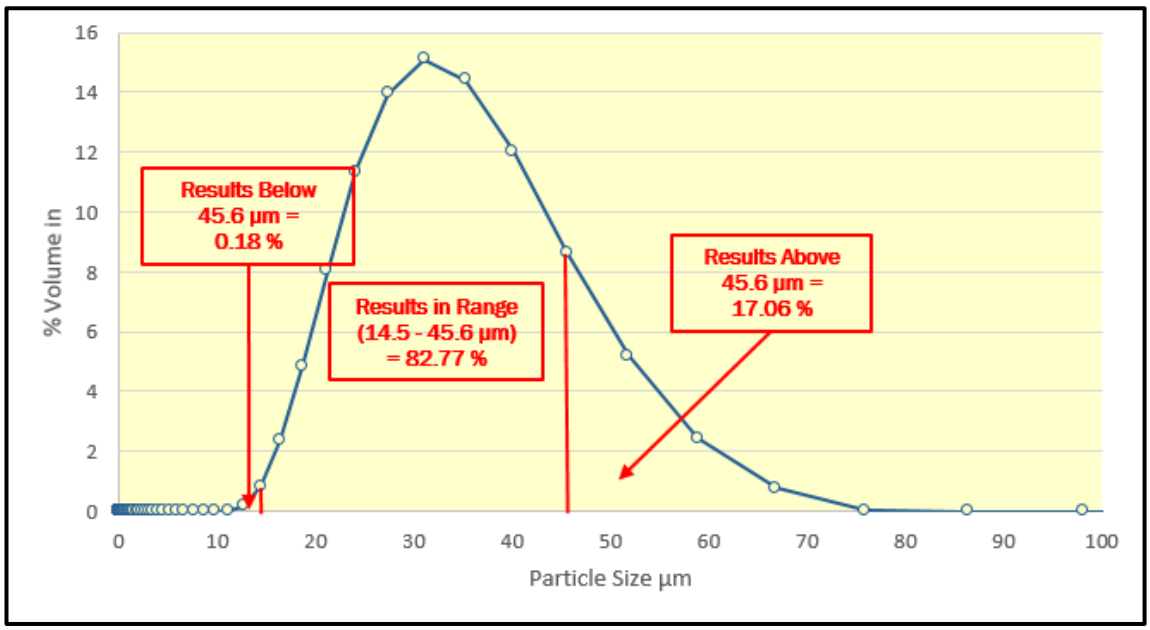

Figure 12 - Graph Showing Average PSD for Build 5 Post Sieved Powder

In contrast,

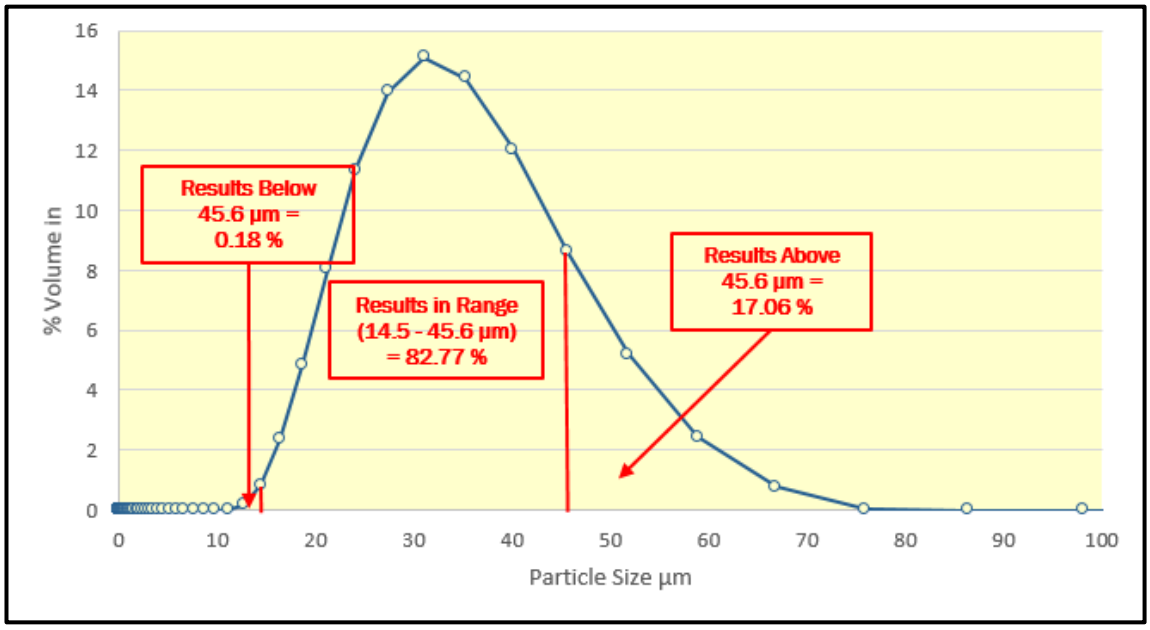

Figure 12 shows the average of five repeat measurements of PSD taken for the powder at the end of the investigation in to the effects of repeated recycling of Ti-6Al-4V powders. This powder sample had been through the SLM process five times. By this stage of recycling, only 82.77 % of the powder particles within the sample analysed were within the desired range, with 0.18 % of the particles being of a diameter less 14.5 µm and 17.06 % of the particles being of a diameter greater than 45.6 µm.

When considering the condition of the powder samples in terms of PSD, Figure 11 and

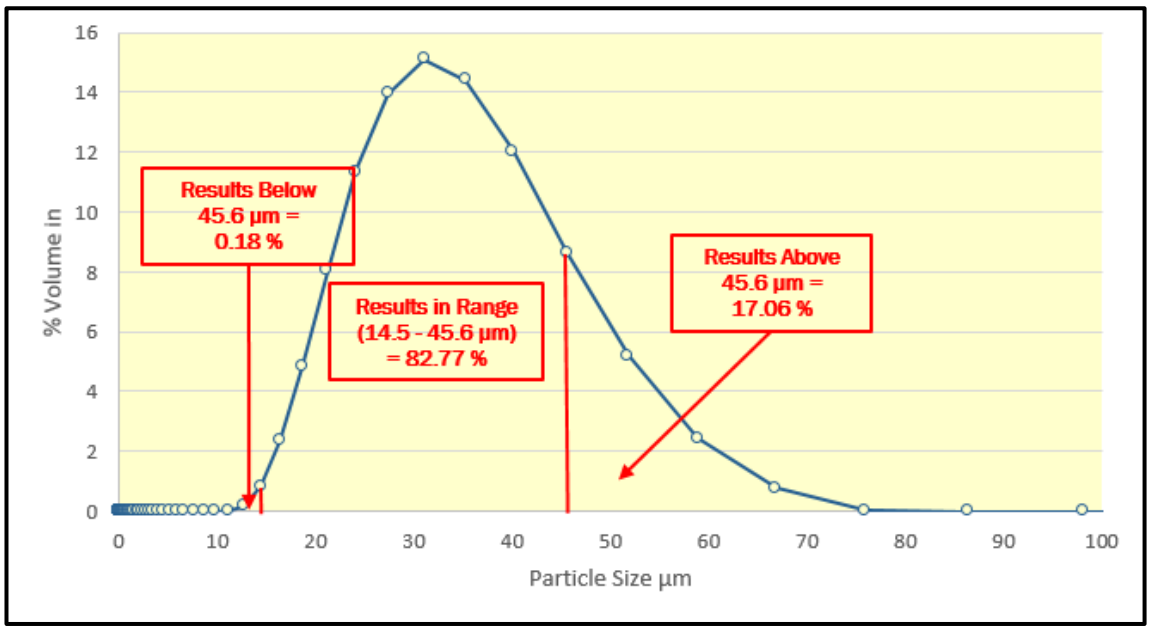

Figure 12 show that there was clearly a reduction in the number of fine particles (< 14.5 µm) within the overall powder population, and an increase in the number of coarse particles (>45 µm) within the powder population. This is further emphasised by the results for Dx(10), Dx(50) and Dx(90) of all powder samples analysed and shown in Figure 13, where a reduction in the number of fine particles shall tend towards increasing values of Dx(10), Dx(50) and Dx(90).

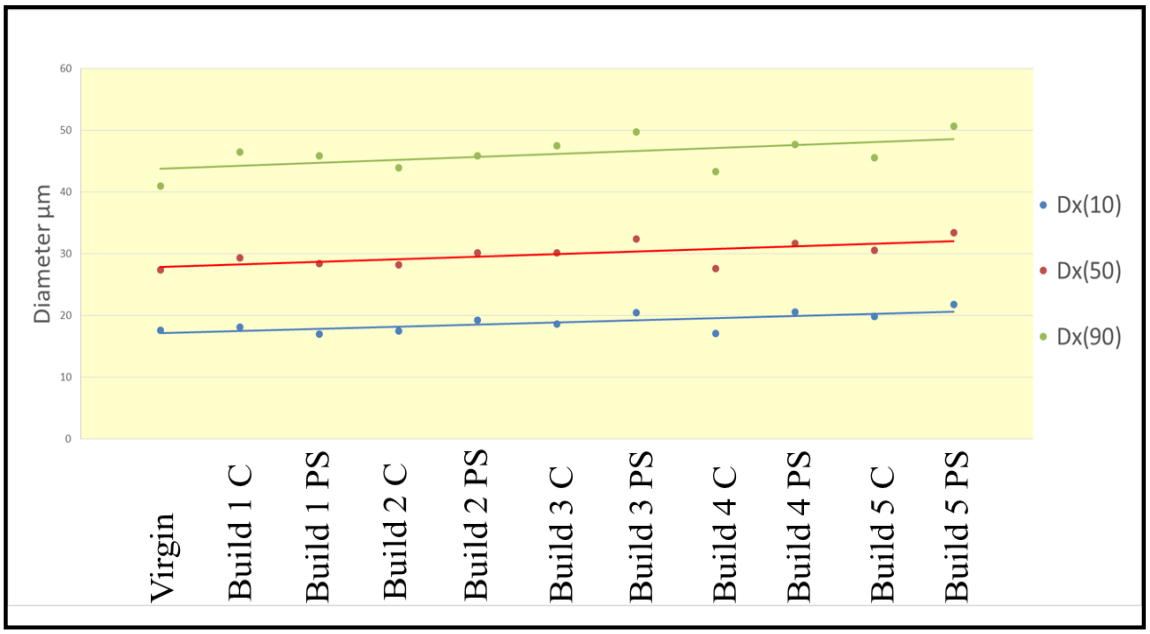

Figure 13 - Graph Showing Dx(10), Dx(50) and Dx(90) for Powder Samples

3.4. Analysis of Variance for Powder Testing Results

The next stage in the assessment of change in PSD through repeated recycling was to perform Analysis of Variance (ANOVA) for the repeat measurements taken for all samples. Additionally, within this section, the results for PSD analysis of the PCB samples, shown in Figure 5 were considered. For all 5 builds, five samples were analysed, which were:

- Feed Powder. This was the powder sample used as the feed stock for each build. That is, the powder used for build 1 was the Feed Stock powder, the powder used for build 2 was the build 1 post sieve powder and so on.
- Chamber Powder. This was the powder sample collected from within the build chamber upon completion of each build. The powder sample was taken extremely close to the build plate, within the gaps between laser melted parts.
- PCB Small. This was the powder sample taken from the small chamber of the powder collection box produced with each build.
- PCB Medium. This was the powder sample taken from the medium chamber of the powder collection box produced with each build.
- PCB Large. This was the powder sample taken from the large chamber of the powder collection box produced with each build.

The process factors to be investigated within this study were:

- Build Number at 5 levels (Build 1, 2, 3, 4 and 5).
- Powder Sample Location at 2 levels (Feed Powder, Chamber Powder).

The measured response variables for each sample were as defined previously and shown in Table 2. Analysis within this section was focused two key areas, which were General Factorial Regression Modelling and Main Effects Analysis.

Minitab (2015) states that:

> "One of the most commonly used methods in statistical decision making is hypothesis testing. In general, a hypothesis test is a process in which you assume an initial claim to be true and then test this claim using sample data. Ordinarily, the initial claim refers to a population

parameter of interest such as the population mean (μ). Hypothesis tests include two hypotheses: the null hypothesis (denoted by H_0) and the alternative hypothesis (denoted by H_1)."

In this instance, the null hypothesis was the initial claim that there was no evidence of statistical significance for the effect being considered. The alternative hypothesis in this case referred to there being evidence of a statistical significance for the effect being considered (Moore 1999). When performing ANOVA for the data to be considered, Minitab tested for the null hypothesis and output a p-value.

The p-values in the ANOVA table were used to determine which of the effects in the model were statistically significant. If the p-value was found to be less than or equal to the α-level (predetermined level of significance), then the null hypothesis was to be rejected and support claimed for the alternative hypothesis. This would mean concluding that there was evidence of statistical significance for the effect considered. If the P-value was above the α-level, the null hypothesis was to be accepted and the conclusion drawn that there was no evidence of statistical significance for the effect considered (Minitab 2015).

When the null hypothesis was true and it was rejected, a type I error would be made. The probability of making a type I error was termed the α-level. The α-level used within this statistical analysis was 0.05 (5 %), meaning that there was a 5 % chance of rejecting the null hypothesis incorrectly and concluding that an effect was statistically significant, when in fact it was not (Moore 1999).

The F-value was used to determine whether different levels of a factor lead to different values of the response variable. It was the value that was used to test the null hypothesis, that the effects of a term in the model (factor or interaction) were significant. F-value was used to determine the p-values calculated (Minitab 2015).

F-value = (MS FACTOR)/(MS ERROR)

Where MS represents the Mean Squares for each factor.

The F-value was to be large where MS FACTOR was much larger than MS ERROR. That meant that when variation within factors was much greater than the variation due to random error, the F-value would be large. The F-value was considered to be a key test statistic (Joiner & Ryan 2001). The larger the F-value, the more likely it was that the factor contributed significantly to the variability in the response variable. A combination of a low p-value and high F-value was thus considered to be indicative of evidence for a statistically significant effect of the factor being considered.

When conducting General Factorial Regression Modelling, ANOVA was performed to fit a model to the input data. This lead to a fitted value, and a residual value for each data point input. A fitted value was the best estimate of the underlying population mean corresponding to the specific data point found through regression modelling. The residual value was the amount by which the specific data point varied from the fitted value (Joiner and Ryan 2010).

The ANOVA table output S, R^2 and Adjusted R^2 values which were measures of how well the model fitted to the data. From Minitab (2015):

> S is measured in the units of the response variable and represents the standard distance that data values fall from the regression line. For a given study, the better the equation predicts the response, the lower S is.
>
> R^2 (R-Sq) describes the amount of variation in the observed response values that is explained by the model and Adjusted R^2 (R-sq(adj)) is a modified R^2 that has been adjusted for the number of terms in the model.

By considering the above, within the analysis, low values of S, combined with high values of R^2 and Adjusted R^2 were desirable, as this suggested a high level of accuracy within the model created, providing a high level of confidence in the results.

Within this analysis, the p-value, F-value, S, R^2 and Adjusted R^2 values were output within the ANOVA tables produced through completing General Factorial Regression Modelling. The p-value and F-value were used to quantify the level of significance that each process factor had on the response variables

measured for each sample. The S, R^2 and Adjusted R^2 values were used to determine the level of accuracy for the model produced.

Table 3 - Analysis of Variance for Dx(10)

Source	DF	Adj SS	Adj MS	F-Value	P-Value
Model	9	81.478	9.0531	191.47	0.000
Linear	5	56.271	11.2542	238.02	0.000
Build Number	4	49.274	12.3184	260.53	0.000
Powder Sampling Location	1	6.997	6.9970	147.98	0.000
2-Way Interactions	4	25.207	6.3017	133.28	0.000
Build Number*Powder Sampling Location	4	25.207	6.3017	133.28	0.000
Error	40	1.891	0.0473		
Total	49	83.369			

Model Summary

S	R-sq	R-sq(adj)	R-sq(pred)
0.217445	97.73%	97.22%	96.46%

Table 3 shows the ANOVA table produced for Dx(10) when General Factorial Regression analysis was performed. Figure 14 shows the residual plots produced. The Normal Probability Plot shows the regression line created by the model, and the residual values deviation from the expected value created by the model.

The S value was shown to be extremely low, suggesting that there was a low standard difference of data points from the fitted value shown by the regression line (0.217 µm). Additionally, R^2 and Adjusted R^2 were calculated as being 97.73 % and 97.22 % respectively. These values were indicative of a highly accurate model, capable of explaining the majority of the data points, providing the author with confidence in the model produced.

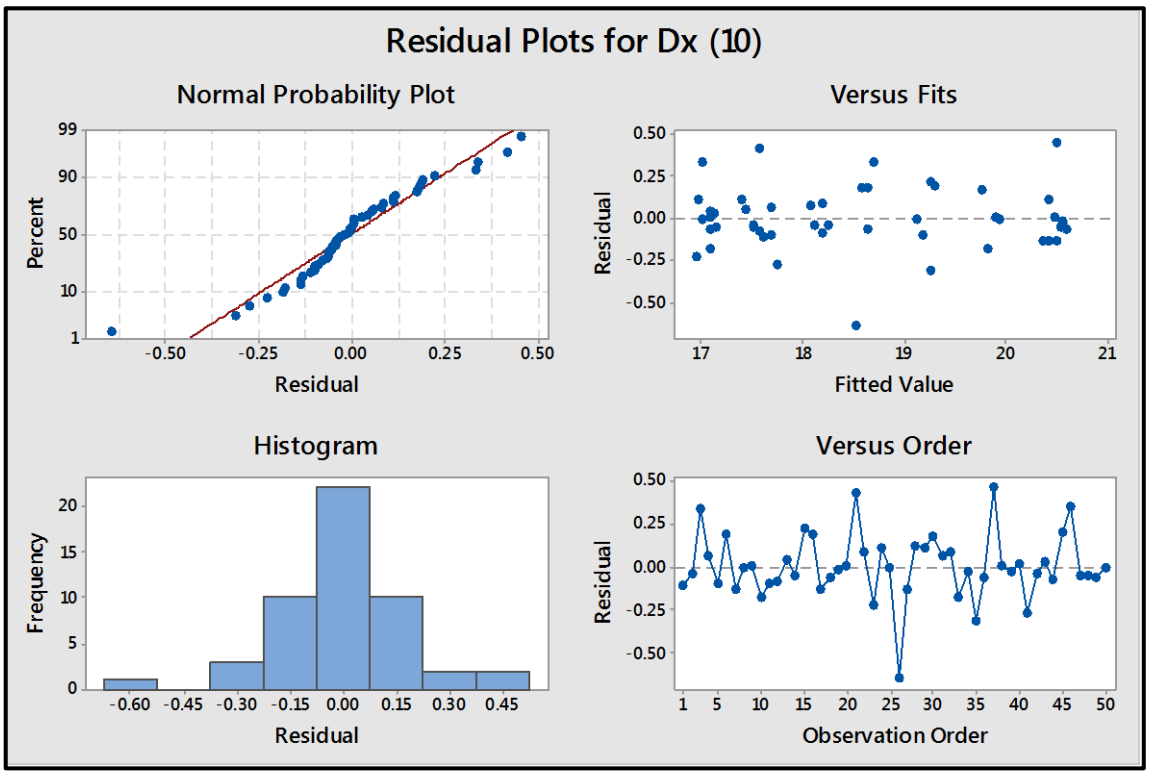

Figure 14 - Residual Plots for Dx(10)

Figure 15 shows the main effects plot produced for the measured variable Dx(10). Main Effects plots may be used in combination with ANOVA in the determination of the effect of a process factor. The main effects plot displays, and allows for the comparison of the average result for each level of the factors being considered (Minitab 2015). In this case, the main effects plot displays the average result of Dx(10) for each of the five builds, as well as the average result of Dx(10) for each of the powder sampling locations.

When considering the effect of the two process factors on Dx(10), review of the p-value and f-value shown in Table 3, along with the comparison of main effects shown in Figure 15 was required. The process factor that was shown to have the most significant effect on the measured variable Dx(10) was Build Number. A p-value of 0.000 (P-value << α-level of 0.05), coupled with a F-value ratio value of 260.53 suggested that there was strong statistical evidence of varying Build Number on Dx(10).

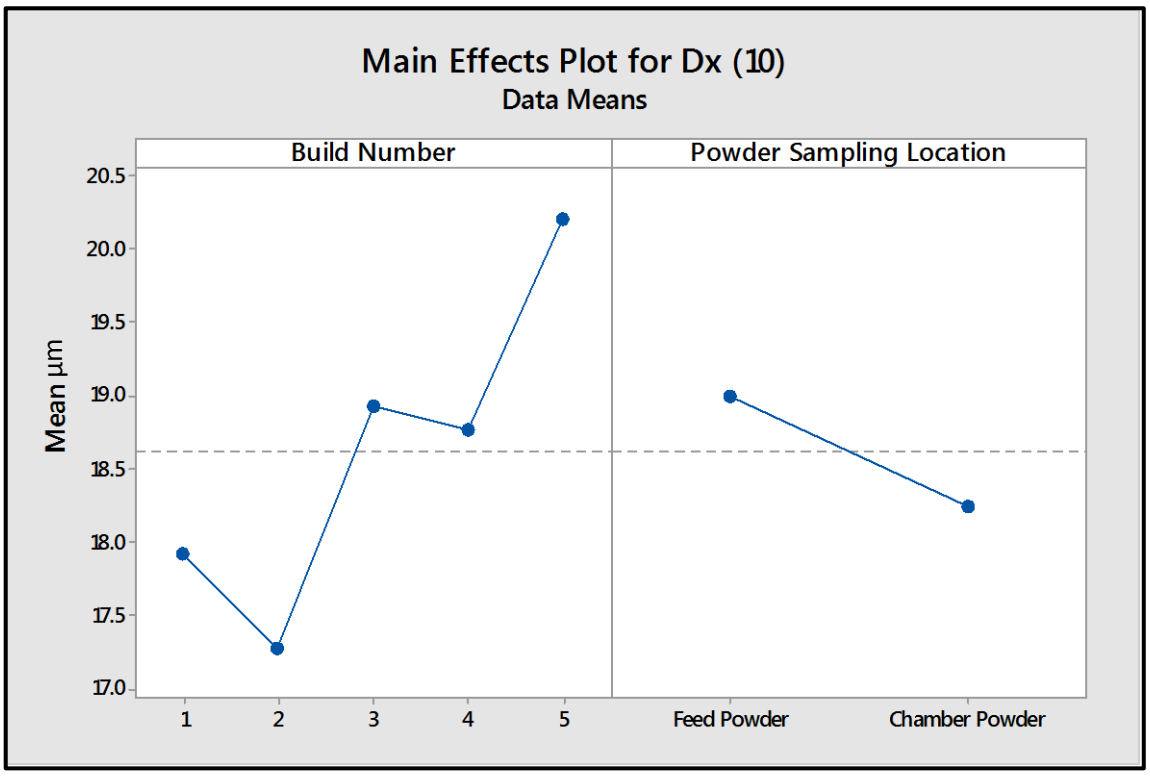

Figure 15 - Main Effects Plot for Dx(10)

The process factor of Powder Sample Location was also shown to have the an effect on the measured variable Dx(10). A p-value of 0.000 (P-value << α-level of 0.05), coupled with a F-value ratio value of 147.98 suggested that there was statistical evidence of varying the Powder Sampling Location on Dx(10). The overall trend was towards an increase in Dx(10) through repeated recycling, that is, moving from level 1 to level 5. Surprisingly, the powder samples for build 2 showed slightly lower values (17.27 µm) for Dx(10) that those for build 1 (17.92 µm). Although the effect of varying the Build Number level from 1 to 5 (recycling the powder) was shown to be statistically significant, the absolute difference in the value of Dx(10) when moving from build 1 through 5 was 2.28 µm.

Table 4 - Analysis of Variance for Dx(50)

Source	DF	Adj SS	Adj MS	F-Value	P-Value
Model	9	129.771	14.4190	109.79	0.000
Linear	5	67.887	13.5773	103.38	0.000
Build Number	4	59.174	14.7934	112.64	0.000
Powder Sampling Location	1	8.713	8.7130	66.34	0.000
2-Way Interactions	4	61.884	15.4710	117.80	0.000
Build Number*Powder Sampling Location	4	61.884	15.4710	117.80	0.000
Error	40	5.253	0.1313		
Total	49	135.024			

Model Summary

S	R-sq	R-sq(adj)	R-sq(pred)
0.362400	96.11%	95.23%	93.92%

Table 4 shows the ANOVA table produced for Dx(50) and Figure 16 shows the residual plots produced. The S value was shown to be extremely low, again suggesting that there was a low standard difference of data points from the fitted value shown by the regression line (0.362 µm). Additionally, R^2 and Adjusted R^2 were calculated as being 96.11 % and 95.23 % respectively. These values were again indicative of a highly accurate model, capable of explaining the majority of the data points, providing the author with confidence in the model produced.

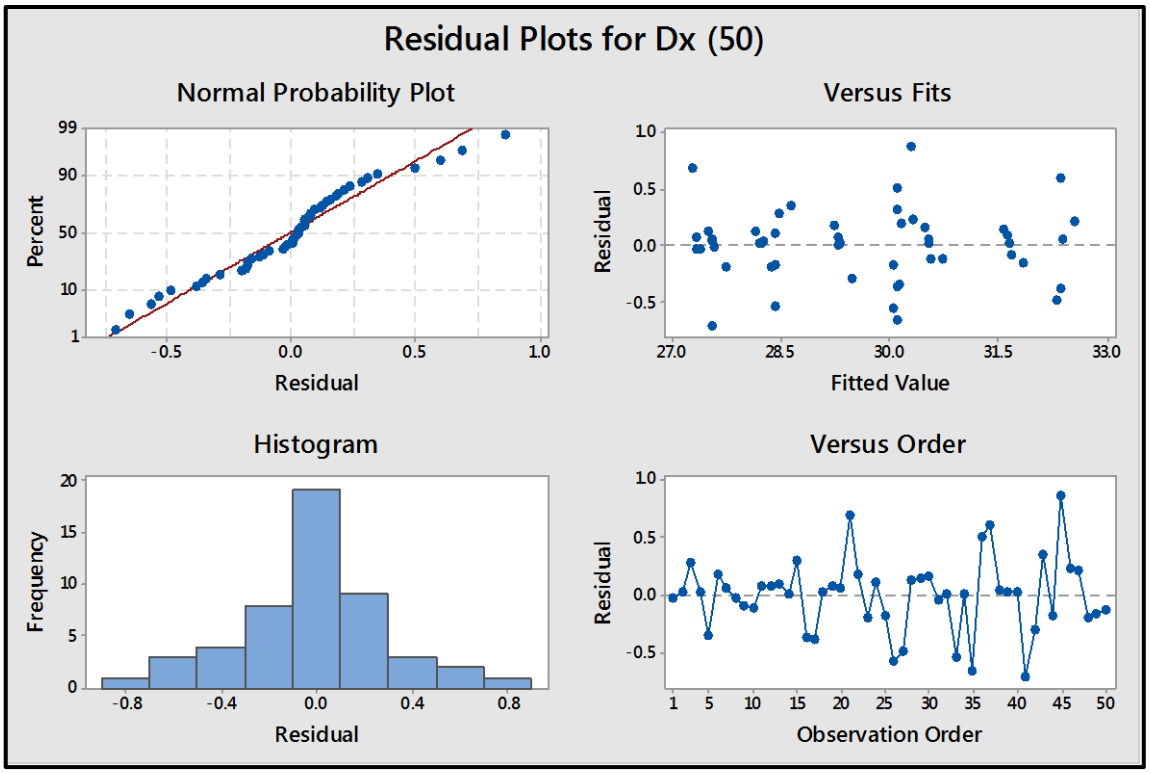

Figure 16 - Residual Plots for Dx(50)

When considering the effect of both Build Number and Powder Sampling Location, both were shown to have an effect on the value of Dx(50) within the samples analysed. Build Number was again show to have the strongest effect on Dx(50). A p-value of 0.000, coupled with a F-value ratio value of 112.64 suggested that there was strong statistical evidence of varying powder sampling location on Dx(50). A p-value of 0.000 for Powder Sampling Location, coupled with a F-value ratio value of 66.34 suggested that there was statistical evidence of varying Powder Sampling Location on Dx(50).

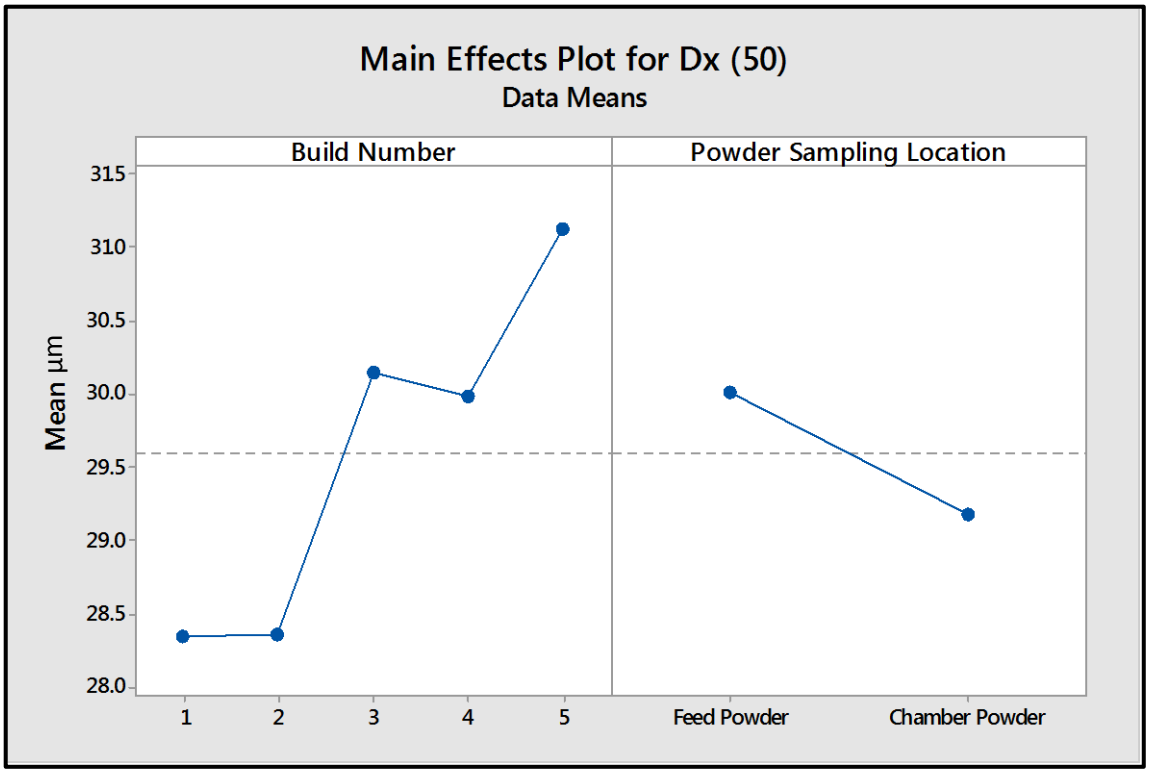

Figure 17 - Main Effects Plot for Dx(50)

Figure 17 shows the Main Effects Plot for Dx(50). The plot showed the same trends observed within the Main Effects Plot for Dx(10) in terms of both an increase in the value of PSD measurements when moving from build 1 to build 5 and a decrease from the feed powder sample to the chamber sample. There was also a difference observed in PSD measurements between the Feed Powder Samples and the Chamber Samples with the average of Dx(50) for the samples being measured as 30.01 and 29.1 µm respectively.

Table 5 - Analysis of Variance for Dx(90)

Source	DF	Adj SS	Adj MS	F-Value	P-Value
Model	9	275.234	30.5815	57.36	0.000
Linear	5	75.960	15.1920	28.50	0.000
Build Number	4	69.885	17.4712	32.77	0.000
Powder Sampling Location	1	6.075	6.0750	11.40	0.002
2-Way Interactions	4	199.274	49.8184	93.45	0.000
Build Number*Powder Sampling Location	4	199.274	49.8184	93.45	0.000
Error	40	21.324	0.5331		
Total	49	296.558			

Model Summary

S	R-sq	R-sq(adj)	R-sq(pred)
0.730141	92.81%	91.19%	88.76%

Table 5 shows the ANOVA table produced for Dx(90) and Figure 86 shows the residual plots produced. The S value was shown to be reasonably low, again suggesting that there was a low standard difference of data points from the fitted value shown by the regression line (0.730 µm). Additionally, R^2 and Adjusted R^2 were calculated as being 92.81 % and 91.19 % respectively. These values were again indicative of a highly accurate model, capable of explaining the majority of the data points, providing the author with confidence in the model produced.

When considering the effect of both Build Number and Powder Sampling Location, both were shown to have an effect on the value of Dx(90) within the samples analysed. Build Number was again show to have the strongest effect on Dx(90). A p-value of 0.000, coupled with a F-value ratio value of 32.77 suggested that there was some statistical evidence of varying powder sampling location on Dx(90). A p-value of 0.002 for Powder Sampling Location, coupled with a relatively low F-value ratio value of 11.40 suggested that there was some statistical evidence of varying Powder Sampling Location on Dx(90). This was clearly displayed within the Main Effects Plot shown in Figure 18.

Again, through repeated recycling, the value of Dx(90) for the powder samples analysed increased from Build 1 to Build 5. The value of Dx(90) decreased again between the powder sample taken from the Feed Stock powder to the Chamber Sample. One may expect the

chamber samples to contain a larger proportion of larger particles when compared to the feed powder samples, due to the chamber samples being taken from close to the site of laser melting, resulting in a higher number larger particles being present. This coupled with the fact that all feed powder samples having been sieved and should contain less large particles, would lead the author to expect higher values for PSD measurement for the chamber powder samples when compared to the feed powder samples. Evidence for the effect of increasing numbers of large particles found close to the site of laser melting shall be presented in a later part of this section of the report.

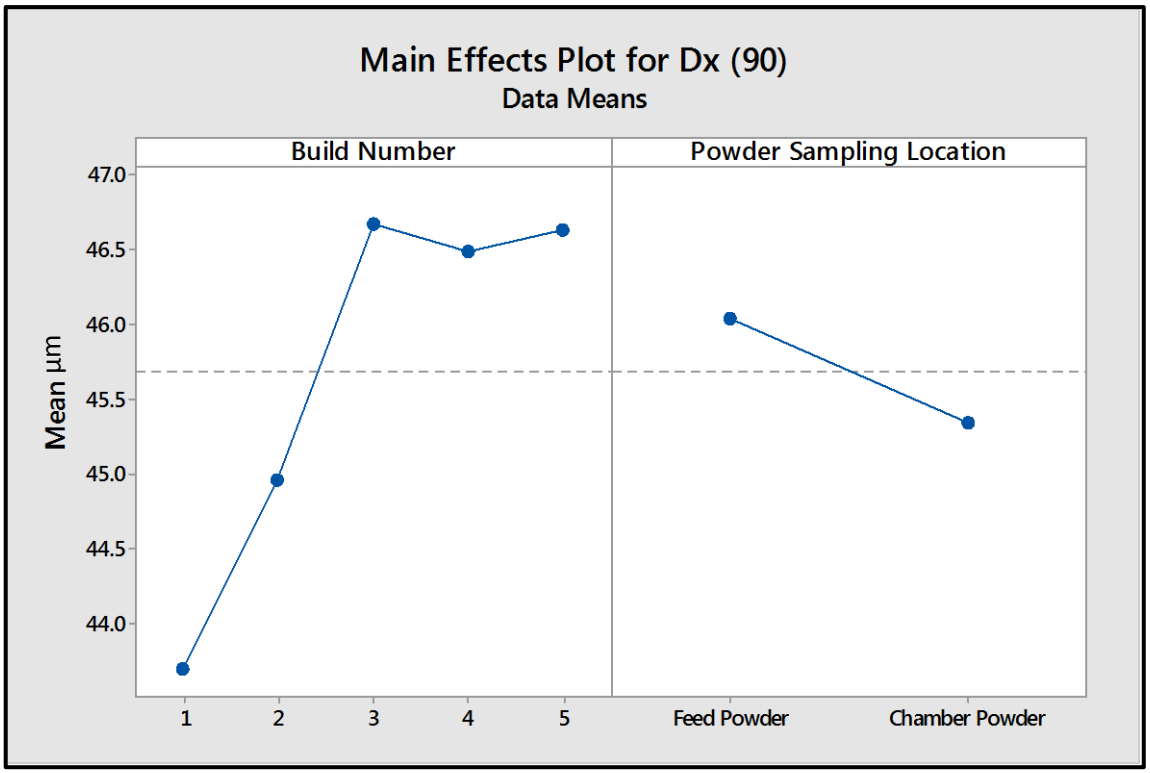

Figure 18 - Main Effects Plot for Dx(90)

A potential reason for this may be as follows:

During the gravity fed sieving process, smaller particles could potentially pass through the sieve and in to the bottom of the container into which they fall. They could pass in the gaps between larger particles, resulting in more small particles at the bottom of the collection container after sieving. The author was not present during powder sample collection and so believed that it was likely that the sample for analysis would have been taken from the top of the conical shaped container used for the collection of sieved powder to be re-introduced into the powder hopper for the subsequent build. This sample taken, containing a potentially lower proportion of small particles could be a potential reason

or the surprising result of the feed powder having larger results for PSD measurements when compared with those of the chamber powder sampled.

Table 6 - Analysis of Variance for Results Below 14.5 µm

Analysis of Variance

Source	DF	Adj SS	Adj MS	F-Value	P-Value
Model	9	71.547	7.9497	150.30	0.000
Linear	5	48.774	9.7548	184.43	0.000
Build Number	4	44.794	11.1986	211.73	0.000
Powder Sampling Location	1	3.980	3.9795	75.24	0.000
2-Way Interactions	4	22.773	5.6933	107.64	0.000
Build Number*Powder Sampling Location	4	22.773	5.6933	107.64	0.000
Error	40	2.116	0.0529		
Total	49	73.663			

Model Summary

S	R-sq	R-sq(adj)	R-sq(pred)
0.229980	97.13%	96.48%	95.51%

Table 6 shows the ANOVA table produced for full analysis of results below 14.5 µm and Figure 87 shows the residual plots produced. The S value was shown to be reasonably low, again suggesting that there was a low standard difference of data points from the fitted value shown by the regression line (0.229 %). Additionally, R^2 and Adjusted R^2 were calculated as being 97.13 % and 96.48 % respectively. These values were again indicative of a highly accurate model, capable of explaining the majority of the data points, providing the author with confidence in the model produced.

When considering the effect of both Build Number and Powder Sampling Location, both were shown to have an effect on the value of Results Below 14.5 µm within the samples analysed. Build Number was again show to have the strongest effect on results below 14.5 µm. A p-value of 0.000, coupled with a F-value ratio value of 211.73 suggested that there was strong statistical evidence of varying Build Number on results below 14.5 µm. A p-value of 0.000 for Powder Sampling Location, coupled with a F-Value ratio value of 75.24 suggested that there was statistical evidence of varying Powder Sampling Location on results below 14.5 µm.

The Main Effects Plot shown in Figure 19 again shows a trend towards a reduction in the proportion of the powder samples being made up of fine particles through repeated recycling of the powders (Moving from Build 1 to Build 5). For this measured variable, however, the Chamber Powder sample contains a higher proportion of particles below 14.5 µm in diameter than the feed powder sample. This was unsurprising having already considered the values of Dx(10, 50 and 90), which were higher for the Feed Powder samples. This was indicative of their populations being made up of a lower proportion of small particles.

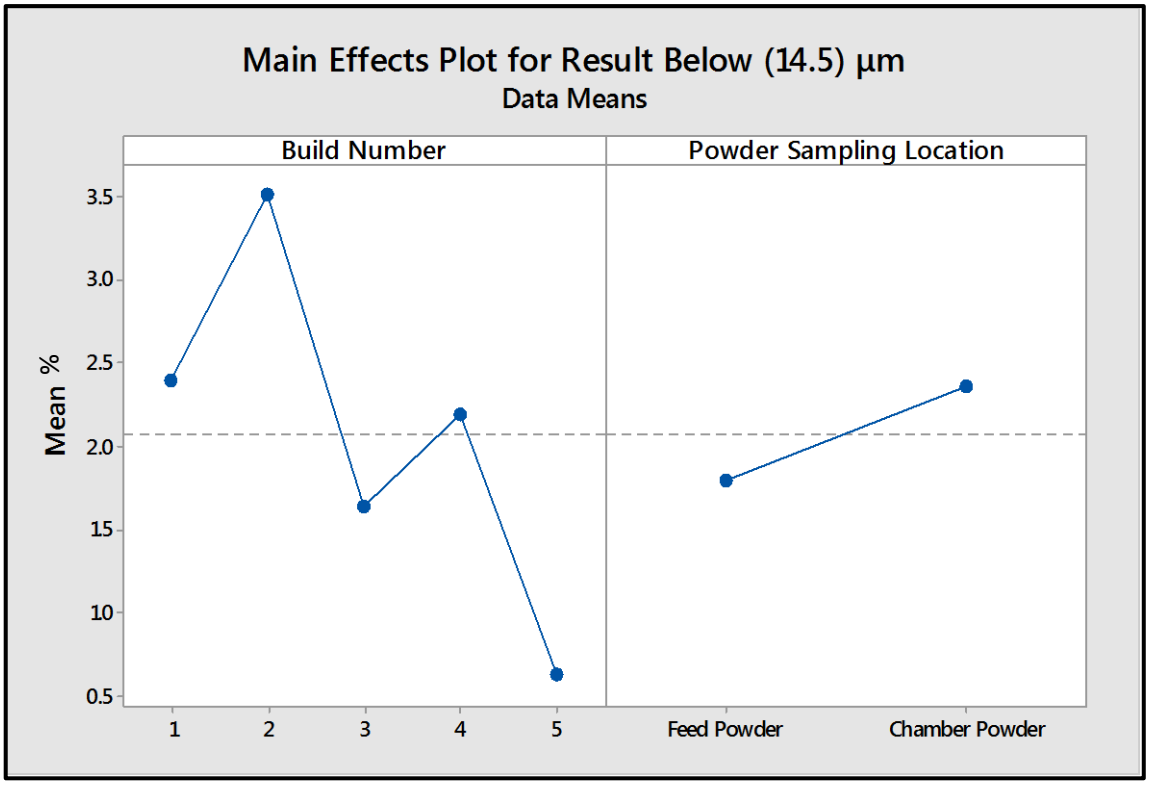

Figure 19 - Main Effects Plot for Results Below 14.5 µm

Table 7 - Analysis of Variance for Results in Range 14.5 - 45.6 µm

Source	DF	Adj SS	Adj MS	F-Value	P-Value
Model	9	328.009	36.4455	40.47	0.000
Linear	5	78.594	15.7189	17.45	0.000
Build Number	4	75.199	18.7998	20.87	0.000
Powder Sampling Location	1	3.395	3.3953	3.77	0.059
2-Way Interactions	4	249.415	62.3537	69.23	0.000
Build Number*Powder Sampling Location	4	249.415	62.3537	69.23	0.000
Error	40	36.026	0.9006		
Total	49	364.035			

Model Summary

S	R-sq	R-sq(adj)	R-sq(pred)
0.949026	90.10%	87.88%	84.54%

Table 7 shows the ANOVA table produced for Results in Range 14.5 – 45.6 µm and Figure 88 shows the residual plots produced. The S value was shown to be acceptable, again suggesting that there was a low standard difference of data points from the fitted value shown by the regression line (0.949 %). R^2 and Adjusted R^2 were lower than those for the previous measured variables ANOVA, and were calculated as being 90.10 % and 87.77 % respectively. These values were again indicative of an accurate model, capable of explaining the majority of the data points, providing the author with confidence in the model produced.

When considering the effect on Results in Range 14.5 – 45.6 µm, only Build Number was shown to have an effect. A p-value of 0.000, coupled with an F-value ratio value of 20.87 suggested that there was some statistical evidence of varying Build Number on Results in Range 14.5 – 45.6 µm. In this case, Powder Sample Location was not found to have a statistically significant effect on the measured variable. A p-value of 0.059 (p-value > α level of 0.05) and a F-Value ratio value of 3.77 (close to 1) suggested that there was not statistical evidence of varying Powder Sampling Location on Results in Range 14.5 – 45.6 µm and that the difference in mean percentage of results in range could be attributed to random error. The Main Effects Plot if shown in Figure 20 and shows a trend towards a reduction in the proportion of the powder samples being within the desired range of 15 – 45 µm.

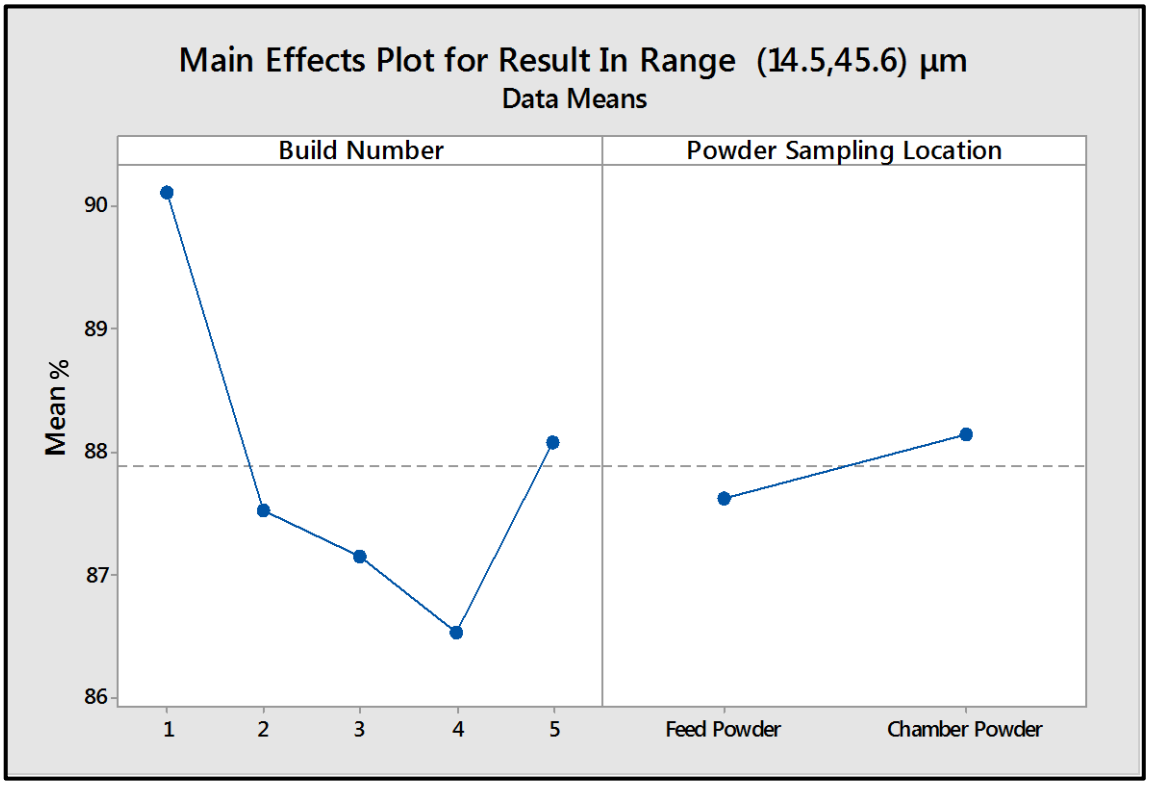

Figure 20 - Main Effects Plot for Results in Range 14.5 - 45.6 µm

Table 8 - Analysis of Variance for Results Above 45.6 µm

Source	DF	Adj SS	Adj MS	F-Value	P-Value
Model	13	81.6671	6.2821	132.89	0.000
Blocks	4	0.1894	0.0474	1.00	0.419
Linear	5	56.2708	11.2542	238.06	0.000
Build Number	4	49.2738	12.3184	260.58	0.000
Powder Sampling Location	1	6.9970	6.9970	148.01	0.000
2-Way Interactions	4	25.2069	6.3017	133.30	0.000
Build Number*Powder Sampling Location	4	25.2069	6.3017	133.30	0.000
Error	36	1.7019	0.0473		
Total	49	83.3690			

Model Summary

S	R-sq	R-sq(adj)	R-sq(pred)
0.217425	97.96%	97.22%	96.06%

Table 8 shows the ANOVA table produced for full analysis of Results Above 45.65 µm and Figure 89 shows the residual plots produced. The S value was shown to be extremely low, again suggesting that there was a low standard difference of data points from the fitted value shown by the regression line (0.217 %). Additionally, R^2 and Adjusted R^2 were calculated as being 97.96 % and 97.22 % respectively. These values were again indicative of a highly accurate model, capable of explaining the majority of the data points, providing the author with confidence in the model produced.

When considering the effect of both Build Number and Powder Sampling Location, both were shown to have an effect on the value of Results Above 45.65 µm within the samples analysed. Build Number was again show to have the strongest effect on Results Above 45.65 µm. A p-value of 0.000, coupled with a F-value ratio value of 260.58 suggested that there was strong statistical evidence of varying Build Number on Results Above 45.65 µm. A p-value of 0.000 for Powder Sampling Location, coupled with a F-Value ratio value of 148.01 suggested that there was statistical evidence of varying Powder Sampling Location on Results Above 45.65 µm.

The Main Effects Plot shown in Figure 21 shows a trend towards an increase in the proportion of the powder samples being made up of large particles through repeated recycling of the powders (Moving from Build 1 to Build 5). For this measured variable, the Chamber Powder sample again showed a lower proportion of particles above 45.6 µm in diameter than the Feed Powder sample.

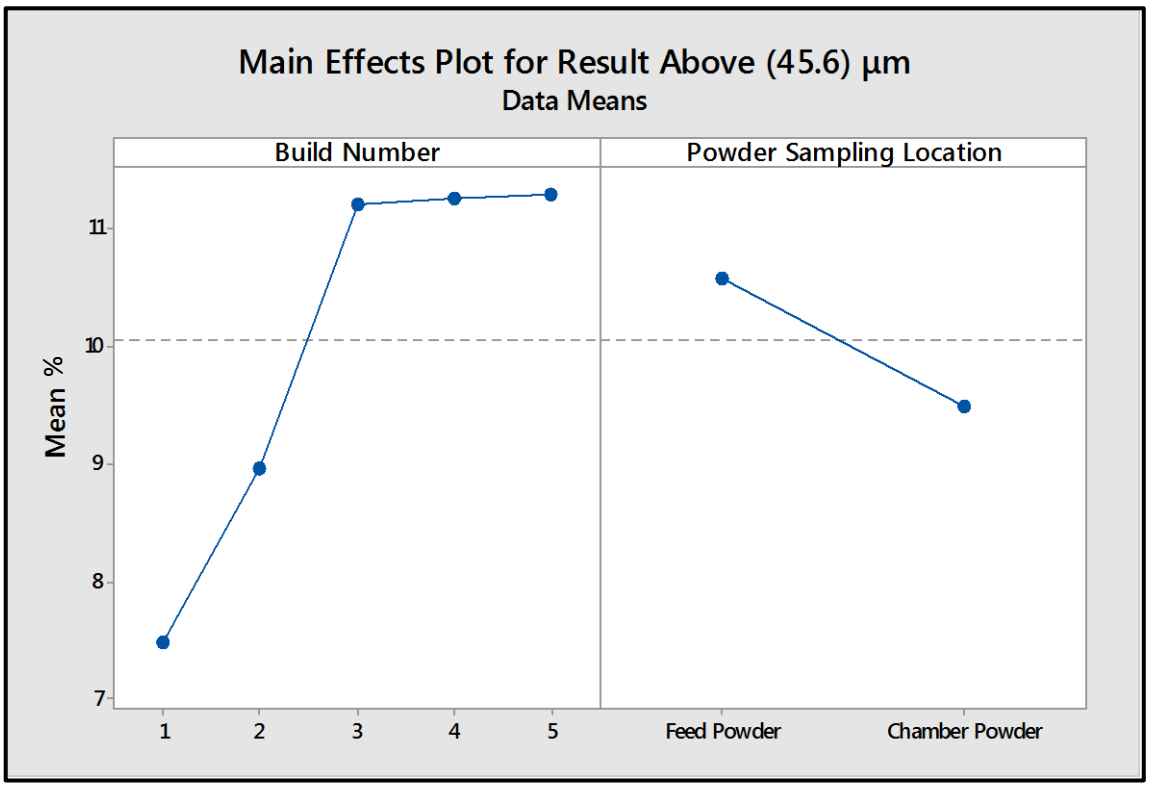

Figure 21 - Main Effects Plot for Results Above 45.6 µm

Next, the powder samples collected using the PCB's were considered and compared with the results from Chamber and Feed Powder samples with Main Effects Plots for Dx(10), Dx(50) and Dx(90) shown in Figure 22, Figure 23 and Figure 24. When considering the results of Dx(10) measured from powder samples contained within the PCB, it was obvious that there was a significant difference in the number of smaller particles contained within the population when compared with the samples taken from within the chamber and feed powder samples, leading to higher values of Dx(10) being displayed. The effect of sampling powder from the three sized boxes was also apparent and clearly displayed in Figure 22. As the size of the PCB chamber decreased, Dx(10) increased. This was also apparent for both Dx(50) and Dx(90).

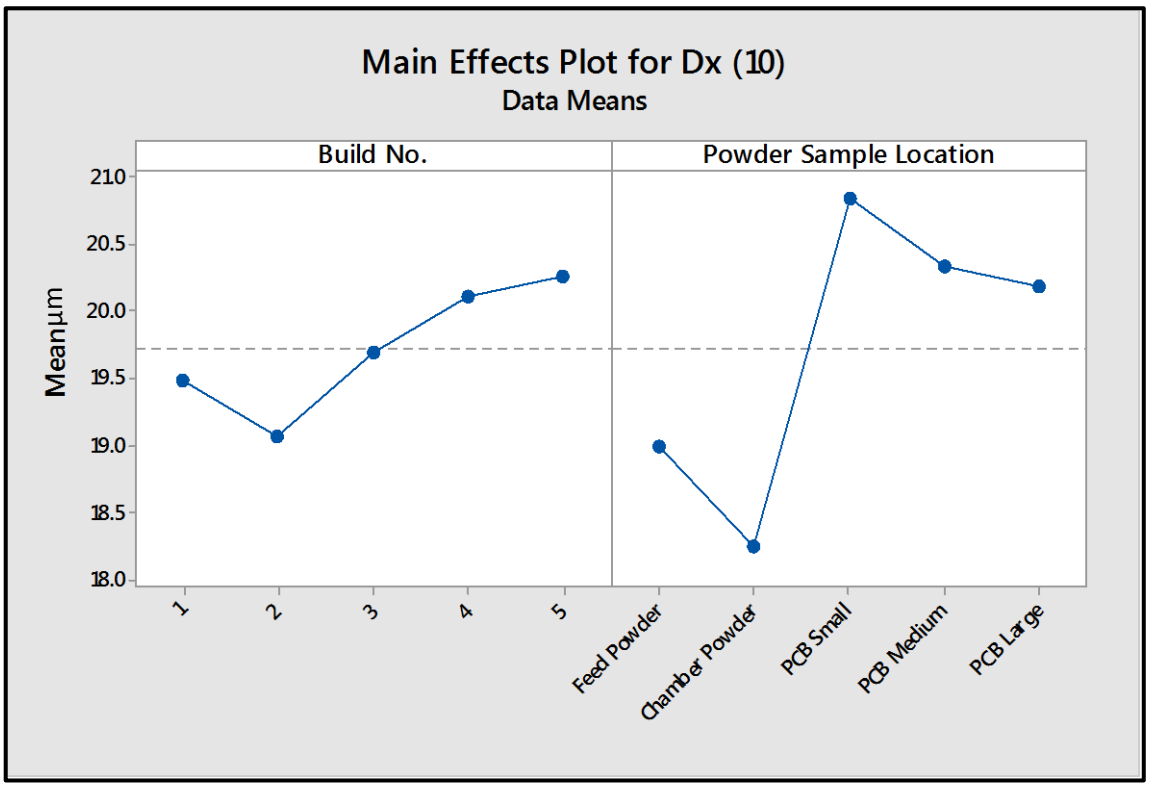

Figure 22 - Main Effects Plot for Dx(10) Including PCB Results

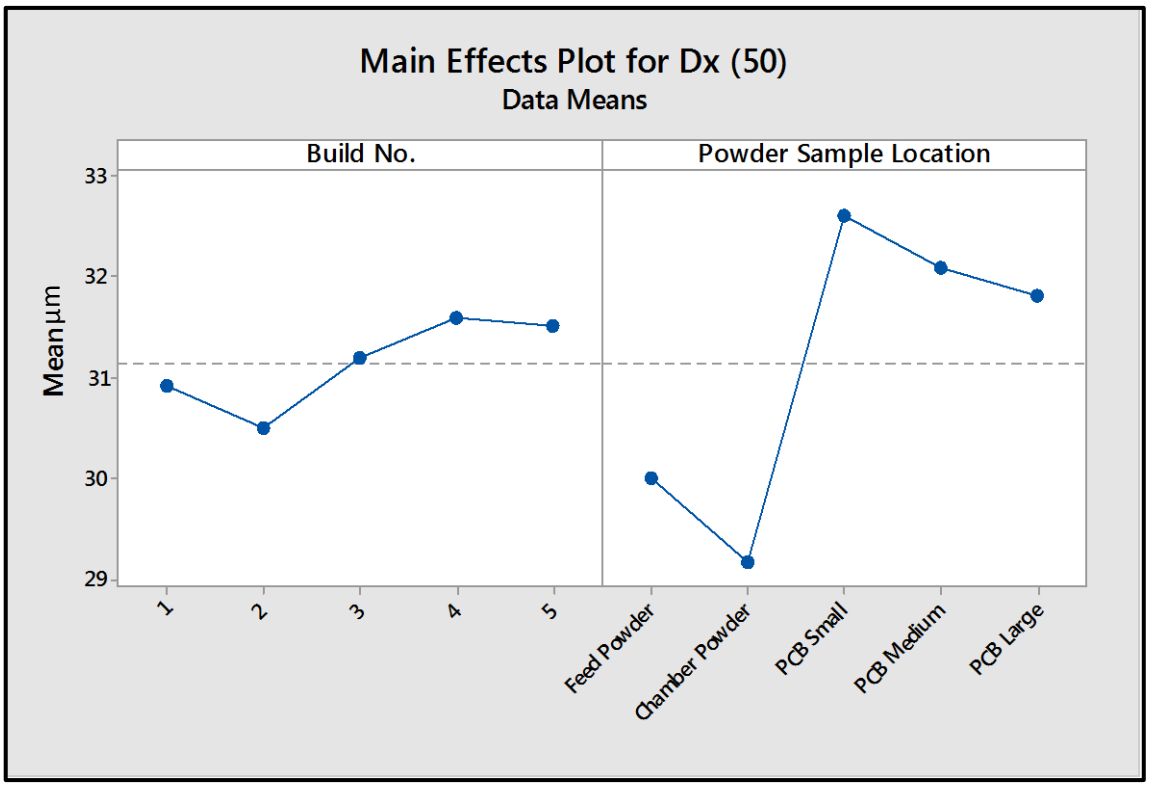

Figure 23 - Main Effects Plot for Dx(50) Including PCB Results

This may be explained by the proximity of the powder samples to the site of laser melting. Powder samples from the small box would have been in close proximity to the walls of the box, and hence laser melting. Powder samples from the large box would not have been in such close proximity to the

walls, and hence laser melting. Powder particles in close proximity to the site of laser melting may experience partial sintering, fusing several particles together. Smaller particles would be expected to require less energy input for melting, thus resulting in a larger number of smaller particles being fused together. This would result in a decrease in the number of small particles, and an increase in the number of larger particles.

This would lead to a smaller angle of light scattering in laser diffraction and an increase in the particle size measured. Values of Dx(10), Dx(50) and Dx(90) increased for all samples analysed and was attributed to a reduction in the number of small particles, coupled with an increase in the number of large particles. It was apparent at this stage that the powder samples collected within the PCB's varied significantly from both those collected within the chamber and after sieving. Samples collected from within the PCB's were thus considered to be unrepresentative for assessment of powder population post-test.

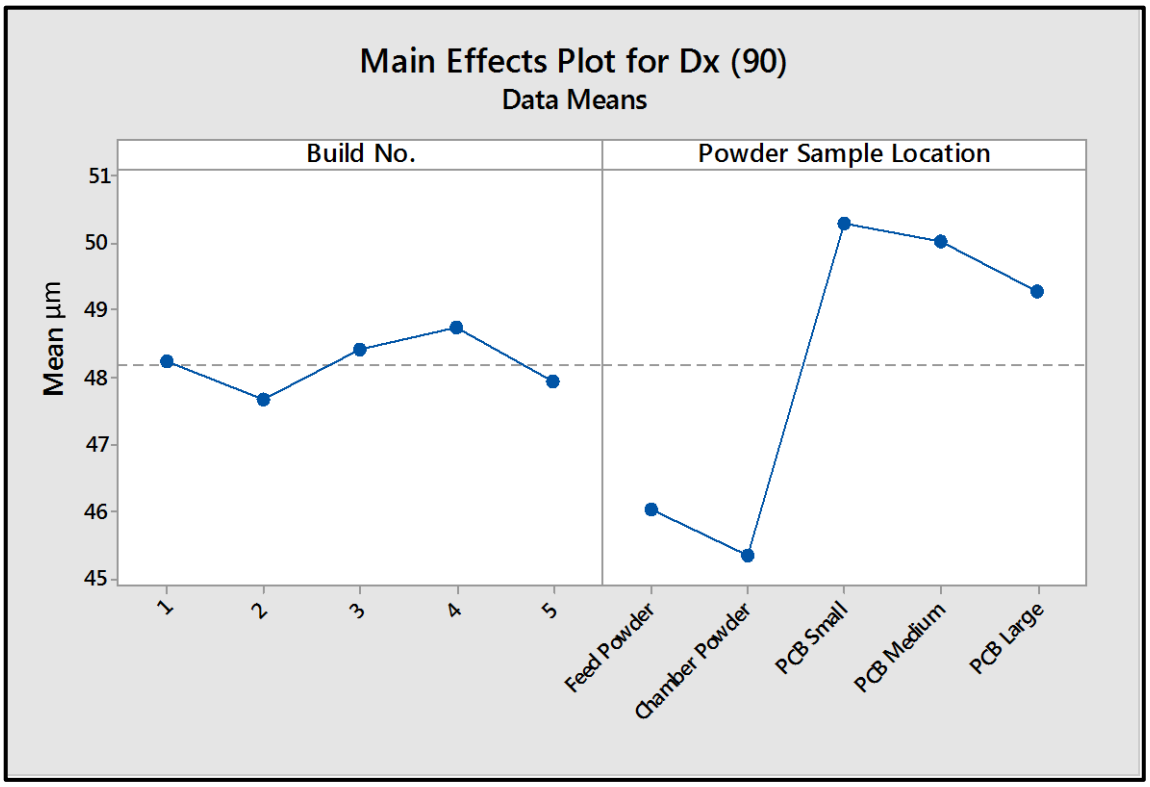

Figure 24 - Main Effects Plot for Dx(90) Including PCB Results

3.5. Powder Morphology

Knowledge of the way in which powders change in terms of their morphology was considered to be another useful piece of information in the characterisation of Ti-6Al-4V powders. As such, Scanning Electron Microscopy was performed. This analysis was also used to confirm the results of particle size obtained through laser diffraction. All powder samples analysed were viewed under SEM in three locations, with some of the key learnings described within this section.

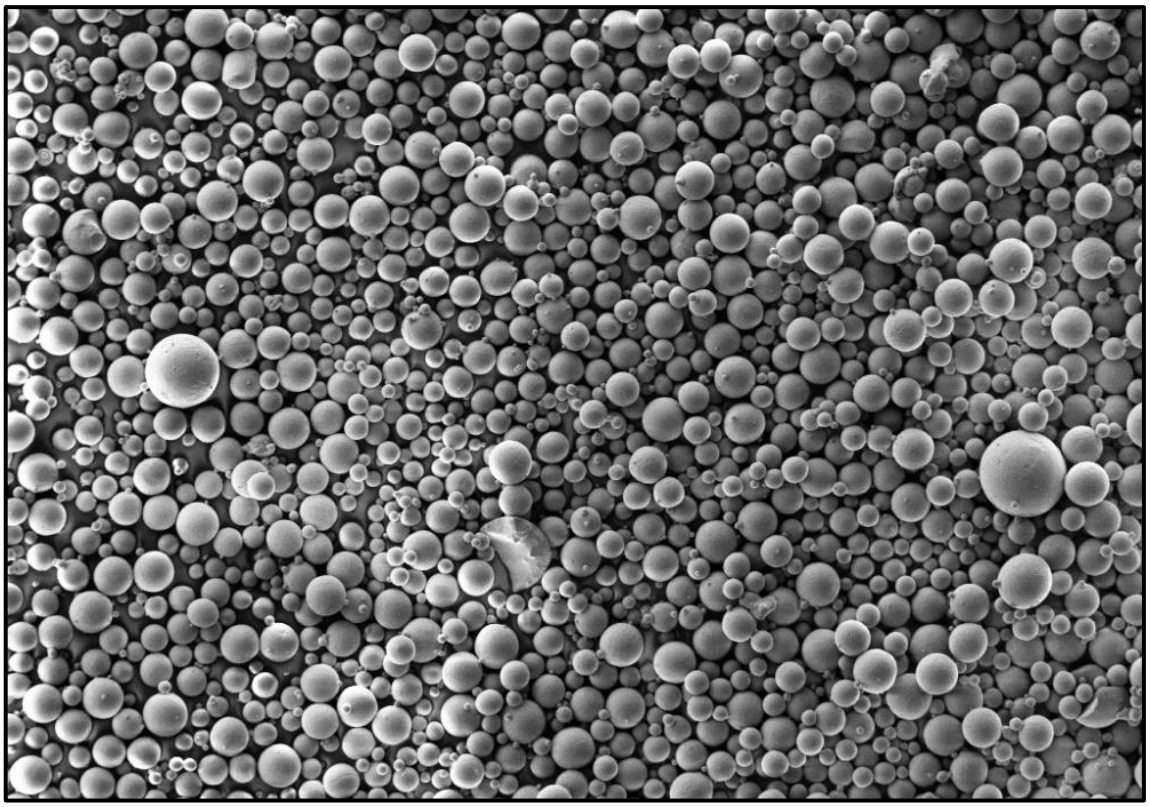

Figure 25 - Feed Stock Powder Sample at X189 Magnification

Feed Stock powder particles showed a high level of sphericity as shown in Figure 25 and Figure 26. This was consistent for the three locations viewed under SEM. When viewing the samples at X1090 magnification, checks on the particle size were performed using both point to point measurements and a circle tool. The high level of sphericity made it easy to draw the circles around the powder particles. The vast majority of the powder particles checked for diameter were within the ranges determined by PSD analysis, confirming the measurements taken. This was the same for all samples analysed.

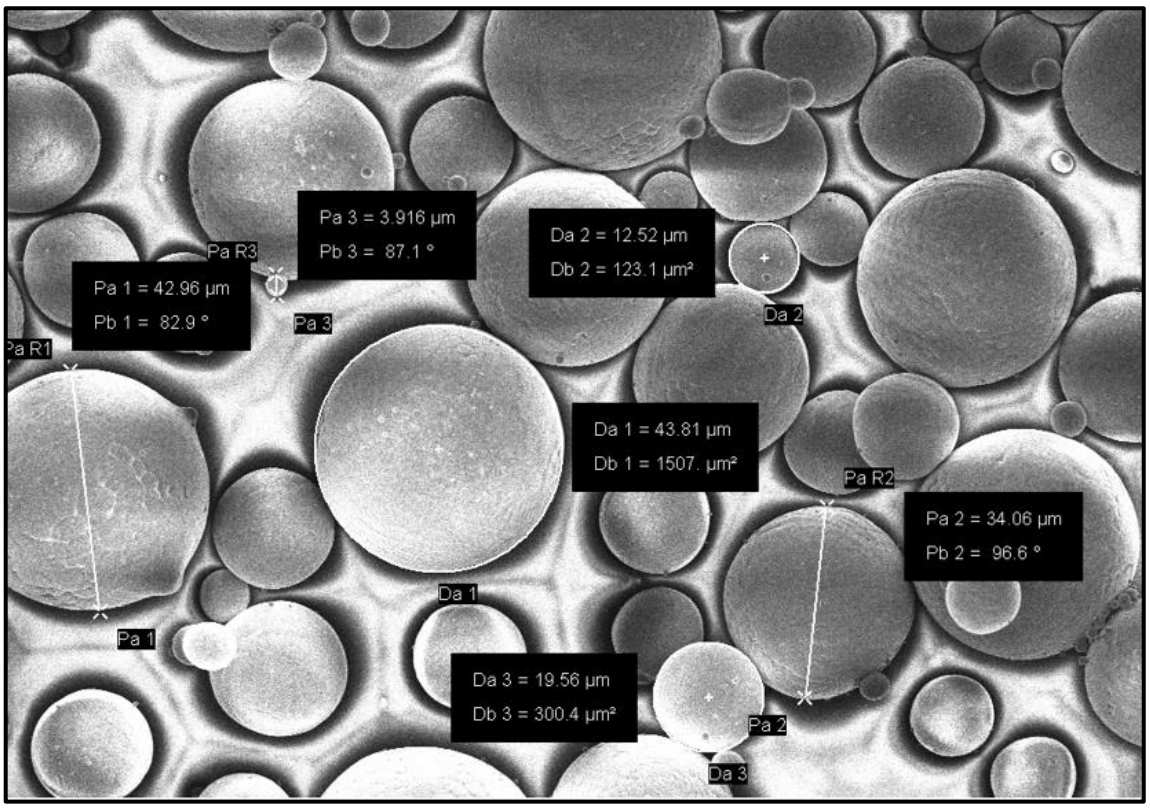

Figure 26 - Feed Stock Powder Sample at X1090 Magnification

Consistently, the presence of satellite particles attached to normally sized particles was observed and shown in Figure 27. In all cases analysed in detail, where satellite particles were observed, there was the presence of extreme fine and nano scale particles attached in the joins. These extreme fine micro and nano scale particles, were not observed at any other point within the samples analysed.

Feed Stock powder, and normally sized particles within all samples exhibited a mixture of coarse acicular martensitic alpha and large equiaxed structures, with a relatively smooth surface which is shown in Figure 28. Consistently within the samples analysed, there was the presence of larger particles that were outside the intended range of particle size. These particles were up to 110 µm in diameter and are shown in Figure 28 and Figure 29.

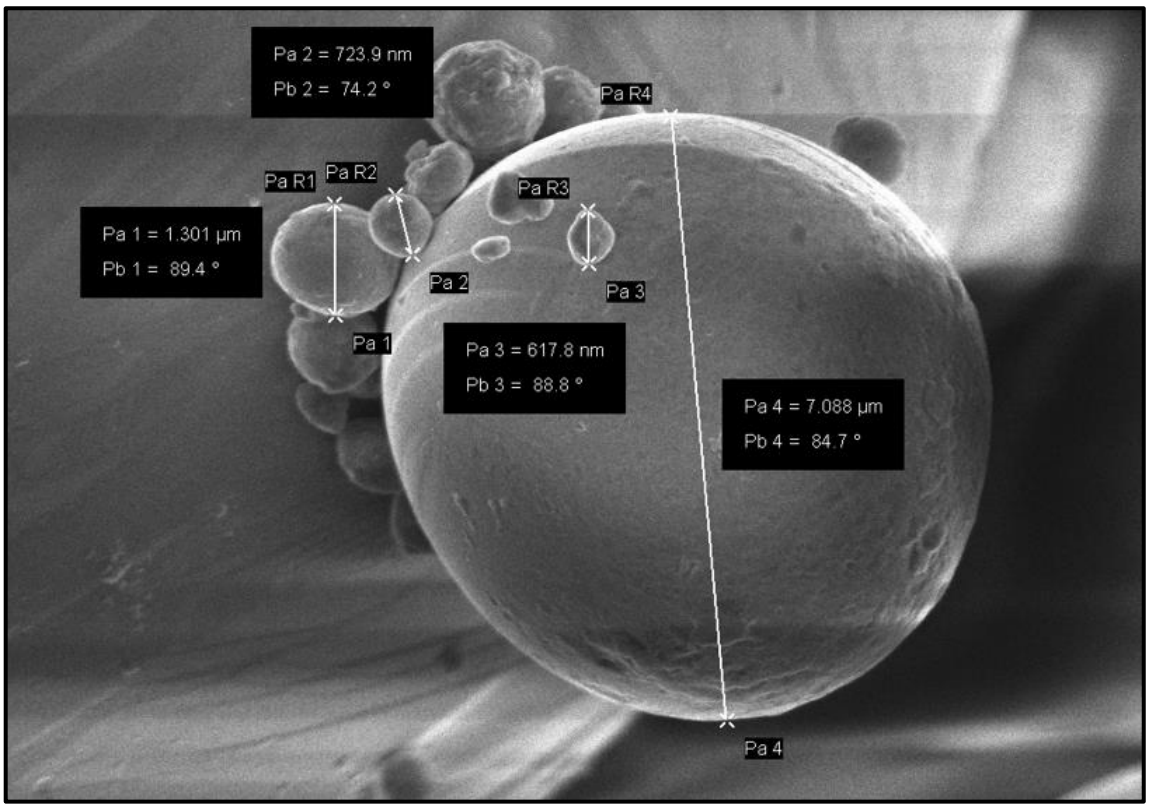

Figure 27 - Satellite Powder Particles from Feed Stock Sample at X16040 Magnification

Figure 29 shows a particle collected from the fourth build within the chamber, meaning that the powder had been sieved three times previously. The large particles consistently exhibited an extremely fine acicular martensitic alpha structure, suggesting extremely rapid cooling from the beta domain of the phase diagram. The high level of sphericity of these particles ruled out partial sintering during the SLM process, which is shown in Figure 31. Such large particles were also observed within the Feed Stock powder samples, meaning that they resulted from improper sieving of the manufacturers powder following their plasma atomization production process. These particles, however, did not exhibit the same extremely fine acicular martensitic alpha structure and instead exhibited the same structure as normally sized particles.

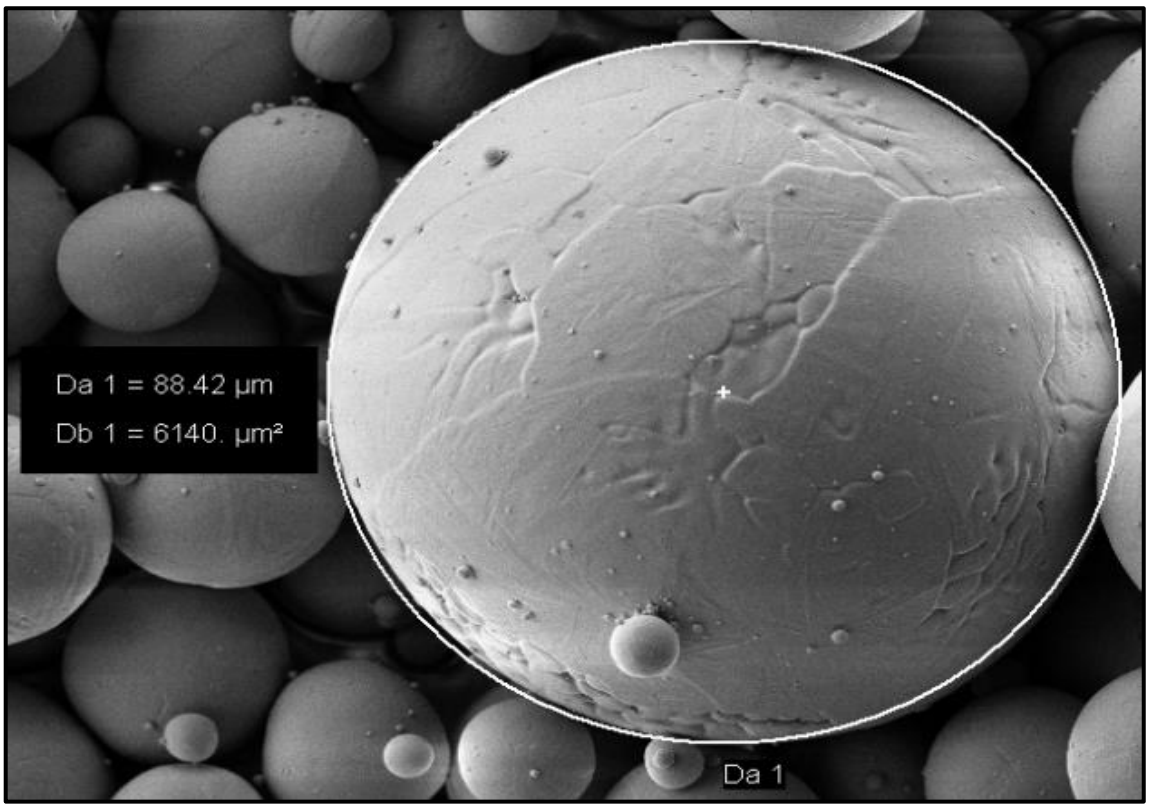

Figure 28 - Large Powder Particle from Feed Stock Sample at X1070 Magnification

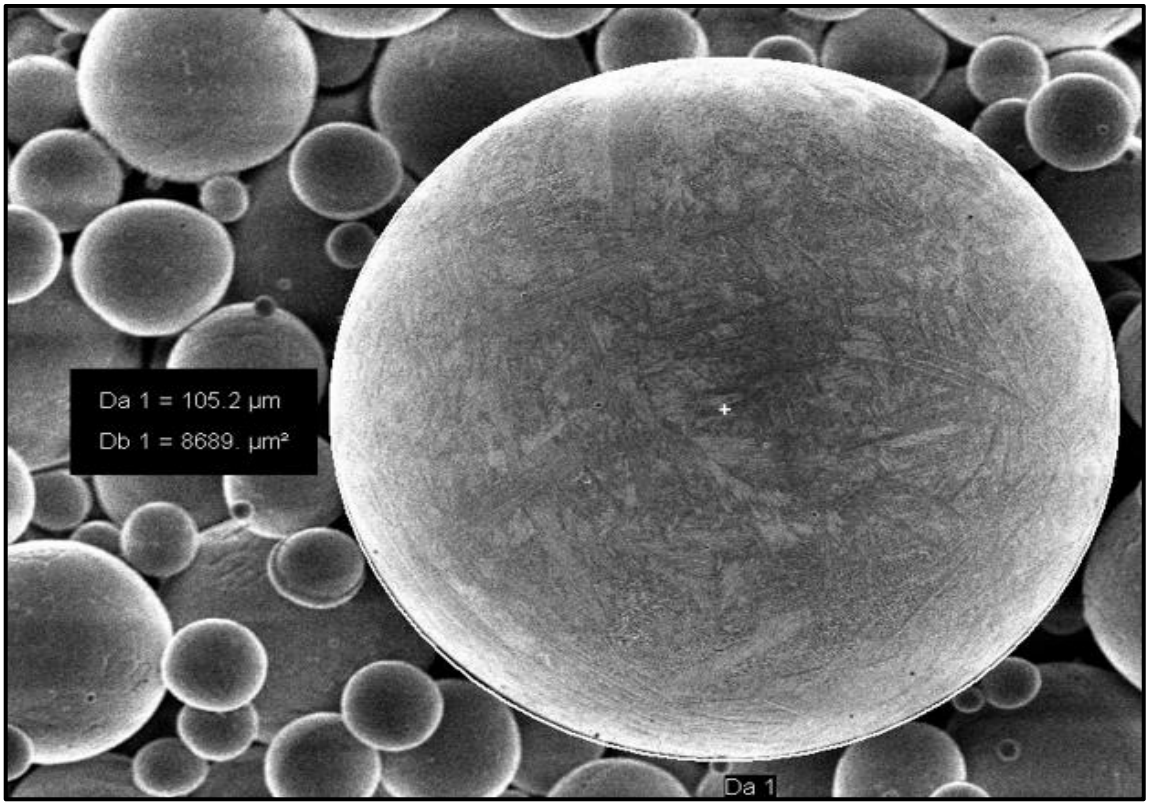

Figure 29 – Large Powder Particle from Build 4 Chamber Sample at X1070 Magnification

Figure 30 - Large Powder Particle from Build 4 Chamber Sample Showing Surface Microstructure at X5500 Magnification

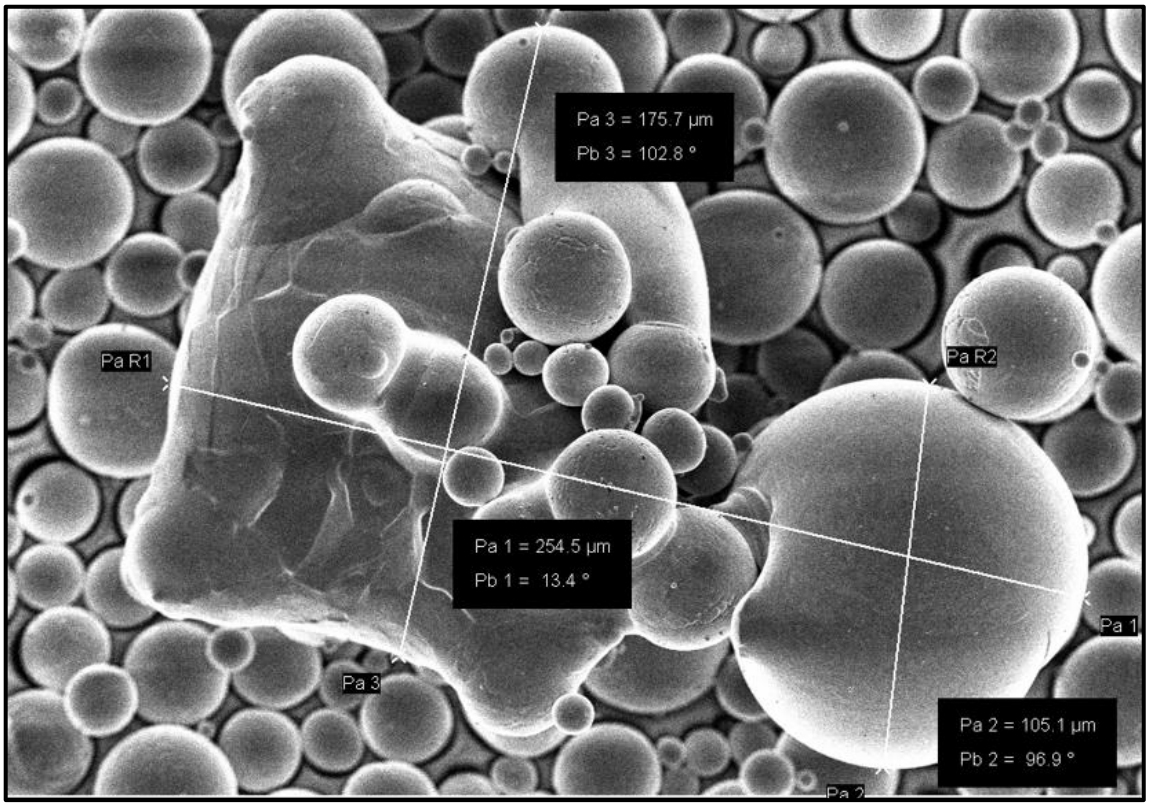

Figure 31 - Partially Sintered Powder from Build 3 Chamber Sample at X699 Magnification

The sieving process which the powder was subjected to involved the use of a 63 µm mesh size. This should have eliminated the presence of larger particles greater than 63 µm in diameter, but did not.

The sieving process used then was not considered to be satisfactory in the active removal of particles outside of the intended size range and methods of improvement should be sought as a continuation of this work.

3.6. Chemical Composition Analysis

Standard specifications for Ti-6Al-4V detail limits of acceptable chemical composition of the material. ASTM F3001-14 and ASTM F2924-14 are the respective standard specifications for Grade 23 (ELI) & Grade 5 for Additive Manufacturing Titanium-6 Aluminum-4 Vanadium with Powder Bed Fusion. The limits of chemical composition, along with tolerances are shown in Table 9.

Table 9 - Chemical Requirements of ASTM F3001-14 & ASTM F2924-14

Element	ASTM F3001-13	ASTM F2924-14	Tolerance Under the Minimum or Over the Maximum Limit % (mass/mass)
	Composition, % (mass/mass)	Composition, % (mass/mass)	
Nitrogen, max	0.05	0.05	0.02
Carbon, max	0.08	0.08	0.02
Hydrogen, max	0.012	0.015	0.002
Iron, max	0.25	0.3	0.1
Oxygen, max	0.13	0.2	0.02
Aluminium	5.5 – 6.5	5.5 – 6.75	0.4
Vanadium	3.5 – 4.5	3.5 – 4.5	0.15
Yttrium, max	N/A	0.005	0.0006
Titanium	balance	balance	N/A

The chemical requirements detailed within Table 9 show that grade 23 possesses a more tightly controlled chemical composition, when compared with grade 5. Grade 23 is referred to as the ELI version, meaning that it possesses lower percentage by mass of the interstitial element oxygen. The Feed Stock powder supplied for this experimentation was of the ELI grade.

An understanding of the way in which the chemical composition of the powders used within the SLM process varied over time and through repeat recycling was considered to be an essential requirement for a thorough understanding of the process as a whole. As such, chemical composition testing was performed on powders sampled at various stages of recycling, as described within Section 3.1 of this report. All Feed Powder samples were tested for chemical composition. Chemical composition testing

focused on determination of the percentage mass of both oxygen and nitrogen contained within each sample analysed. These two interstitial elements were believed to be the most problematic for the mechanical performance of produced parts when containing excessive amounts of interstitial elements.

The ASTM standards F3001-14 & F2924-14 both call for the same chemical composition test methodology. For determination of both oxygen and nitrogen within titanium alloys, the following standard test is required: ASTM E1409-13 - Test Method for Determination of Oxygen and Nitrogen in Titanium and Titanium Alloys by Inert Gas Fusion. The results of chemical composition testing are shown in Table 10 and Figure 32.

Table 10 - Chemical Composition of Powder Results

Sample	Oxygen, %mass	Within acceptable limit? 0.13 %	Nitrogen, %mass	Within acceptable limit? 0.05 %
Feed Stock	0.131	No > 0.13 %	0.014	Yes < 0.05 %
Build 1	0.113	Yes < 0.13 %	0.014	Yes < 0.05 %
Build 2	0.120	Yes < 0.13 %	0.015	Yes < 0.05 %
Build 3	0.129	Yes < 0.13 %	0.017	Yes < 0.05 %
Build 4	0.124	Yes < 0.13 %	0.013	Yes < 0.05 %
Build 5	0.141	No >0.13 %	0.018	Yes < 0.05 %

Comparison of the results obtained for each of the powder samples shows some fluctuation in the percentage mass of both oxygen and nitrogen within the samples. It should be noted that the Feed Stock powder supplied initially contained 0.131% oxygen. This was just outside the allowable limit of the nominal maximum chemical requirement for oxygen and likely to cause an issue when considering the chemical composition of laser melted parts. Titanium in its molten state has an extremely high affinity for both oxygen and nitrogen. The presence of either of these elements within the build chamber, could result in an increase in the chemical composition of laser melted parts, through reaction between molten material and residual interstitial gasses.

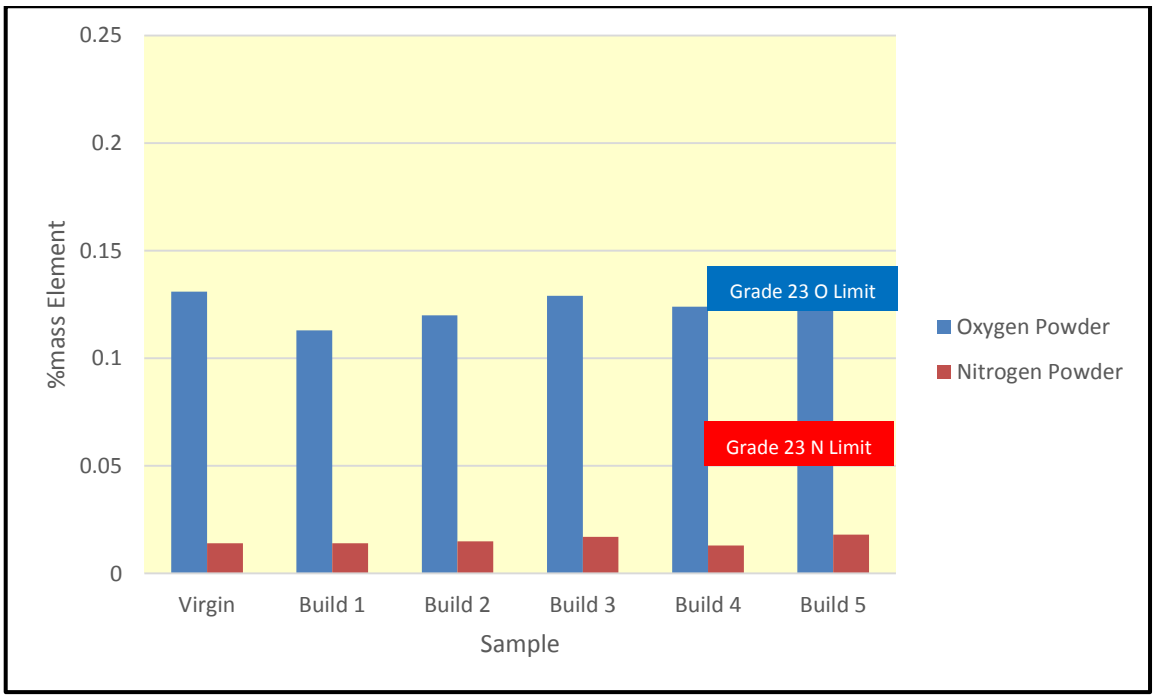

Figure 32 – Graph Showing Results of Determination of %Mass of Oxygen and Nitrogen in Titanium and Titanium Alloys by Inert Gas Fusion for Powder Samples.

There was little change observed in the percentage mass of both oxygen and nitrogen within the powders as they were recycled. Ti-6Al-4V powders have been shown to possess a stable oxide film on their outermost surface comprised of a mixture of TiO_2 and Al_2O_3 (Axelsson 2012). With the presence of such a film, it was likely that additional oxidation of the powders was prevented.

4.0. Mechanical Characterisation of Laser Melted Parts: Results and Discussion

Upon completion of the powder characterisation work, and identification of the effect of recycling the powder up to five times had on the composition of the powder, there was a requirement to understand the effects that changes in powder quality and composition had on the mechanical, chemical and metallurgical properties of laser melted parts. This section of the report details the steps taken to identify these changes.

A series of test pieces were designed to be able to address each of the properties of laser melted parts required. These are shown in Figure 33 and are as follows:

1. Tensile test specimens.
2. Fatigue test specimens.
3. Rotating bend test specimens.
4. Pyramids for evaluation of porosity and microstructure.
5. Chemical test cubes.
6. Powder collection box (powder characterisation section).

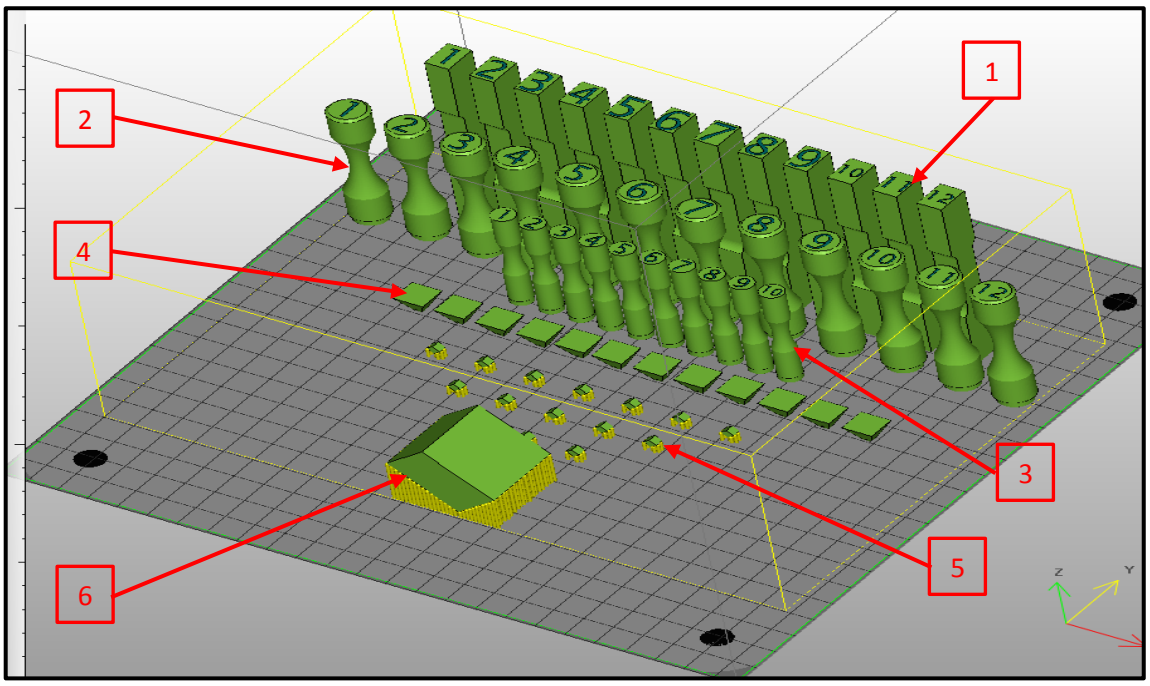

Figure 33 - Test Build showing all Test Pieces

Each build was completed using the laser parameters described within Table 11 at a layer thickness of 40 µm. Following the completion of each build, the build plate was removed from the SLM machine and all of the parts were separated from the build plate. Six of both the pyramids and chemical test cubes were separated for analysis, along with the powder collection box. The rest of the parts were subjected to a heat treatment cycle within a vacuum furnace as described below.

Table 11 - Laser Process Parameters used for SLM

	Volume border	Volume area	Supports
Power (W)	200	200	170
Point Distance (µm)	50	70	60
Exposure time (µs)	35	65	50
Scan strategy	-	Meander hatch	-

- Vacuum on. 1 hour ramp to 350 °C.
- Hold at 350 °C for 0.5 hours.
- 1 hour ramp to 850 °C.
- Hold at 850 °C for 1 hour.
- Furnace cool to 100 °C.

A vacuum furnace was used for the heat treatment process to try to mitigate the effect of interstitial element absorption during heat treatment. The removal of six of the chemical test cubes prior to heat treatment was for the investigation of such interstitial absorption. Heat treatment was required to reduce residual stresses resulting from the SLM process and to produce an acceptable level of ductility (Donachie 2000). The heat treatment opted for was annealing in the α + β region of the Ti-6Al-4V phase diagram shown in Figure 34.

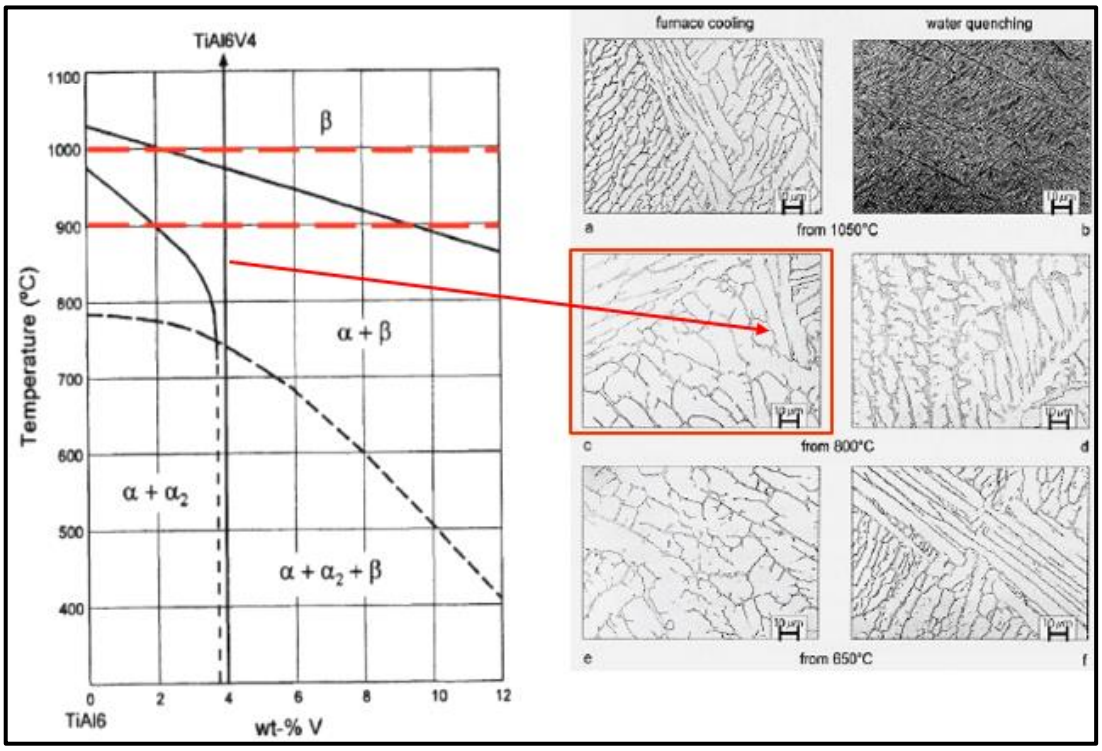

Figure 34 - Microstructures Possible for Several Heat Treatment Methods for Ti-6Al-4V, Reproduced from Donachie (2000).

4.1. Tensile Testing

One of the aims of this project was to be able to determine whether the parts produced would be capable of meeting the requirements specified by standards governing the use of Ti-6Al-4V for surgical implantation applications. The requirements in terms of mechanical performance for the ELI grade of Ti-6Al-4V are detailed within ASTM F136-13: Standard Specification for Wrought Titanium-6Aluminum-4Vanadium ELI Alloy for Surgical Implant Applications, and are detailed within Table 12.

Table 12 - Annealed Mechanical Properties of Bar, Wire, and Forgings, Reproduced from ASTM F136 (2013).

Nominal Diameter or Distance Between Parallel Sides, in. (mm)	Tensile Strength min, psi (MPa)	Yield Strength (0.2 % offset) min, psi (MPa)	Elongation[A] in 4D or 4W min, %		
			L	LT	ST
			—	—	—
Under 0.187 (4.75) thickness or diameter	125 000 (860)	115 000 (795)	10	...	...
0.187 (4.75) to under 1.75 (44.45), incl	125 000 (860)	115 000 (795)	10	...	...
1.75 (44.45) to under 2.50 (63.50), incl	120 000 (825)	110 000 (760)	8	...	...
2.50 (63.50) to 4.00 (101.60), incl	120 000 (825)	110 000 (760)	8	8[C]	8[C]

ASTM F136 requires that tensile tests be performed in accordance with ASTM E8/E8M-15a: Standard Test Methods for Tension Testing of Metallic Materials. ASTM E8/E8M details acceptable designs for tensile test pieces and so the tensile test pieces built as part of this testing were designed to match required dimensions for a sub-size specimen, as shown in Figure 35. In order to achieve the required dimensional accuracy, and a good surface finish, the parts were built over sized by 1 mm in all directions and then machined to size.

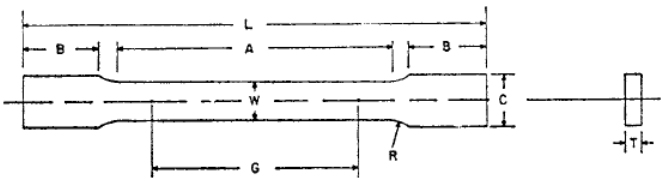

	Dimensions		
	Standard Specimens		Subsize Specimen
	Plate-Type, 40 mm [1.500 in.] Wide	Sheet-Type, 12.5 mm [0.500 in.] Wide	6 mm [0.250 in.] Wide
	mm [in.]	mm [in.]	mm [in.]
G—Gage length (Note 1 and Note 2)	200.0 ± 0.2 [8.00 ± 0.01]	50.0 ± 0.1 [2.000 ± 0.005]	25.0 ± 0.1 [1.000 ± 0.003]
W—Width (Note 3 and Note 4)	40.0 ± 2.0 [1.500 ± 0.125, -0.250]	12.5 ± 0.2 [0.500 ± 0.010]	6.0 ± 0.1 [0.250 ± 0.005]
T—Thickness (Note 5)		thickness of material	
R—Radius of fillet, min (Note 6)	25 [1]	12.5 [0.500]	6 [0.250]
L—Overall length, min (Note 2, Note 7, and Note 8)	450 [18]	200 [8]	100 [4]
A—Length of reduced section, min	225 [9]	57 [2.25]	32 [1.25]
B—Length of grip section, min (Note 9)	75 [3]	50 [2]	30 [1.25]
C—Width of grip section, approximate (Note 4 and Note 9)	50 [2]	20 [0.750]	10 [0.375]

Figure 35 - Dimensions Required for Subsize Tensile Specimen, Reproduced from ASTM E8/E8M (2015).

The machine used for testing was a Zwick Z100 materials testing machine with extensometer attached. Initial attempts to run a strain controlled test proved unsuccessful and so a stress controlled test was run instead. The extensometer remained attached to the specimen until 2 percentage elongation was attained, before removal of the extensometer. At this stage, displacement measurement was switched and linked to the crosshead displacement.

With the smooth surface attained through machining of the samples, the machine grips could not hold onto the samples, resulting in slip of the sample within the grip. Several methods were attempted to

overcome this problem until a solution was found. All samples required a roughening of the surface on the grip sections through grit blasting. An example of a prepared sample is shown in Figure 36.

Figure 36 - Image of Machined Tensile Test Specimen.

With 60 samples tested, there was simply too much numerical data to display within this report and so excel files are provided within the memory stick provided with this dissertation.

ANOVA was again used in order to assess the effect of powder condition on the mechanical performance of laser melted parts. General Factorial Regression analysis was performed in the same manner as for powder characterisation analysis.

The process factors to be investigated within this study were:

- Build Number at 5 levels (Build 1, 2, 3, 4 and 5).
- Build Position at 12 levels (1, 2, 3, 4, 5, 6, 7, 8, 9, 10, 11, 12). Build position relates to the numbering of parts as shown in Figure 33.

The measured responses on which the effect of the process factors were acting were:

- Ultimate tensile strength
- Yield strength (0.2% offset)
- Elongation

All stress strain and force elongation graphs for each specimen testes are contained within the CD provided with this report.

Table 13 - Analysis of Variance for Ultimate Tensile Strength

Analysis of Variance

Source	DF	Seq SS	Contribution	Adj SS	Adj MS	F-Value	P-Value
Model	15	75141	88.84%	75141	5009.4	21.77	0.000
Linear	15	75141	88.84%	75141	5009.4	21.77	0.000
Build No.	4	1432	1.69%	1488	372.0	1.62	0.188
Build Position	11	73709	87.15%	73709	6700.8	29.12	0.000
Error	41	9435	11.16%	9435	230.1		
Total	56	84576	100.00%				

Model Summary

S	R-sq	R-sq(adj)	PRESS	R-sq(pred)
15.1696	88.84%	84.76%	18149.3	78.54%

Table 13 shows the ANOVA table produced for full analysis of UTS and Figure 37 shows the residual plots produced. The S value was shown to be 15.2 MPa, meaning that the standard difference of data points from the fitted value shown by the regression line were not too high. Additionally, R^2 and Adjusted R^2 were calculated as being 88.84 % and 84.76 % respectively. These values showed that the model created was capable of explaining the vast majority of the data points.

When considering the effect of Build Number on UTS, a P-value of 0.188 coupled with a F-Value of 1.62 was indicative of no statistical evidence of varying the level of Build Number on UTS. This meant that even though the condition of the powder had been shown to vary from build to build, the effect on UTS for each build was not significant. Build Position was shown to have a significant effect on UTS of the samples tested. A P-value of 0.000, coupled with a F-value of 29.12 showed that there was strong evidence of the effect of varying the build position on UTS. Additionally, 88.76 % of the contribution to variability was attributed to Build Position.

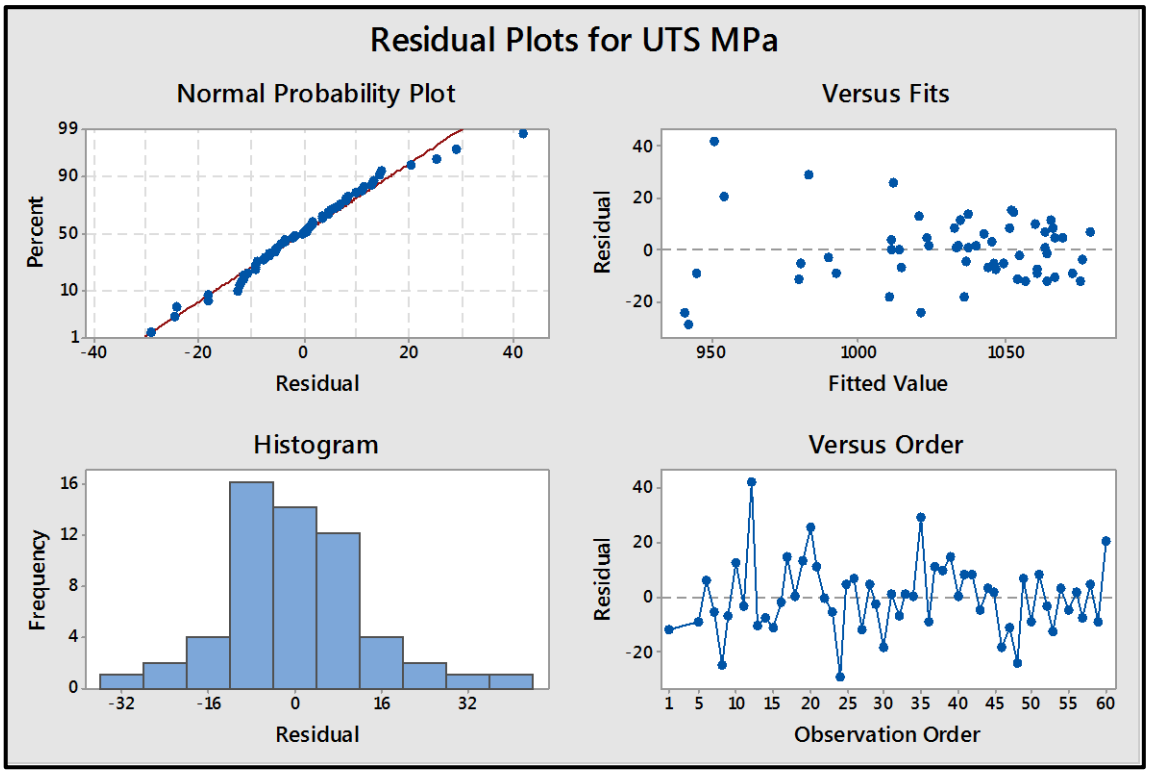

Figure 37 - Residual Plots for UTS

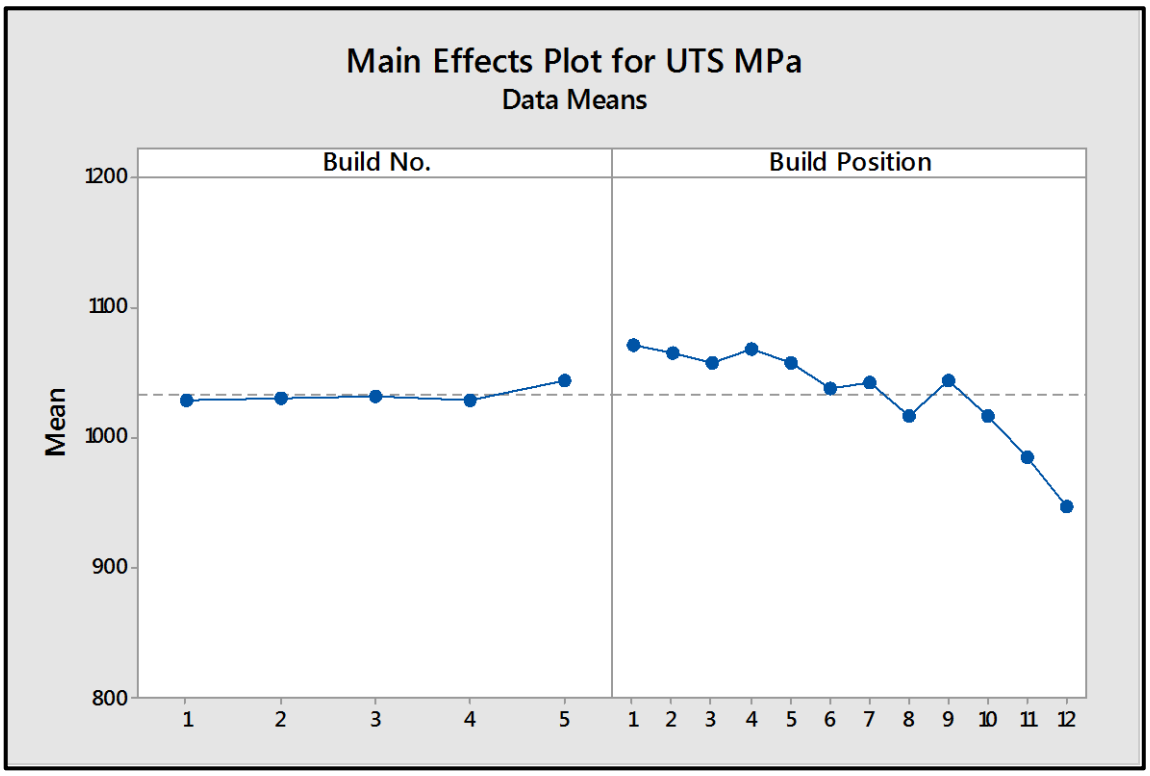

Figure 38 - Main Effects Plot for UTS

The effect of varying build position was significant for the effect on measured UTS during tensile testing. Figure 38 shows the Main Effects Plot for UTS, in which it is clear to see that the data means for build position decrease significantly when moving from position 1 to position 12. The data means for build number do not vary significantly when moving from build 1 to build 5 which again emphasised the lack of effect of varying powder characteristics on UTS. Figure 39 shows the contour plot of UTS for both build number and build position. This plot again shows the lack of variation between build number, and the variation in build position. Figure 40 shows the result for UTS of each of the samples analysed for both build position and build number.

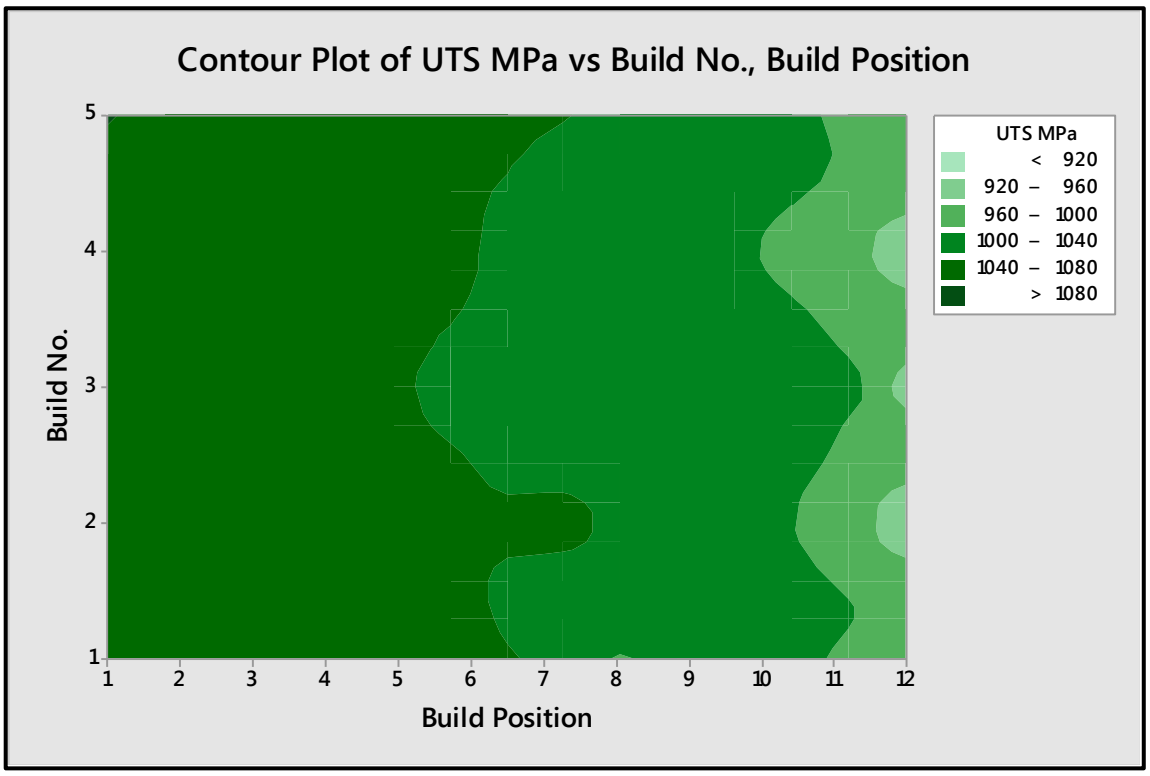

Figure 39 - Contour Plot for UTS

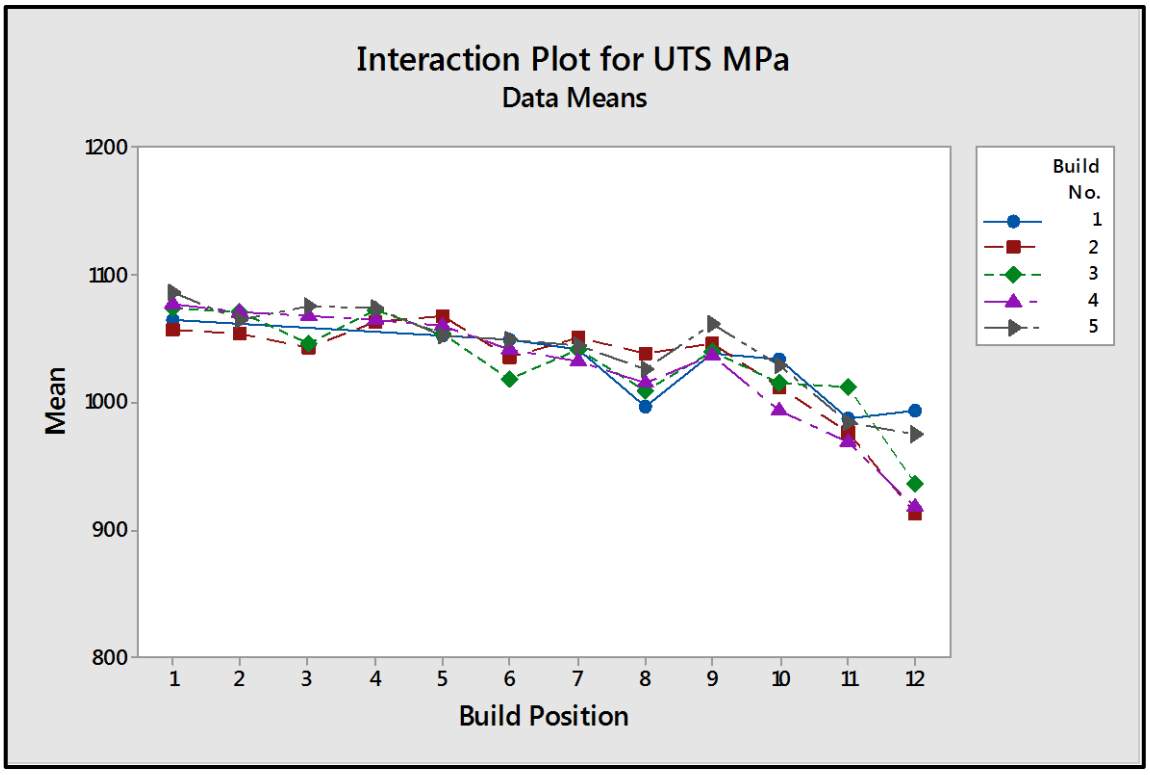

Figure 40 - Interaction Plot for UTS

Table 14 - Analysis of Variance for Yield Strength

Analysis of Variance

Source	DF	Seq SS	Contribution	Adj SS	Adj MS	F-Value	P-Value
Model	15	19085	80.58%	19085	1272.3	11.34	0.000
Linear	15	19085	80.58%	19085	1272.3	11.34	0.000
Build No.	4	1719	7.26%	1609	402.2	3.59	0.013
Build Position	11	17366	73.33%	17366	1578.7	14.08	0.000
Error	41	4598	19.42%	4598	112.2		
Total	56	23683	100.00%				

Model Summary

S	R-sq	R-sq(adj)	PRESS	R-sq(pred)
10.5903	80.58%	73.48%	8990.96	62.04%

Table 14 shows the ANOVA table produced for full analysis of Yield Strength and Figure 41 shows the residual plots produced. The S value was shown to be 10.6 MPa, meaning that the standard difference of data points from the fitted value shown by the regression line was relatively low. Additionally, R^2 and Adjusted R^2 were calculated as being 80.58 % and 73.48 % respectively. These values showed that the model created was capable of explaining the majority of the data points.

When considering the effect of Build Number on Yield Strength, a P-value of 0.013 coupled with an F-Value of 3.59 was indicative of some statistical evidence of varying the level of Build Number on the Yield Strength. The percentage contribution to variability of build position was 7.26 %. Build Position was again shown to have a significant effect on Yield Strength of the samples tested. A P-value of 0.0, coupled with a F-value of 11.34 showed that there was evidence of the effect of varying the build position on Yield Strength. Additionally, 73.33 % of the contribution to variability was attributed to Build Position.

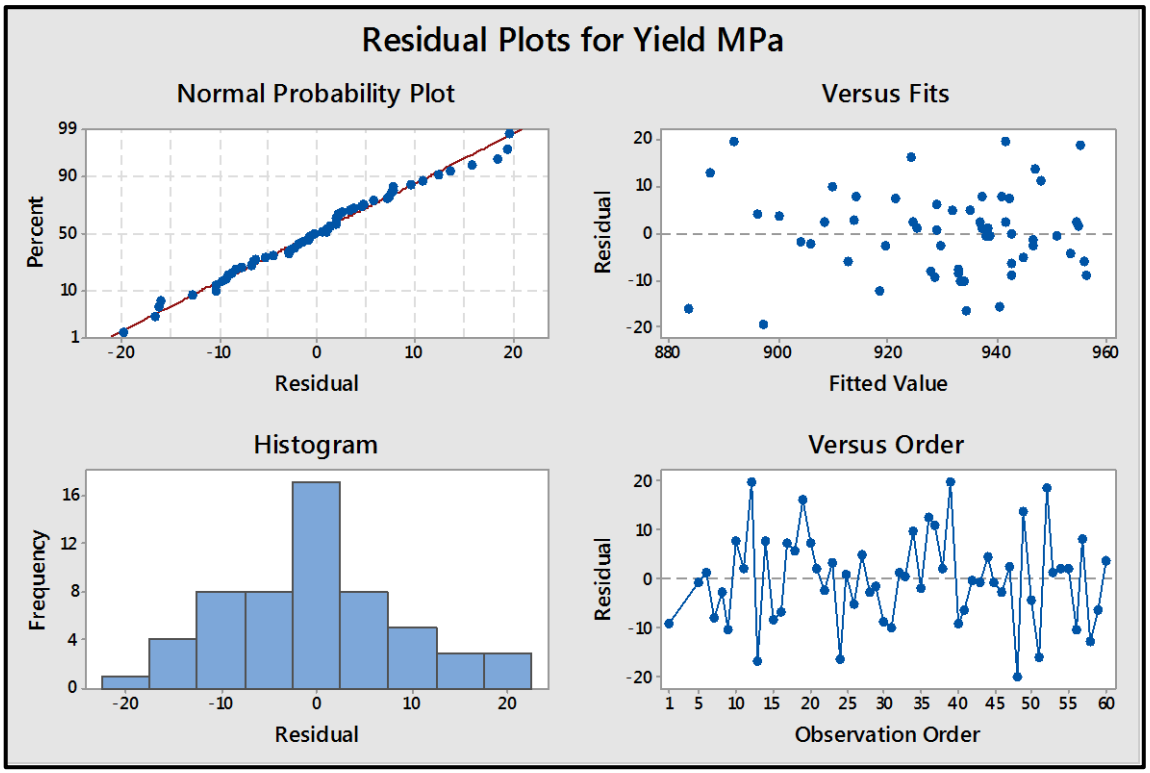

Figure 41 - Residual Plots for Yield Strength

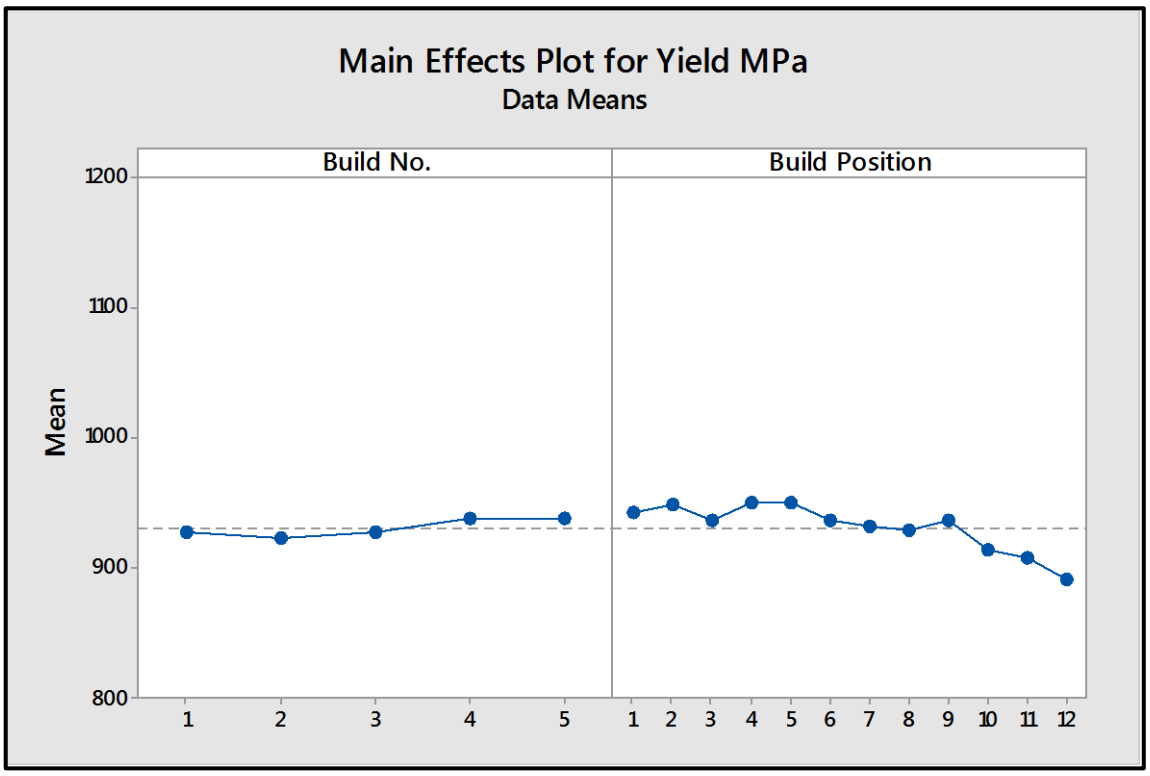

Figure 42 - Main Effects Plot for Yield Strength

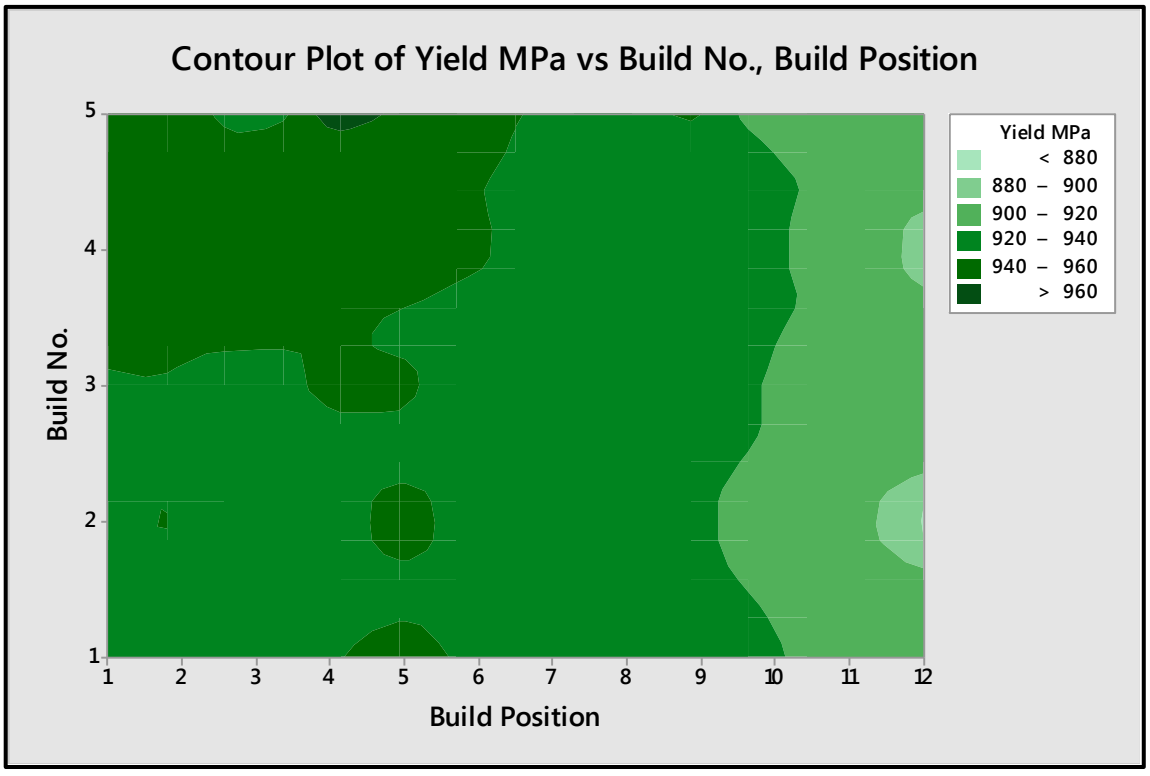

Figure 43 - Contour Plot for Yield Strength

The effect of varying build position was significant for the effect on measured Yield Strength during tensile testing. Figure 42 shows the Main Effects Plot for Yield Strength, in which it is clear to see that the data means for build position decrease when moving from position 1 to position 12. The data

means for build number do not appear to vary significantly when moving from build 1 to build 5, however consideration of the tightness of grouping of results shown in Figure 44 would explain the significant p-value output. Figure 43 shows the contour plot for Yield Strength for both build number and build position. This plot again shows the variation in Yield Strength when moving along build position, and additionally shows the difference in Yield Strength when moving between builds. Figure 44shows the result for Yield Strength of each of the samples analysed for both build position and build number.

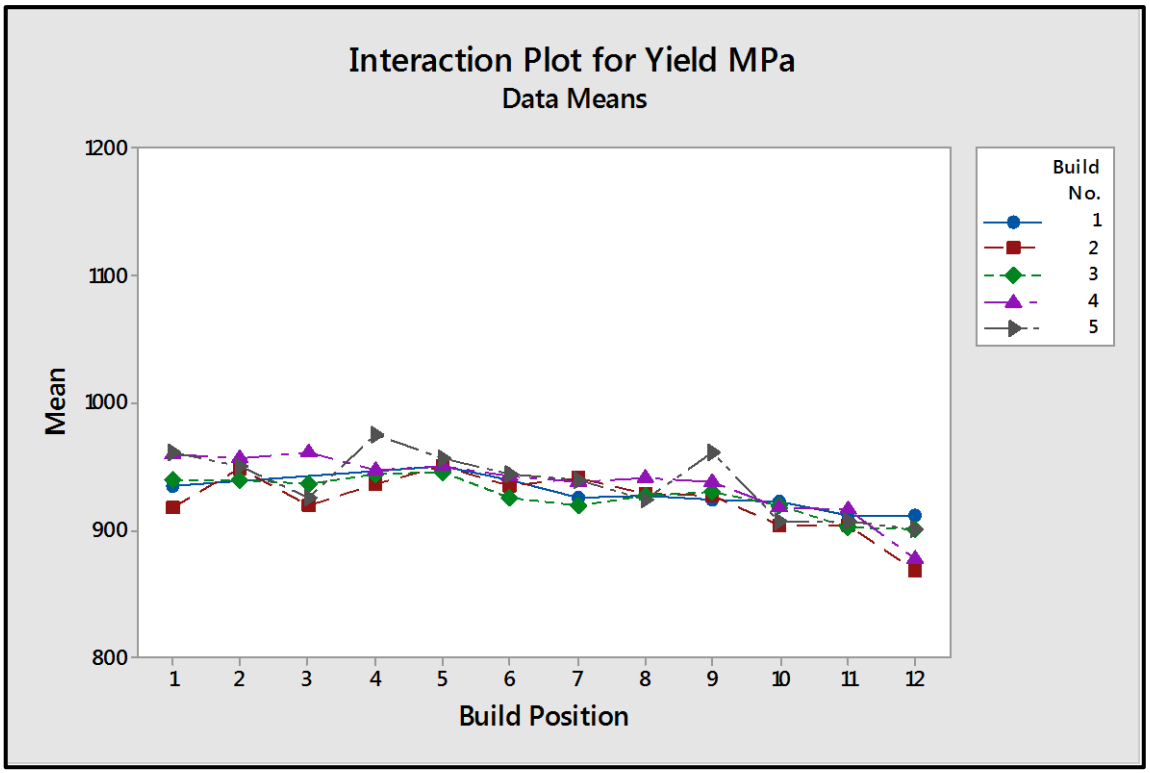

Figure 44 - Interaction Plot for Yield Strength

Table 15 - Analysis of Variance for Elongation

Analysis of Variance

Source	DF	Seq SS	Contribution	Adj SS	Adj MS	F-Value	P-Value
Model	15	235.321	82.88%	235.321	15.688	13.24	0.000
Linear	15	235.321	82.88%	235.321	15.688	13.24	0.000
Build No.	4	7.201	2.54%	5.076	1.269	1.07	0.383
Build Position	11	228.120	80.35%	228.120	20.738	17.50	0.000
Error	41	48.593	17.12%	48.593	1.185		
Total	56	283.914	100.00%				

Model Summary

S	R-sq	R-sq(adj)	PRESS	R-sq(pred)
1.08867	82.88%	76.62%	97.9416	65.50%

Table 15 shows the ANOVA table produced for full analysis of UTS and Figure 45 shows the residual plots produced. The S value was shown to be 1.1 %, meaning that the standard difference of data points from the fitted value shown by the regression line was not low, owing to several relatively large residuals as shown in the residual plots. R^2 and Adjusted R^2 were calculated as being 82.88 % and 76.62 % respectively. These values showed that the model created was capable of explaining the majority of the data points.

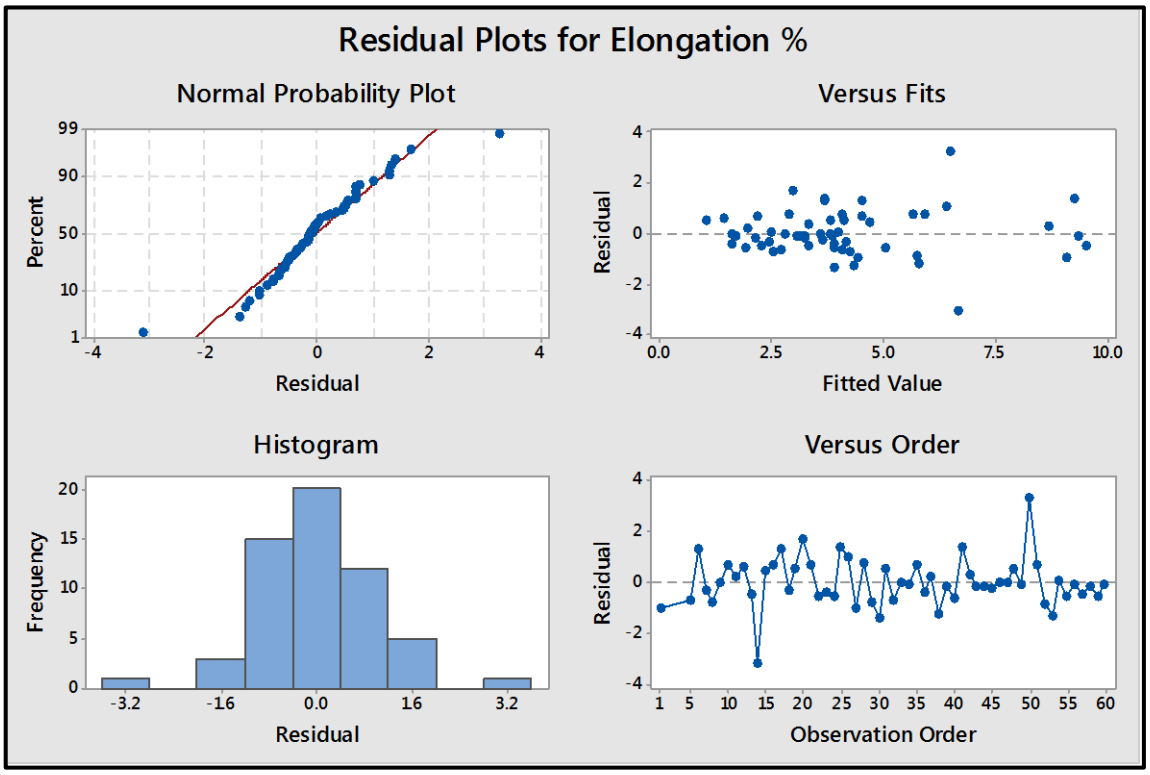

Figure 45 - Residual Plots for Elongation

When considering the effect of Build Number on Elongation, a P-value of 0.383 coupled with a F-Value of 1.07 was indicative of no statistical evidence of varying the level of Build Number on Elongation. Again, this meant that even though the condition of the powder had been shown to vary from build to build, the effect on Elongation for each build was not significant. Build Position was shown to have a significant effect on Elongation of the samples tested. A P-value of 0.0, coupled with a F-value of 13.24 showed that there was strong evidence of the effect of varying the build position on Elongation. Additionally, 80.35 % of the contribution to variability was attributed to Build Position.

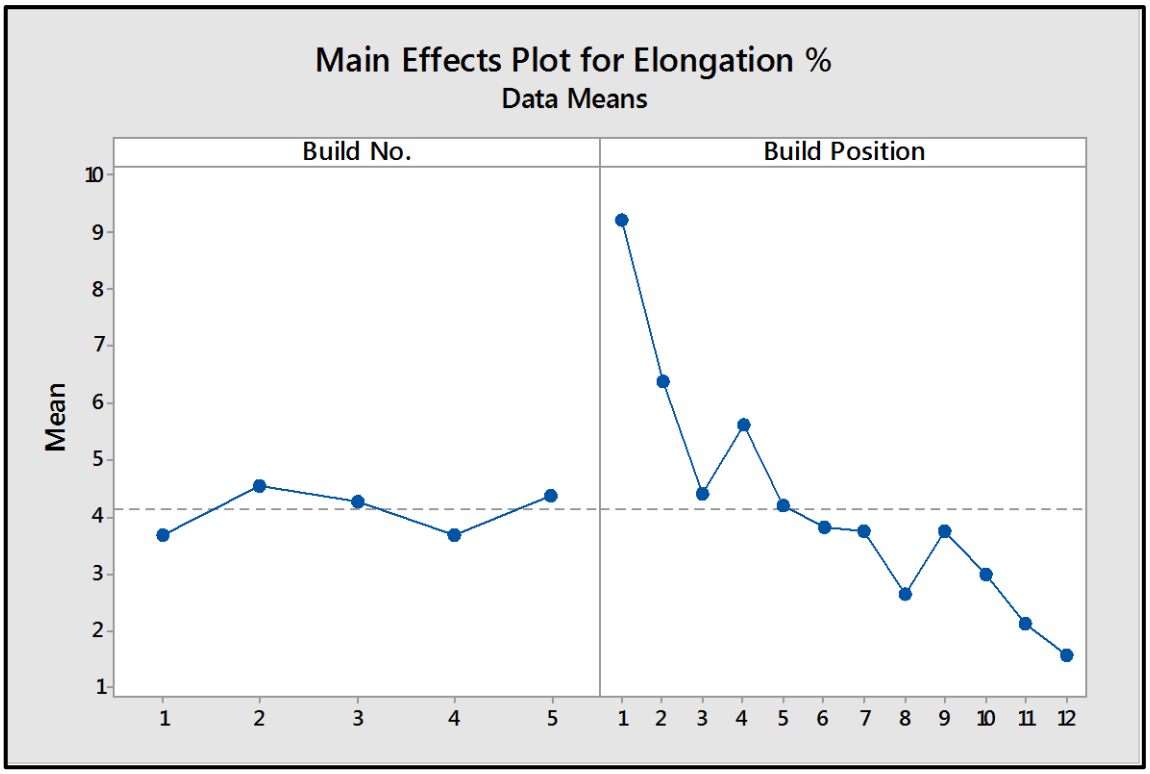

Figure 46 - Main Effects Plot for Elongation

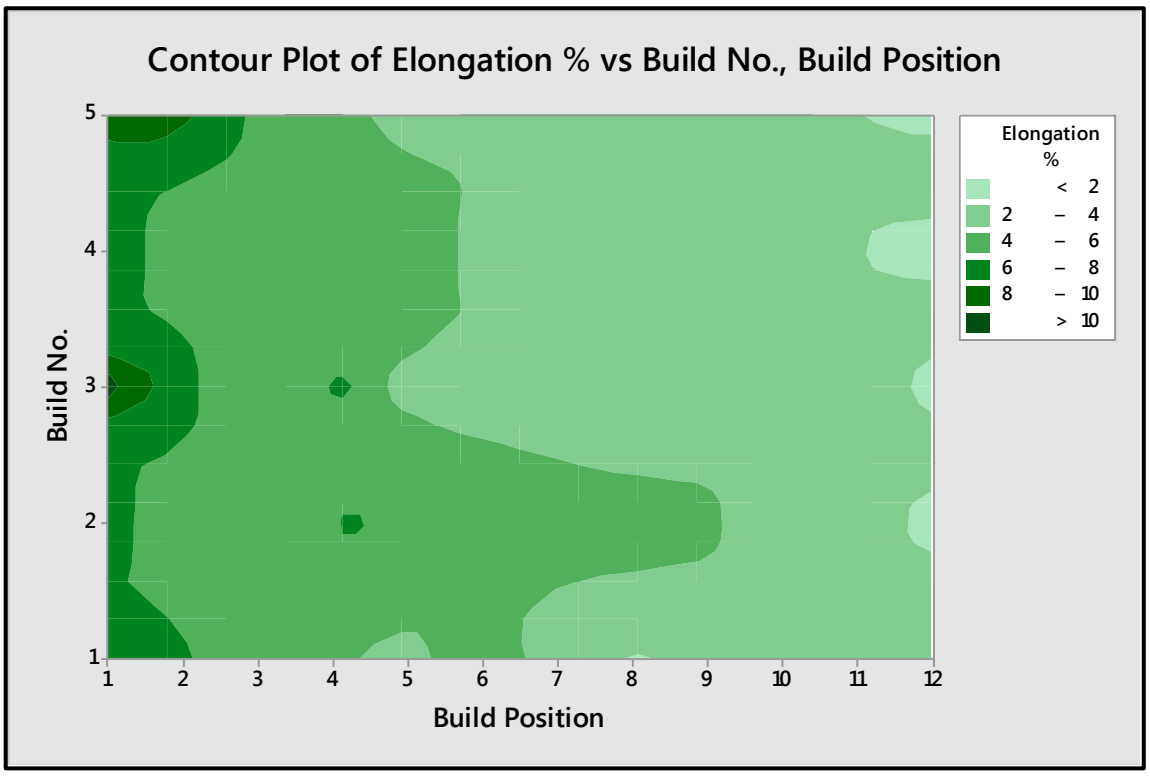

Figure 47 - Contour Plot for Elongation

The effect of varying build position was significant for the effect on measured Elongation during tensile testing. Figure 46 shows the Main Effects Plot for Elongation, in which it is clear to see that the data means for build position decrease drastically when moving from position 1 to position 12. The average result of elongation for position 1 was 9.205 % and the average result for position 12 was 1.563. The data means for build number do not vary significantly when moving from build 1 to build 5 which again emphasised the lack of effect of varying powder characteristics on Elongation. Figure 47 shows the contour plot of Elongation for both build number and build position. This plot again shows the lack of variation between build number, and the variation in build position. Figure 48 shows the result for Elongation of each of the samples analysed for both build position and build number.

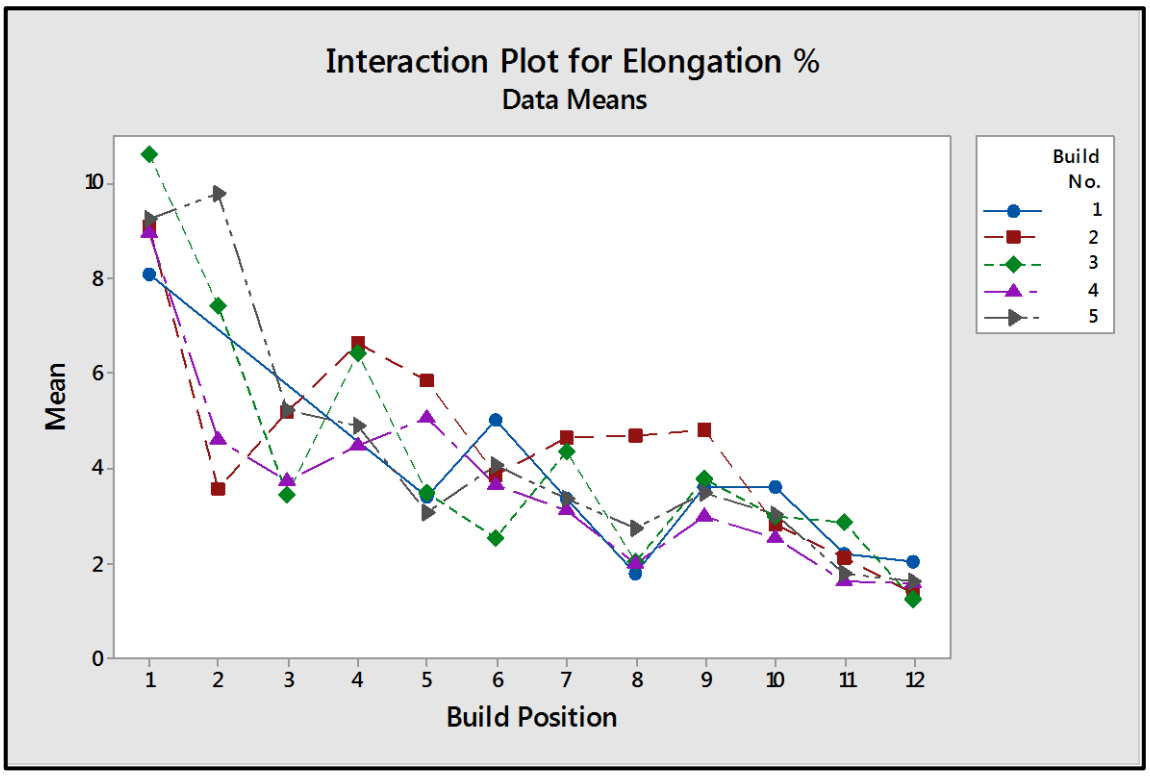

Figure 48 - Interaction Plot for Elongation

4.2. Fatigue Testing

The initial plan for this investigation in the effects of recycling powder on mechanical performance of laser melted parts was to perform a traditional fatigue test as described within ASTM E466-07: Standard Practice for Conducting Force Controlled Constant Amplitude Axial Fatigue Tests of Metallic Materials. This standard describes the procedure for the performance of uniaxial, un-notched dynamic axial force fatigue testing to determine material fatigue strength. ASTM E466 offers the option for a cylindrical specimen with a continuous radius between ends as shown in Figure 50, and so fatigue test pieces were built and machined to the dimensions shown in Figure 49, with D = 5 mm.

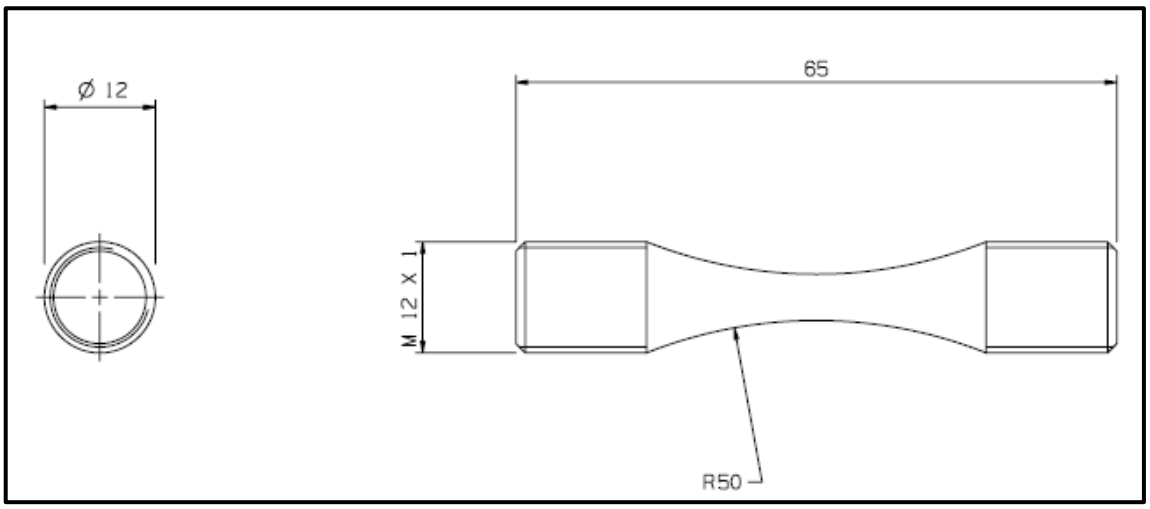

Figure 49 - Drawing of Machined Fatigue Test Specimen.

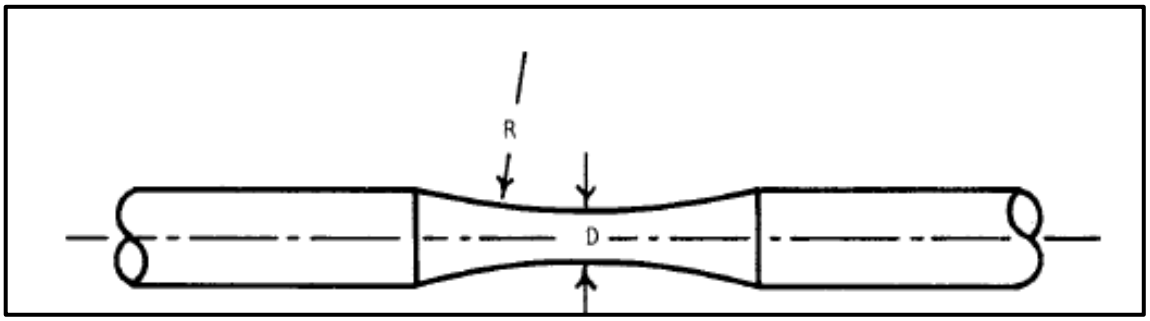

Figure 50 - Specimen with a Continuous Radius between Ends, Figure Reproduced from ASTM E466 (2007)

The machine to be used for the fatigue tests was an Instron 8801 servo-hydraulic fatigue testing system, powdered by its own hydraulic power unit. The system was suitable for performing both high and low cycle fatigue testing. The system utilised hydraulic grip sections for clamping of specimens. ASTM E446 (2007) states:

> To minimize bending stresses (strains), specimen fixtures should be aligned such that the major axis of the specimen closely coincides with the load axis throughout each cycle. It is important that the accuracy of alignment be kept consistent from specimen to specimen.

In order to be sure that specimens were aligned along the load axis, special sample adapters were designed by the author with the intention of ensuring alignment. The assembly for these adapters is shown in Figure 51. The assembly consisted of three parts.

1. Ball section in to which the fatigue sample would thread. A bolt was screwed in from the bottom to clamp the sample in place and prevent any rotation during dynamic testing.

2. Cup section with matching radii to ball section. This allowed the ball section to rotate within it for alignment of the sample when load was applied. This section was threaded at the base to allow it to attach to the clamp part.
3. Clamp part which would fit into Instron 8801 hydraulic grip section preventing movement of the assembly during dynamic fatigue testing.

When the samples were loaded onto the Instron 8801, part 2 was not fully threaded on to part 3, leaving a clearance between the two. This allowed part 1 at both ends to move freely. When load was applied to the assembly, the two ball sections, connected by the fatigue sample would self-align within their respective assembly. The assembly may be viewed in Figure 52.

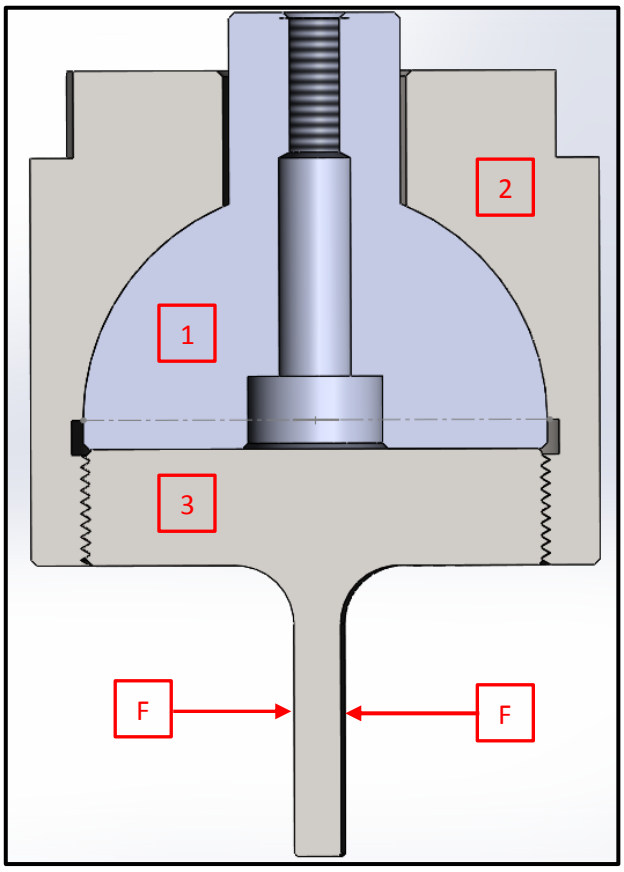

Figure 51 - Fatigue Test Adapter Assembly

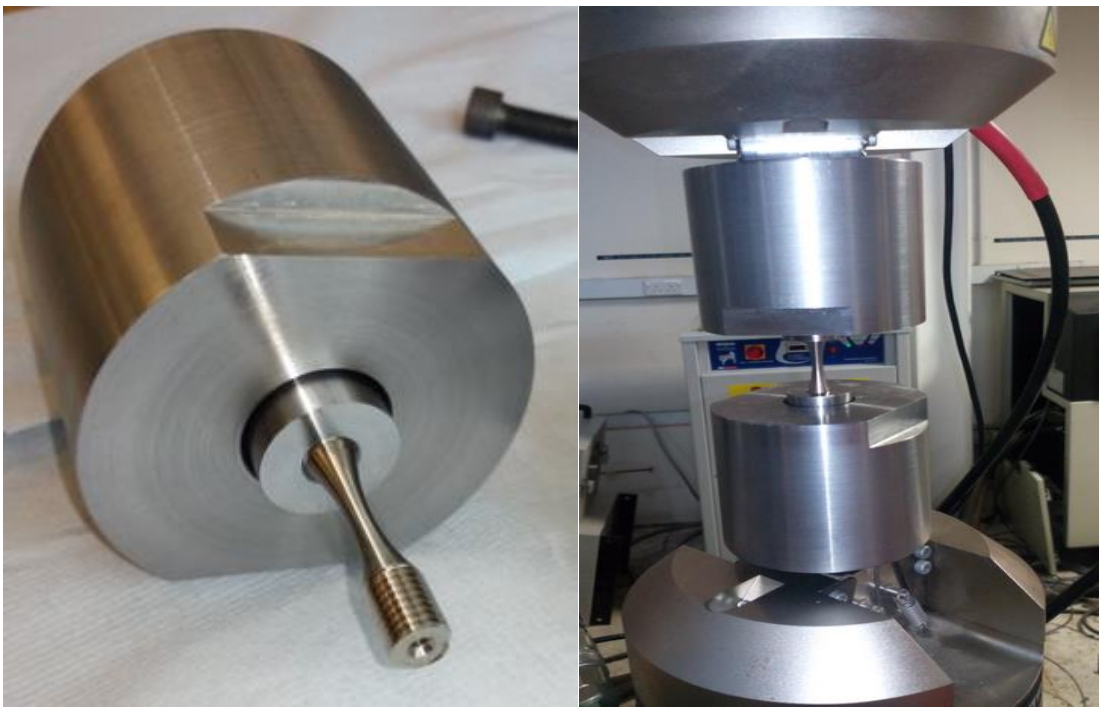

Figure 52 - Left, Fatigue Assembly with Fatigue Test Piece, Right, Fatigue Assembly set up on Instron 8801.

Upon analysis of the tensile test results, it was immediately apparent a test in which fatigue strength was determined in response to varying stress levels would not be suitable. The variation in mechanical performance observed for positions across the build plate made such a test impractical. As a result, the author opted for a constant force for all samples to perform a uniaxial fatigue test. Time constraints led the author to select a relatively high maximum stress of approximately 700 MPa. Slight variations in the minimum diameter measured for each sample meant that stress fluctuated slightly. The test conditions were as follows:

- Force varied between 1.5 and 14 kN.
- Test run at a frequency of 20 Hz.
- Cycles to failure was the test output.

Upon commencing testing, it was important to ensure that the cycle and load desired and input to the control system was in fact the cycle and load being performed. To achieve this, an oscilloscope was used to tune the gain from the machine. This was achieved and an example of the force vs time measurement showing the cycle applied is shown in Figure 53.

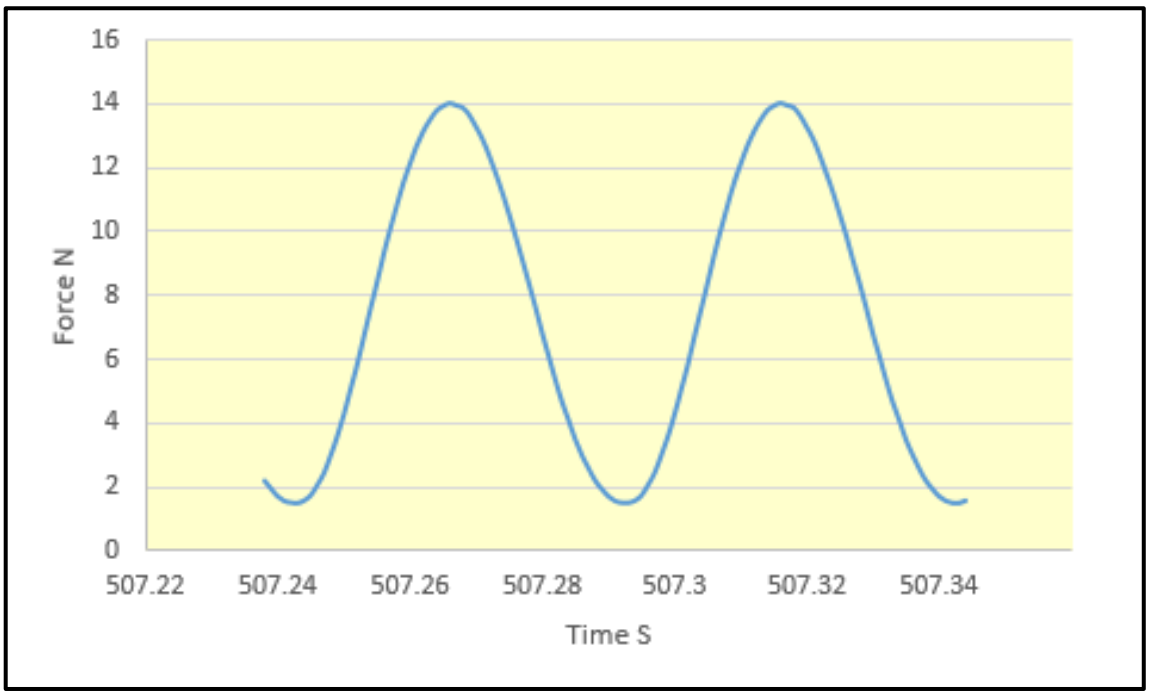

Figure 53 – Graph Showing measured Force vs Time Measurements from Cyclic Fatigue Test of Sample 4-12

Upon completion of all fatigue testing, ANOVA was performed in the same method as described for the tensile test data analysis. The ANOVA table for cycles to failure at FMax = 14 kN is shown in Table 16, along with the results of all fatigue tests in Figure 54. Unfortunately, samples 2-1, 2-3, 2-5 and 2-7 were destroyed in setting up the machine and tuning out the gain. Future work should make use of additional sacrificial specimens that would prevent the loss of test specimens.

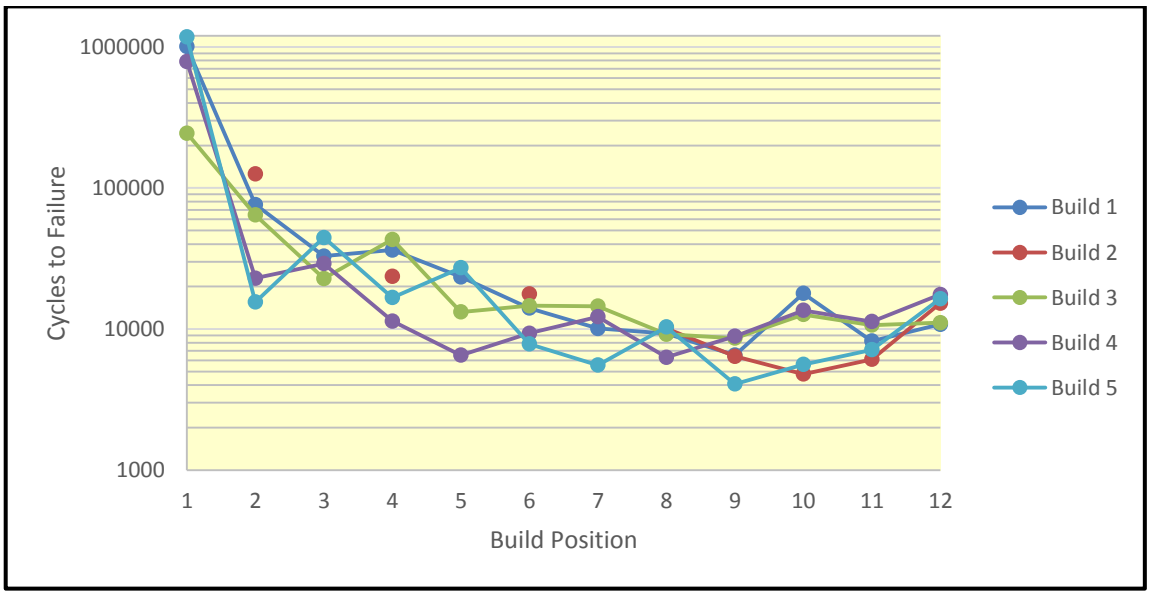

Figure 54 – Graph Showing Cycles to Failure at FMax = 14 kN.

Table 16 - Analysis of Variance for Cycles to Failure at FMax = 14 kN

Analysis of Variance

Source	DF	Seq SS	Contribution	Adj SS	Adj MS	F-Value	P-Value
Model	15	2.33841E+12	83.45%	2.33841E+12	1.55894E+11	13.45	0.000
Linear	15	2.33841E+12	83.45%	2.33841E+12	1.55894E+11	13.45	0.000
Build No.	4	60895168397	2.17%	39151631394	9787907849	0.84	0.506
Build Position	11	2.27751E+12	81.28%	2.27751E+12	2.07047E+11	17.86	0.000
Error	40	4.63727E+11	16.55%	4.63727E+11	11593183950		
Total	55	2.80214E+12	100.00%				

Model Summary

S	R-sq	R-sq(adj)	PRESS	R-sq(pred)
107672	83.45%	77.25%	9.72367E+11	65.30%

When considering the effect of Build Number on cycles to failure, a P-value of 0.506 coupled with a F-Value of 0.84 suggested that there was no statistical evidence of varying the level of Build Number on the measured variable Cycles to Failure. Build Position was shown to have an effect on the number of cycles to failure. A P-value of 0.00, coupled with a F-value of 13.45 showed that there was strong evidence of the effect of varying the build position on cycles to failure. This can be visualised in Figure 55. Additionally, 81.28 % of the contribution to variability was attributable to Build Position.

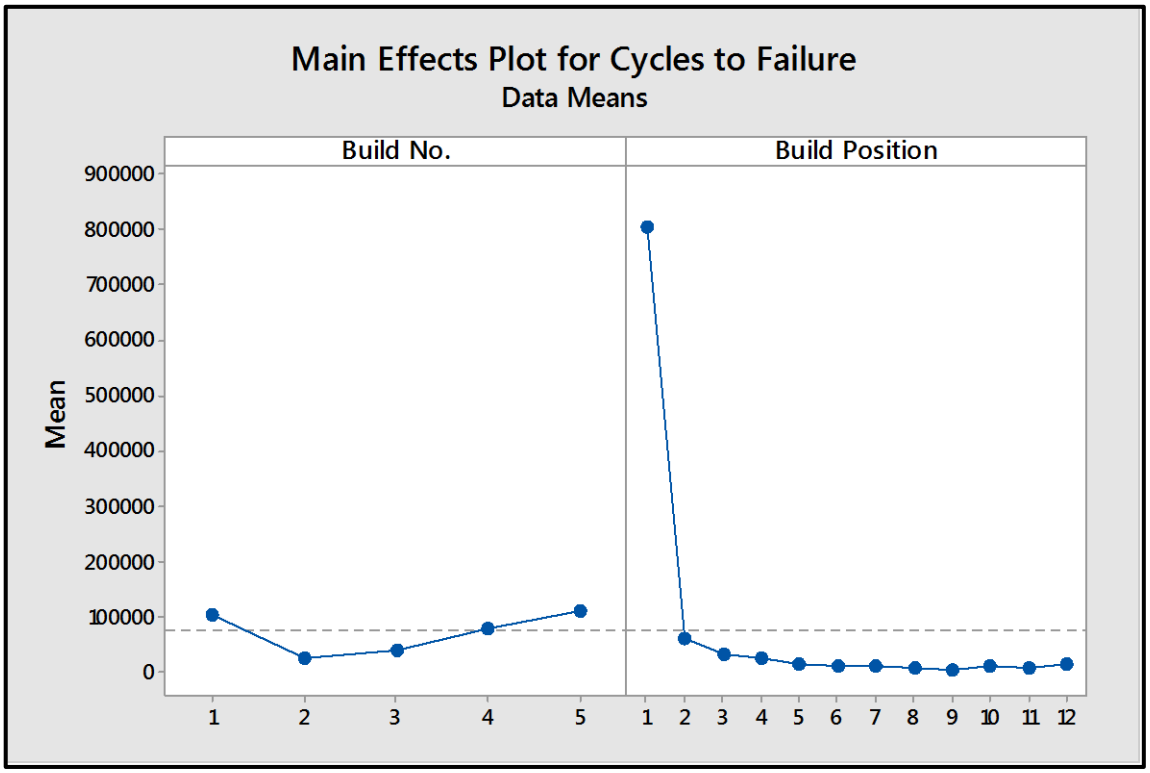

Figure 55 - Main Effects Plot for Cycles to Failure at FMax = 14 kN

What was most obvious was the magnitude of difference in the number of cycles to failure when moving from position 1 to all other positions. Parts built in position 1 showed an average number of

805536 cycles to failure. When moving to position 2, this dropped to 60949 cycles to failure. Clearly, there were factors associated with build position 1 that had a profound effect on the fatigue strength of laser melted parts analysed within this investigation. The difference in the condition of the powder between builds did not have a significant effect on fatigue strength.

5.0. Chemical and Metallurgical Characterisation of Laser Melted Parts: Results and Discussion

5.1 Porosity Analysis

The extreme variation in the mechanical performance of laser melted parts by build position observed through tensile and fatigue testing required the author to investigate the reason behind such variation. One such stage was to investigate the difference in porosity within the laser melted samples. The pyramids created for the purpose of investigating porosity within parts were intended to determine variation between builds, not by position. As such, they were not labelled by position, meaning that the author had no confidence in determining the position on the build plate from which they came. In any future work there is a clear benefit for position references to be added to these pyramids.

To investigate any potential variation in the porosity of laser melted parts by build position, the grip sections of the tensile specimens tested were sectioned for analysis. The grinding and polishing of metallographic specimens was known to be an incredibly laborious and time consuming process. As such, the decision was taken to analyse the porosity of tensile samples from only four build position levels, for all levels of build number. The position levels selected were:

- Position 1
- Position 5
- Position 8
- Position 12

Samples for porosity analysis were prepared following the guidelines detailed within ASTM E3-11: Standard Guide for Preparation of Metallographic Specimens. Initially, the samples were hot mounted within a Bakerlite resin and marked for identification. Specimen preparation then required the following (ASTM E3 2011):

- Planar or rough grinding to flatten an irregular surface caused by section cutting, and to remove substantial amounts of specimen material in order to reach the required plane for subsequent polishing.
- The next stage required was fine grinding using successively finer abrasive papers in order to remove the damage to the surface incurred through the rough grinding process.
- All samples required cleaning between each grinding stage to remove any grit remaining.
- The final stages were fine polishing steps using both diamond and oxide slurries embedded on a suitably fine cloth.

Table 17 - Grinding and Polishing Steps Taken in the Preparation of Metallographic Specimens

Stage	Conditions	Speed & Force
Planar Grinding	Wet grinding with 120 grit SiC Paper	250 rpm / variable
Planer Grinding	Wet grinding with 320 grit SiC Paper	250 rpm / variable
Fine Grinding	Wet grinding with 500 grit SiC Paper	250 rpm / variable
Fine Grinding	Wet grinding with 1000 grit SiC Paper	250 rpm / variable
Fine Grinding	Wet grinding with 2000 grit SiC Paper	250 rpm / variable
Fine Grinding	Wet grinding with 4000 grit SiC Paper	250 rpm / variable
Fine Polishing	Struers 1 µm Diamond Polishing aerosol spray embedded on velvet cloth	250 rpm / variable
Fine Polishing	Struers SiO_2 slurry embedded on velvet cloth	250 rpm / variable

All grinding and polishing stages were performed by hand. Following the successful completion of metallographic specimen preparation, all samples were viewed under Optical Microscope (OM) and imaged. Six images were taken per sample to generate a full picture of the plane to be analysed for porosity. The image processing software “ImageJ” was used to process the images taken. Spaces in the specimen plane showed as darkened regions when compared to the fully dense regions as shown in Figure 56.

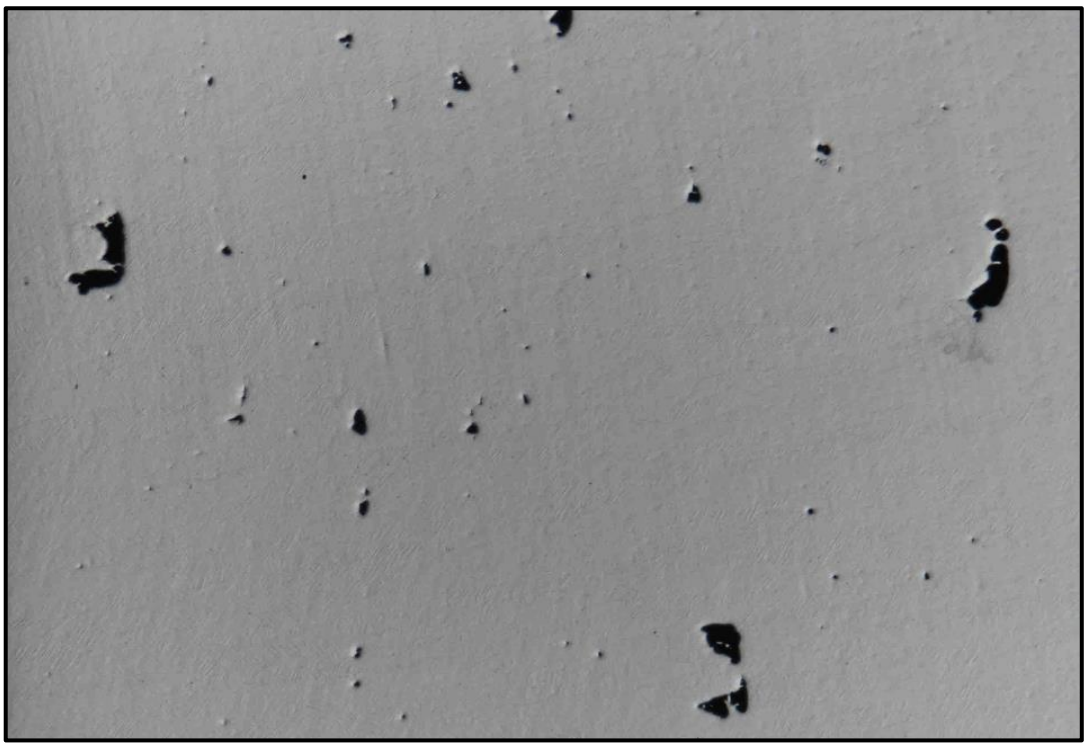

Figure 56 – Original OM Image of Middle Left Section of Sample 1-8.

When using ImageJ to process an image, the user sets a contrast threshold which identifies the darkened porous regions of samples and fills them in with a red colour, as shown in Figure 57. The software was then able to plot outlines of the red sections as shown in Figure 58. Comparison of the Figure 56 and Figure 57 shows just how effective ImageJ was in identifying the darkened regions. The scale of the images was set prior to this and so the software calculated the percentage of the area of the image that was coloured red. Six images were processed for each sample analysed, and the total shaded area was calculated as a percentage of the total area analysed. The results are shown in Table 18 and Figure 59.

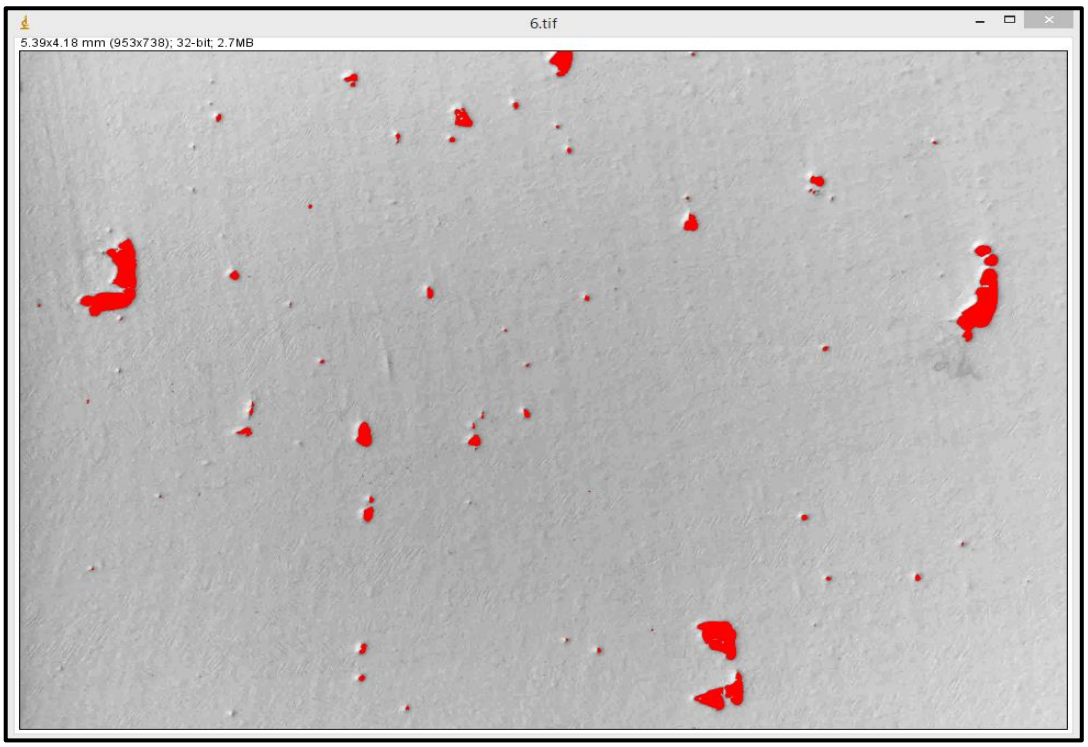

Figure 57 - Processed Image Using ImageJ for Porosity Calculation for Middle Left Section of Sample 1-8 (0.98 %).

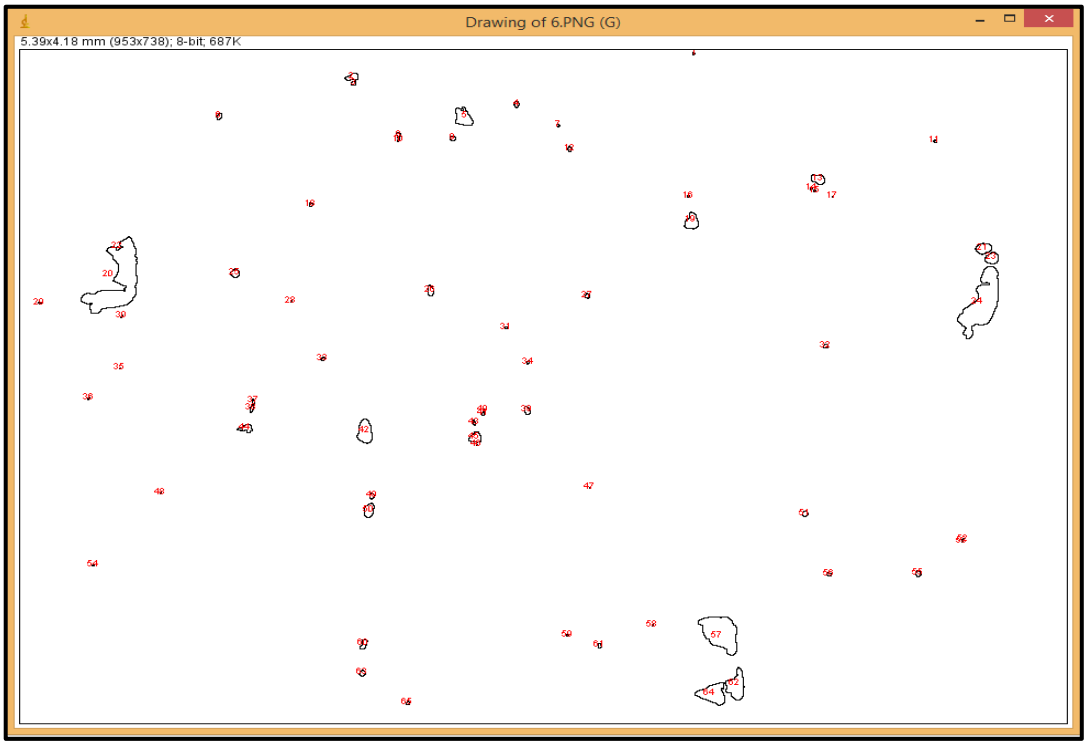

Figure 58 - Outlines Plot Showing Regions Calculated as Porosity for Sample 1-8

Table 18 - Table Showing Calculated Porosity for all Samples Analysed with Tensile Test Data

Sample	Position	Porosity %	UTS MPa	Proof Stress MPa	Elongation %
1-1	1	0.050	1063.57	933.84	8.08
1-5	5	0.387	1052.48	950	3.41
1-8	8	0.544	996.57	927	1.77
1-12	12	0.331	993.09	911.66	2.03
2-1	1	0.102	1056.01	917.83	9.07
2-5	5	0.139	1067.28	949.8	5.84
2-8	8	0.280	1037.76	928.82	4.69
2-12	12	1.194	912.89	867.42	1.37
3-1	1	0.067	1074.03	939.43	10.64
3-5	5	0.106	1052.72	945.04	3.50
3-8	8	0.128	1008.33	926.64	2.04
3-12	12	0.183	935.40	900.23	1.24
4-1	1	0.079	1077.15	959.14	8.97
4-5	5	0.046	1059.52	949.81	5.08
4-8	8	0.143	1014.73	939.89	1.98
4-12	12	1.160	916.79	877.47	1.56
5-1	1	0.088	1085.61	960.88	9.26
5-5	5	0.309	1051.86	956.53	3.085
5-8	8	0.290	1026.12	923.71	2.74
5-12	12	0.439	974.48	899.96	1.62

Figure 59 – Graph Showing Porosity Calculated as Percentage of Overall Area

When considering the results of percentage porosity measured, it was clear to see that generally there was an increase observed from position 1 to position 12. Position 12 for builds 2 and 4 clearly contained the highest levels of porosity measured with values of 1.19 and 1.16 % respectively. Position 12 for builds 1, 3 and 5 showed significantly lower levels of porosity with values of 0.33, 0.18 and 0.439%. Mechanical performance of titanium parts are known to be affected by porosity with Russell and Lee (2005, p185) describing a rapid drop in fatigue strength for parts with increasing levels of porosity.

The tensile test data obtained for each of the samples sectioned is also provided in Table 18 and the results obtained for percentage Elongation are shown in Figure 60. If porosity was the only factor influencing mechanical performance, one may expect the values for percentage Elongation for position 12 to vary significantly with such variation in porosity measured within the samples. Clearly, the results of percentage elongation for position 12 are tightly grouped within Figure 60.

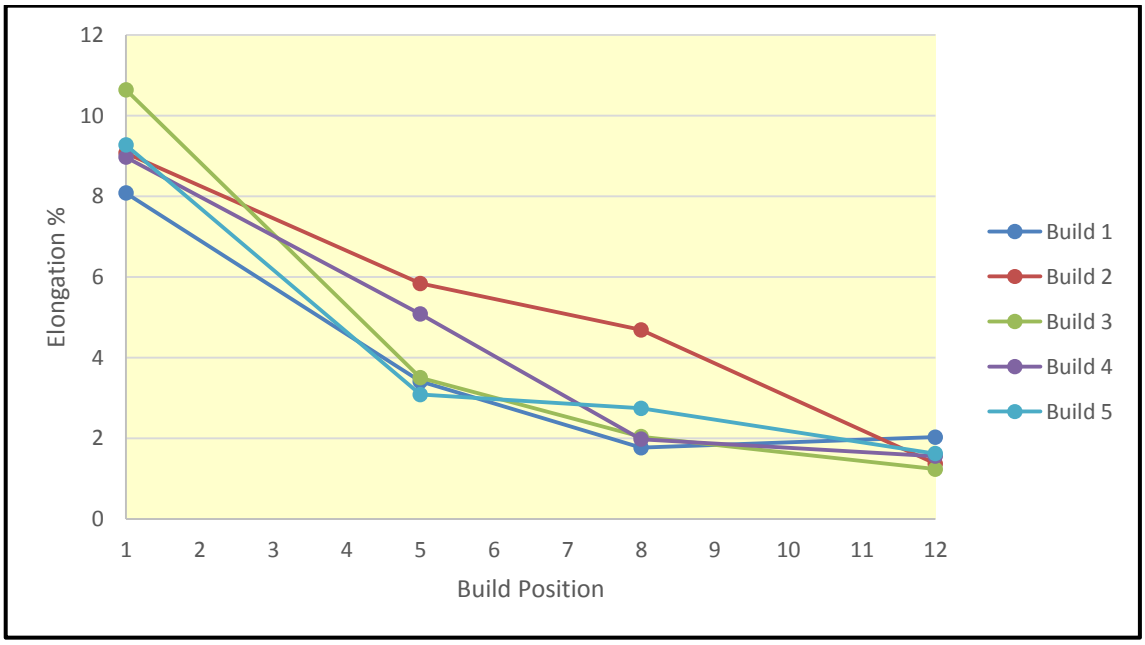

Figure 60 - Graph Showing % Elongation Measured During Tensile Testing

When considering the results of porosity measured for build 1, an increase in porosity was observed from position 1 through to position 8, with a reduction in porosity for position 12. Values of 0.05, 0.39, 0.54 and 0.33 % porosity were measured for samples 1-1 (example of sample with low porosity shown in Figure 61 and Figure 62), 1-5, 1-8 and 1-12 respectively. Clearly samples 1-5 and 1-8 contained a

higher level of porosity than sample 1-12, however, values of tensile strength, yield strength and elongation all decreased when moving from position 1 through to position 12. This led the author to state with confidence that porosity measured was not the only factor affecting the mechanical properties of laser melted parts.

Figure 61 - Original OM Image of Bottom Left Section of Sample 1-1.

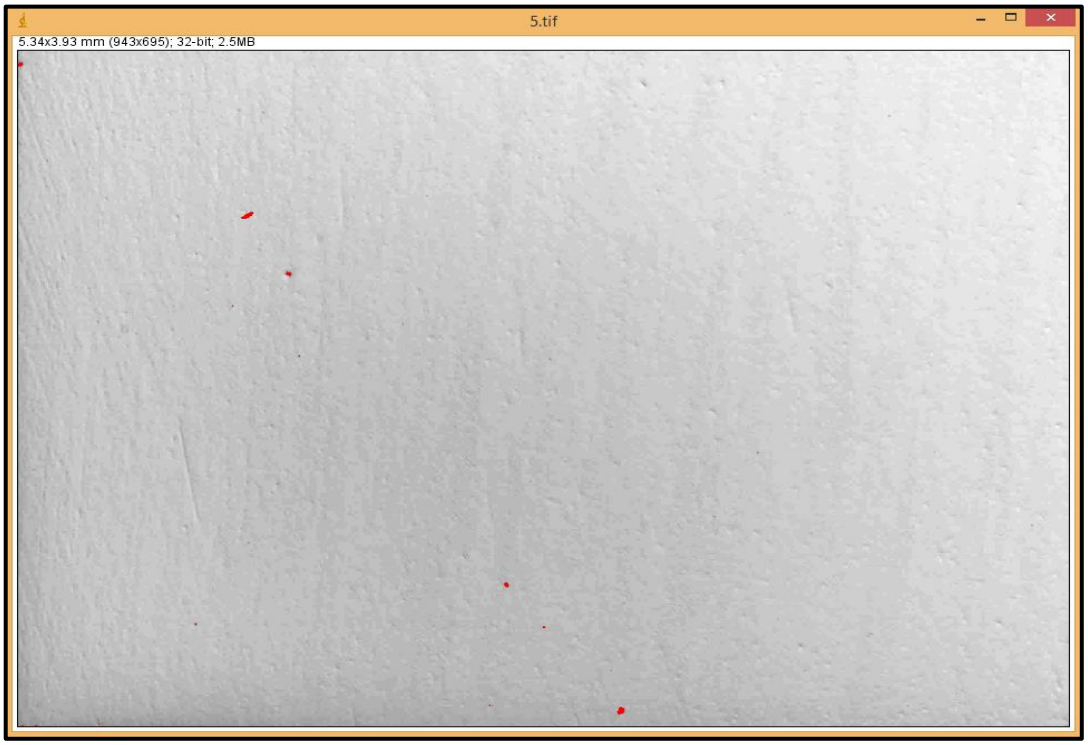

Figure 62 - Processed Image Using ImageJ for Porosity Calculation for Bottom Left Section of Sample 1-1 (0.017 %).

5.2 Chemical Analysis

Due to titanium and aluminium possessing a high affinity for reaction with interstitial elements, an understanding of the level of interstitial elemental absorption during SLM was required. To address this requirement, chemical test cubes were manufactured within each build. Six of these cubes were removed from the build plate prior to any heat treatment and six were subjected to the heat treatment process. This had the added benefit of being able to determine any, and the level of, interstitial element absorption during the heat treatment process. These parts were not marked for build position.

The chemical test cubes were designed to be 27 mm^3 in volume, which was the approximate volume required for chemical analysis. Again, the test methodology described within ASTM E1409-13 was used to determine the mass by percentage of both oxygen and nitrogen within the chemical test cubes. The results for the laser melted chemical test cubes that were removed from the build plate prior to heat treatment are shown along with the results obtained previously for the powder used as the feed stock for the parts in Figure 63.

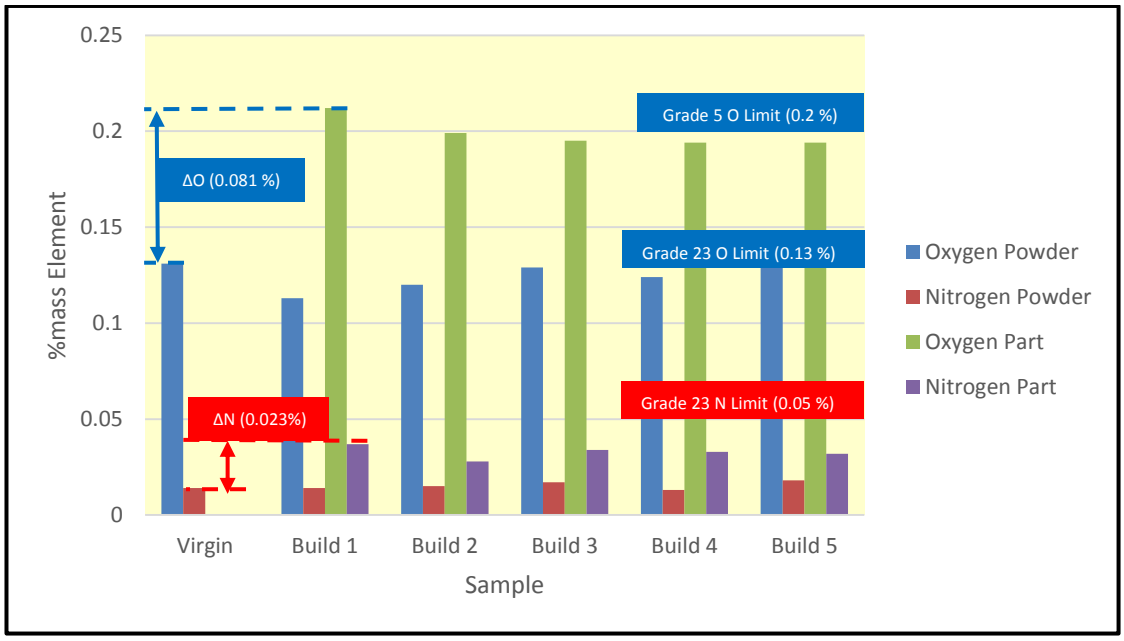

Figure 63 - Graph Showing Results of Determination of % Mass of Oxygen and Nitrogen in Titanium and Titanium Alloys by Inert Gas Fusion for Powder and Laser Melted Samples.

The powder analysed for the Feed Stock sample was used as the feed stock powder for the laser melting of parts in Build 1. The powder analysed for the Build 1 sample was used as the feed stock powder for the parts laser melted in Build 2, and so on. This graph allows for the visualisation of the level of absorption of both oxygen and nitrogen into laser melted parts within the laser melting process. The increase in both oxygen and nitrogen from Feed Stock powder to chemical cube test samples produced as part of build 1 are also shown in Figure 63. An increase of 0.081 % oxygen and an increase of 0.023 % nitrogen was observed.

The position on the build plate from which the chemical test cubes were taken could not be stated with any certainty. It was therefore not possible to determine whether oxygen and nitrogen content within laser melted parts varied with the position in which they were built. Variation in interstitial elemental percentage weight may be considered to be a possible explanation for the variation in mechanical properties observed.

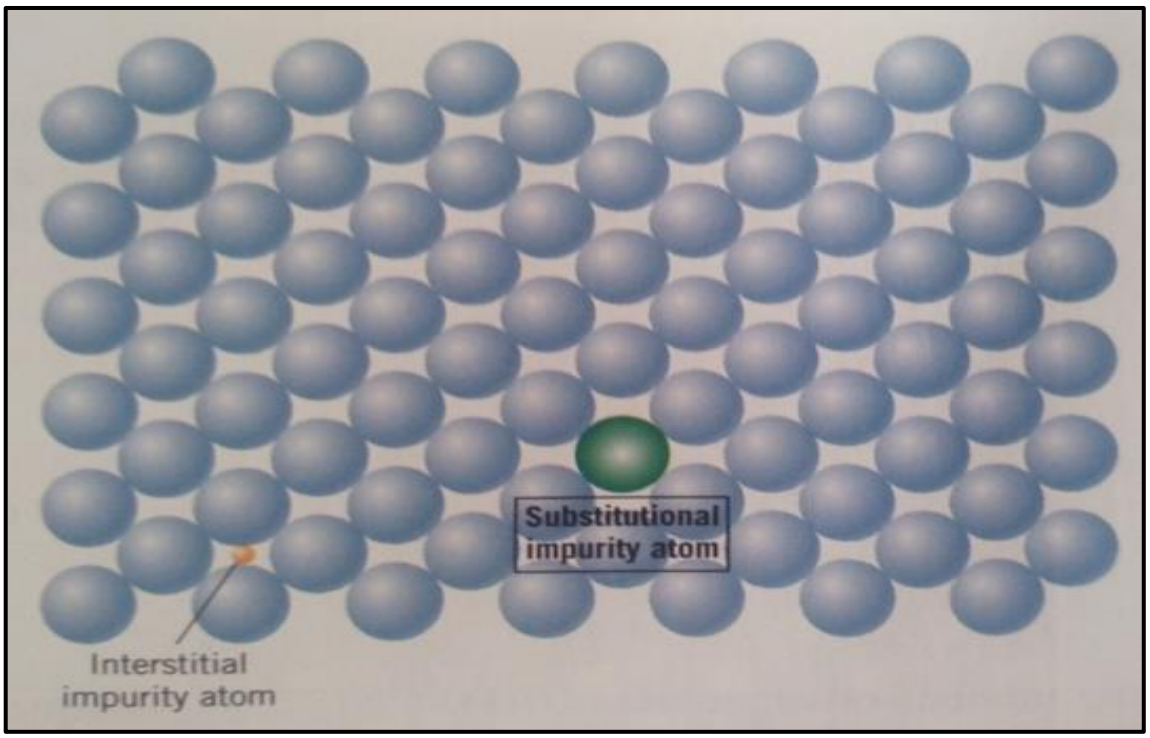

Figure 64 - Two-dimensional Schematic Representation of Interstitial Impurity Atoms, Figure Reproduced From Callister (2007, p. 84).

Oxygen and nitrogen content within titanium alloys has been shown to have a profound effect on the strength and ductility of parts. Increases in both oxygen and nitrogen cause a decrease in toughness until the material becomes brittle (Donachie 2000, p. 97). Additionally, it was shown by Oh et al.

(2011) that elongation of Ti-6Al-4V tensile test specimens decreased with increasing oxygen concentration. Interstitial impurities are typically larger in diameter than the spaces between crystal lattice chains. This has the effect of inducing lattice strains on adjacent host atoms (Callister 2007, p. 85). This may be viewed in Figure 64.

The chemical test cubes that were subjected to heat treatment were sent to a certified laboratory for the same analysis as the chemical test cubes that were removed prior to heat treatment. Unfortunately, at the time of writing, the analysis had not been completed. It was therefore not possible to quantify any change in chemical composition of laser melted parts as a result of the heat treatment process.

Based on the results obtained for chemical composition of laser melted parts, there was clearly some absorption of interstitial elements into the parts. It is unclear at this stage whether chemical composition varied with build position. Any future work concerned with the investigation in to the reason behind such variation in mechanical properties observed for differing positions along the build plate should investigate any difference in chemical composition of parts. The tensile samples produced and tested as part of this project are available for chemical composition testing.

5.3 Microstructure Analysis

An additional consideration in identifying differences in the samples built through laser melting was determining any difference in material microstructure. The analysis of the material microstructure was to be performed on the samples that had undergone metallographic preparation and porosity analysis. The methodology described within ASTM E407-07: Standard Practice for Microetching Metals and Alloys was to be used.

This standard specifies a variety of chemical etchants that may be used to bring out the material microstructure. The author had decided to use etchant number 187 which constituted:

- 10 ml HF.
- 30 ml HNO_3.

- 50 ml H_2O.

This was the recommended etchant by per ASM (1972). The sample was to be swabbed for 10 – 20 seconds (ASTM E407 2007), then being cleaned under a source of warm running water before running under alcohol and dried under a hand drier (ASM 1973).

The use of HydroFluoric acid (HF) within the authors' university was tightly controlled. The author was unable to gain access to the laboratory in which etching using HF would be allowed during the time available. Any future work concerned with this project should include chemical etching of the already prepared metallographic specimens used for porosity analysis, and analysis of the microstructures to investigate any variation between them. An example of the expected microstructure based on the heat treatment cycle applied is shown in Figure 65.

Figure 65 - Expected Microstructure of Ti-6Al-4V Furnace Cooled from 850 °C, Reproduced from Donachie (2000).

6.0. Discussion

6.1. Powder Characterisation Discussion

Section 3.0 of this report detailed the steps taken in the characterisation of powder that had been recycled up to five times within the SLM process. Powder samples were subjected to a variety of analysis techniques, which included PSD analysis to determine particle size, SEM analysis to determine particle morphology and chemical composition analysis to determine any variation in chemical composition. Overall, 26 powder samples were collected. Samples were taken from the initial feed stock powder, from within the build chamber for each build, and from post build sieved powder, which was to act as the feed stock powder for the subsequent build. Additionally, PCB's were produced with the aim of developing a methodology for powder sampling within builds and to investigate the effect of proximity to the site of laser melting on powder.

PSD analysis was conducted using a Malvern Mastersizer 3000, which used the laser diffraction technique and the Mie theory of light scattering to determine the sizes of particles held within a suspension. All of the powder samples underwent five repeat tests with the outputs of PSD analysis being:

- Φ Dx(10) µm
- Φ Dx(50) µm
- Φ Dx(90) µm
- % Result In Range (14.5 – 45.6 µm)
- % Result Below (14.5 µm)
- % Result Above (45.6 µm)

Initial analysis indicated a trend towards an increase in the values of Dx(10), Dx(50) and Dx(90) through repeated recycling. Additionally, the percentage of the powder sample population which exhibited diameters within the required range of 15 – 45 µm decreased with repeated recycling. To confirm this,

ANOVA was conducted on the results obtained from PSD analysis, with the process factors under investigation being:

- Powder Sampling Location at two levels: Feed stock powder for each build and post sieving powder sample after each build.
- Build Number: Build 1, 2, 3, 4 and 5.

The purpose of such an investigation was to determine the effect of repeated recycling on powder characteristics. Through the use of ANOVA, the effect of recycling the powder up to five times was shown to be statistically significant in terms of the effect on the powder population for the measured variables: Φ Dx(10) µm, Φ Dx(50) µm, Φ Dx(90) µm, which showed a trend towards increasing values through repeated recycling.

The effect of build number was also shown to be statistically significant for the measured variables % Result in Range (14.5 – 45.6 µm), % Result Below (14.5 µm), which showed a decrease through repeated recycling and % Result Above (45.6 µm), which showed an increase through repeated recycling. This meant that there was statistical evidence of the effect on the powder characteristics in terms of their PSD when recycling the powder up to five times.

When considering the effect of powder sampling location, there was also a statistically significant difference between the samples taken from within the build chamber, and those taken post sieving. The post sieving samples consistently were found to be made up of larger particles within their population when compared to those taken within the build chamber. This was an unexpected result and attributed to the fine particles falling through the sieve mesh and congregating at the bottom of the containers in to which sieved powder fell. The author was not present for powder sampling and so felt it probable that samples were taken from the top of the sieved powder container, where there would have been a larger proportion of larger particles, which may not have been entirely representative of the overall sieved powder population.

ANOVA was also performed on powder samples collected from within the PCB's built with each build with the same analysis performed as with the chamber and sieved samples. This time however, there were five levels for sampling location, with the additional levels being:

- PCB Small Chamber
- PCB Medium Chamber
- PCB Large Chamber

The analysis performed using the PCB samples again showed a statistical significance when moving from build 1 to build 5 with the same effect observed on all measured variables as the analysis with only two levels of powder sampling location. When considering the effect on powder characteristics of using the three sizes of chamber, the conclusions were as follows:

- The small PCB chamber consistently contained a higher proportion of larger particles and exhibited the highest values for Dx(10), Dx(50) and Dx(90). This was likely due to the higher proportion of partially sintered powder particles as a result of the powder population being in such close proximity to the site of laser melting.
- The medium PCB Chamber showed slightly lower values of Dx(10), Dx(50) and Dx(90), which decreased again for the large PCB chamber.
- For all three chambers, there was a large difference in the powder characteristics in terms of PSD when compared to the chamber and sieved samples. Samples collected from the PCB's were thus not considered to be representative of the overall powder populations of powder to be recycled and are not a suitable means for in process powder sampling.

SEM analysis was conducted to ascertain any difference in the morphology and surface microstructure of recycled powders. The main outcomes of this analysis were:

- Through repeated recycling, a roughening of the powder surface with a reduction in particle sphericity was observed.

- Large particles greater than 60 µm were observed in all powder samples analysed, including the feed stock powder provided by the manufacturer. The high level of sphericity of such powders negated the possibility of them resulting from partial sintering.
- Such large particles which had been through the SLM process exhibited an extremely fine acicular martensitic surface microstructure, which was not observed on large particles provided by the manufactured in the initial feed stock powder. This surface structure could be attributed to rapid heating and cooling of the powders from within the β domain of the Ti-6Al-4V phase diagram.
- Normally sized and large particles from within the initial batch of manufacturer's powders exhibited a mix of coarse acicular martensitic alpha and large equiaxed surface structure. The reason for such variation with the large particles was not clear.
- Nano scale particles were only observed within the joins between satellite particles. There were no unattached nano scale particles found within any powder sample analysed.
- Large and partially sintered particles greater than the mesh diameter of 63 mµ, used for sieving were consistently found within recycled powder, leading to questions regarding the efficacy of the sieving process for removing such particles outside of the required PSD range.

Chemical composition testing was conducted as per ASTM E1409-13 – Test Method for Determination of Oxygen and Nitrogen in Titanium and Titanium Alloys. One sample for each of the builds was sent for such analysis. The results indicated that the feed stock powder supplied by the manufacturer contained a percentage by mass of oxygen that was greater than the allowable limit stipulated for the grade of Ti-6Al-4V that the powder was said to be produced to. The limit was 0.13 %, with the result from testing showing a result of 0.131 %. The level of oxygen fluctuated for each sample tested and ranged from a minimum of 0.113 % to a maximum of 0.141 %. Nitrogen content within all powder samples analysed was below the maximum allowable percentage by mass of 0.05 %.

6.2. Chemical and Mechanical Characterisation Discussion

The previous sections had detailed the steps taken in the characterisation of parts produced through laser melting with the intention of investigating the effect of recycling of Ti-6Al-4V powders. Test

specimens were created and tested to investigate the mechanical, chemical and metallurgical properties of the laser melted parts. An understanding of the effect of changes in powder characteristics on the performance of laser melted parts was considered to be of paramount importance for the production of loaded production parts.

Tensile testing was performed on tensile test pieces using a Zwick Z100 Materials Testing Machine, with the outputs of testing being UTS, Yield strength and elongation. Cyclic constant force tests were performed using an Instron 8801 Fatigue Test System with the intention of determining the fatigue strength of parts produced and the output of testing being cycles to failure at 700 MPa. Chemical composition testing was performed to determine changes in the amount of both oxygen and nitrogen contained within the parts. Porosity analysis was also conducted. Unfortunately, time constraints prevented any investigation in to the potential variation of microstructure of parts produced.

Tensile testing was conducted on 12 parts produced per each of the five builds. All parts produced satisfied the minimum requirement of both UTS and Yield Strength stipulated within ASTM F136-13 and ASTM F2924-14. Only one test piece satisfied the minimum requirement of attaining an elongation of 10%. This specimen was from build 3, position 1.

Through ANOVA, there was shown to be no statistical effect on UTS, Yield Strength and Elongation when moving between builds, meaning there was no effect of the change in powder characteristics measured on the mechanical properties of laser melted parts for powder that had been recycled up to five times.

The effect of moving from position 1 to position 12 on UTS was significant with parts produced at position 1 showing average UTS results of 1071 MPa, falling to 947 MPa for position 12. When moving from position 1 to position 12, the average Yield strength decreased from 1071 MPa to 947 MPa. The effect of moving from position 1 to position 12 on elongation was profound with parts produced at position 1 showing an average elongation 9.2 %, falling to 1.6 % for position 12. Clearly, there was a significant effect of position within the build chamber on the strength and ductility of parts produced.

Cyclic fatigue testing followed an identical pattern to that of fatigue testing with there being no statistical effect of moving between builds, meaning that there was no effect of the change in powder characteristics measured on the fatigue strength of laser melted parts for powder that had been recycled up to five times. The difference in the average number of cycles to failure recorded for samples produced at 1, when compared to the average of those produced at position 12 was astounding. Parts produced at position 1 lasted an average of 805,536 cycles, and parts produced at position 12 lasting an average of 14,210 cycles.

In order to attempt to answer the question of why such significant variation in mechanical properties was observed for laser melted parts produced at different positions on the build plate, porosity analysis was conducted. Samples 1, 5, 8 and 12 for all builds were sectioned and polished to allow for such analysis. Results indicated that there was a general trend towards increased porosity when moving from position 1 to position 12. Porosity was not however, considered to be the only factor affecting the mechanical performance of parts produced. When considering build 1, samples 5 and 8 showed higher levels of porosity than position 12, however, the sample produced at position 12 showed significantly lower results for UTS, Yield, Elongation and cycles to failure. This led the author to believe that additional factors were affecting the mechanical performance of parts produced.

Chemical composition testing was performed on chemical test cubes produced for each build. At the time of testing, the level of variation in performance of parts produced at different build positions was not anticipated and so the parts were only intended to determine the difference in chemical composition between builds, and level of interstitial element absorption. The position of the chemical test cubes on the build plate was thus not recorded and so there was no way to determine the position on the build plate from which they had originated.

There was a significant increase in oxygen observed when comparing the % composition of the powder used to produce the parts, and the parts themselves. The limits stipulated for % composition of oxygen are 0.13 % and 0.20 % for ASTM F136-13 and ASTM F2924-14 respectively, with the powder being of the ELI grade of Ti-6Al-4V to match ASTM F136-13. None of the parts produced and tested satisfied the

maximum chemical composition in terms of oxygen for ASTM F136-13. In fact, most of the parts were shown to have a chemical composition that barely satisfied ASTM F2924-14, with the parts from build 1 not satisfying the limit. All parts satisfied the limit for nitrogen of 0.05 %.

7.0. Conclusions & Future Work

7.1. Conclusions

- Recycling powder has a statistically significant effect on powder characteristics.
- This change in powder characteristics had no effect on mechanical performance of laser melted parts.
- Build position was shown to have a strongly significant effect on mechanical performance of laser melted parts in terms of:
  - UTS.
  - Yield Strength.
  - Elongation.
  - Fatigue Strength.
- In process interstitial elemental absorption was significant .
- Porosity varied with build position.
- Parts satisfied the minimum requirement of UTS, Yield strength and nitrogen content in all cases considered.
- Parts did not satisfy the minimum requirement of elongation in all but one case, or oxygen content in all cases considered.
- It was not possible to say what the usable life of the powder would be as a result of this analysis.

Some of the methodologies presented within this report had been used previously for the characterisation of powders. This study has combined several methodologies used previously in an attempt to provide a methodology for full characterisation of powders to be used within SLM, and provide a methodology that can be used in the future to fully investigate the link between powder and produced part characteristics. The methodology can be continued for increasing numbers of recycling to determine the end of life for Ti-6Al-4V powders.

The project has produced a quantitative way of presenting the information in a manner that is both approachable and easily understandable. Contributions have been made towards the process of recycling of powders and attention has been drawn to a significant current limitation of the process in terms of variability of parts with build position. Steps may now be taken to address this issue and rectify the problem. The author's industrial sponsors may now confidently use the powder up to five

times, safe in the knowledge that the powders characteristics shall not influence the performance of parts produced. This report has also highlighted the high level of repeatability of the process.

Two main process related factors have been investigated; build number and build position. Important knowledge has been produced in relation to each of these. By completing and analysing five builds, the effect of recycling the powder up to five times was shown to be statistically significant in terms of the effect on the powder PSD population, with a trend towards increasing particle size values through repeated recycling. There was however no statistical effect found on laser melted parts in terms of UTS, Yield Strength and Elongation when moving between builds 1 and 5. This indicateed that the change in powder characteristics measured had no effect on the mechanical properties of laser melted parts for powder that had been recycled up to five times. Fatigue testing followed the same pattern with no statistical build number related effect. Again, this would indicate that there was no effect of the change in powder characteristics measured on the fatigue strength of laser melted parts for powder that had been recycled up to five times.

When considering the effect of powder sampling location, there was a statistically significant difference between the samples taken from within the build chamber, and those taken post sieving.

A clear and significant effect has been identified in regard to the position within the build chamber. The strength and ductility of parts produced has been shown to vary when moving from position 1 to position 12. All the mechanical properties underwent significant changes. The difference in the average number of cycles to failure recorded for samples produced at 1, when compared to the average of those produced at position 12 was astounding. In seeking the reason for such a change a general trend was determined towards increased porosity when moving from position 1 to position 12. Porosity cannot however be considered to be the only factor effecting the mechanical performance and additional factors must be effecting the mechanical performance of parts produced, such as the chemical composition of parts.

7.2. Future Work

Any future work concerned with investigating the effects of recycling of Ti-6Al-4V powders should thoroughly investigate the difference in chemical composition of laser melted parts produced a different position on the build plate, to ascertain any variation in, and the effect of changes in chemical composition of parts. This could be a potential reason for the variation in mechanical performance observed. Additionally, variation in microstructure of parts should be conducted to determine if there was any difference between parts produced at different build positions.

Future work should also include a longer ranging investigation in to the effect of recycling powders. The number of times that the powder had been recycled was shown to have no effect for powder recycled up to five times. It was not possible to say that this lack of effect of recycling would continue indefinitely and so powder should be recycled an increased number of times in order to determine the end life of the powder. This would represent a significant challenge, primarily due to the cost of running such a study as well as the time required. The methodology used within this study represents a testing guide that could be followed for both characterising powders used, and parts produced within such an investigation.

8.0. Appendices

8.1. Appendix 1 – Additional Figures

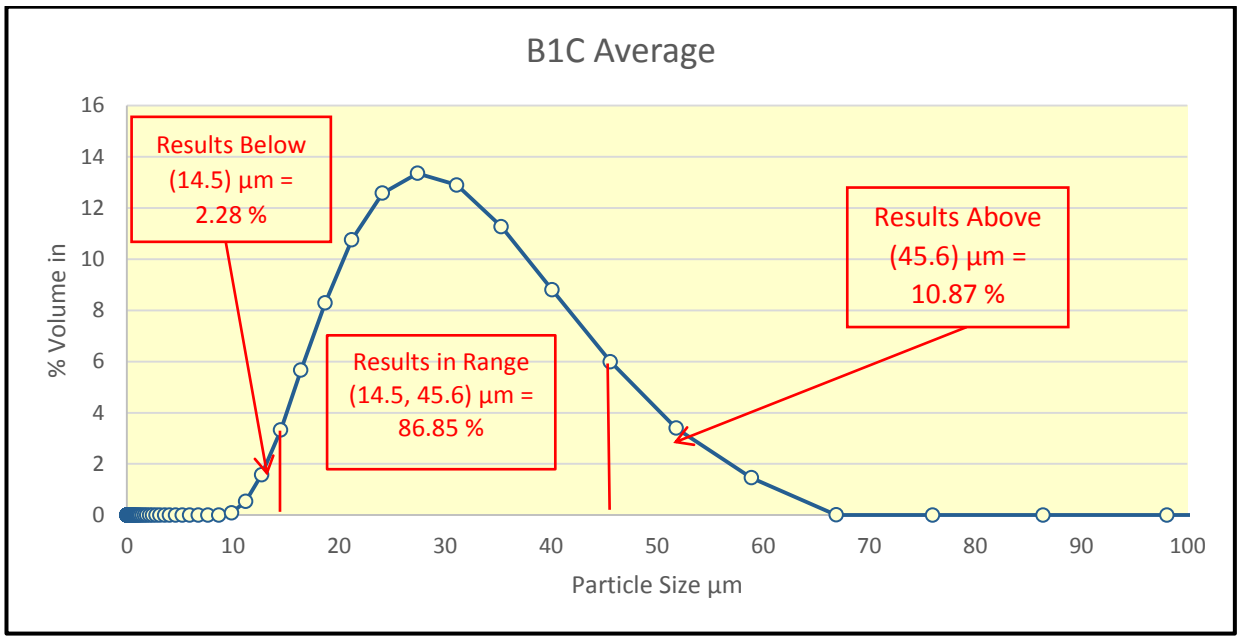

Figure 66 - Graph Showing Average PSD for B1C Powder Sample

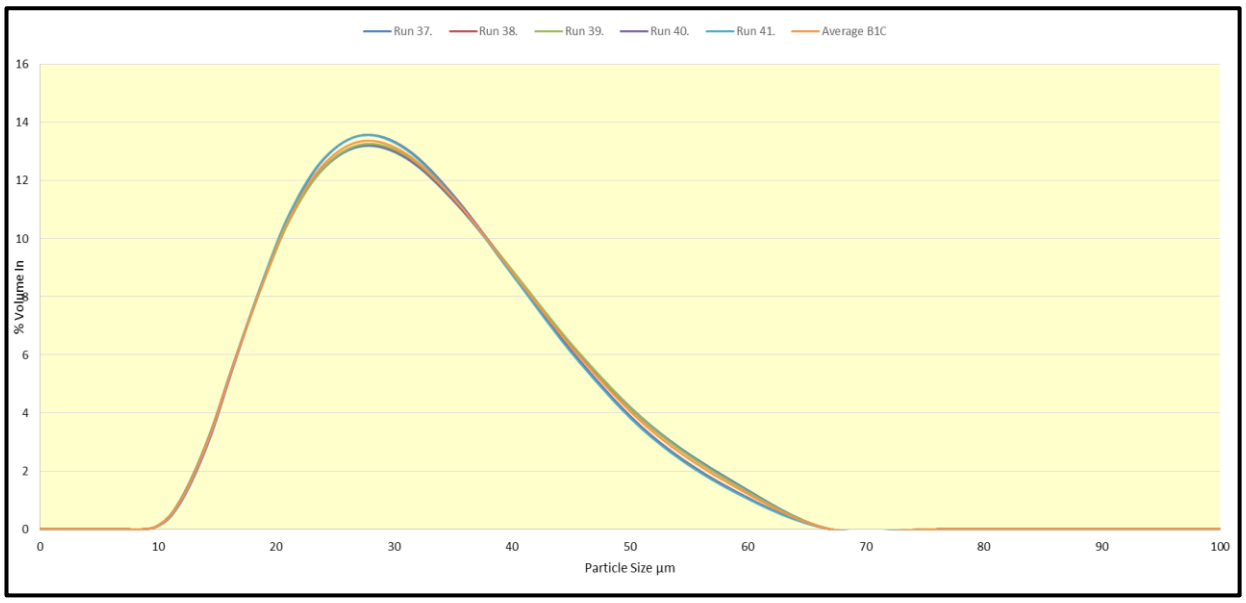

Figure 67 - Graph Showing PSD for B1C Powder Sample

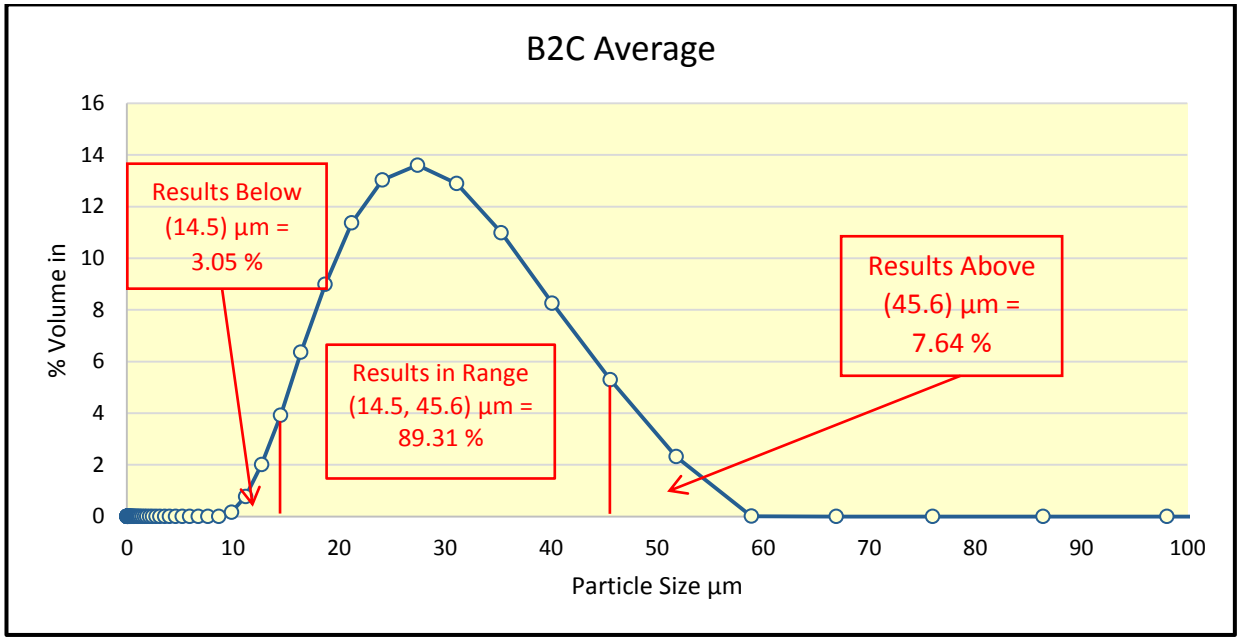

Figure 68 - Graph Showing Average PSD for B2C Powder Sample

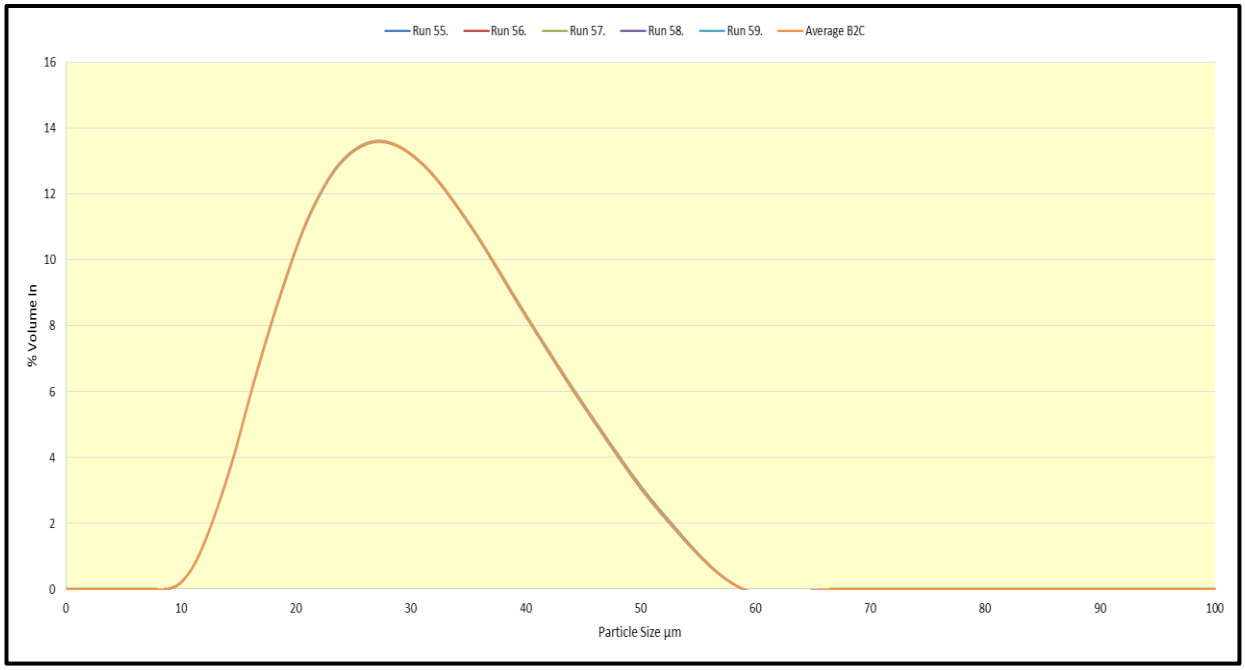

Figure 69 - Graph Showing PSD for B2C Powder Sample

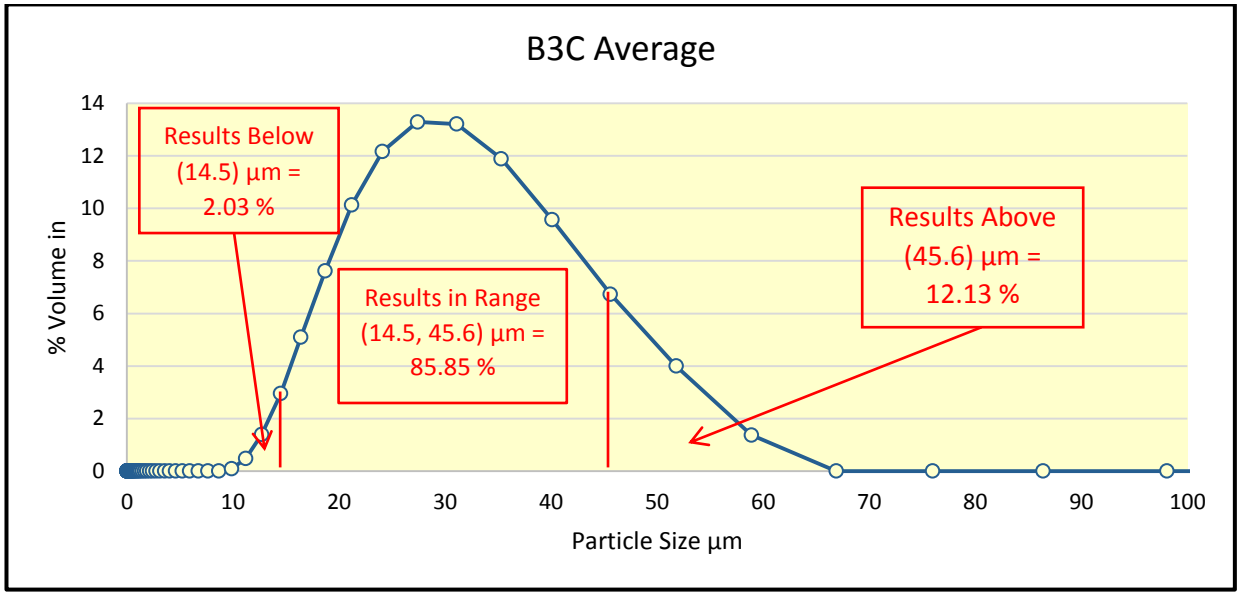

Figure 70 - Graph Showing Average PSD for B3C Powder Sample

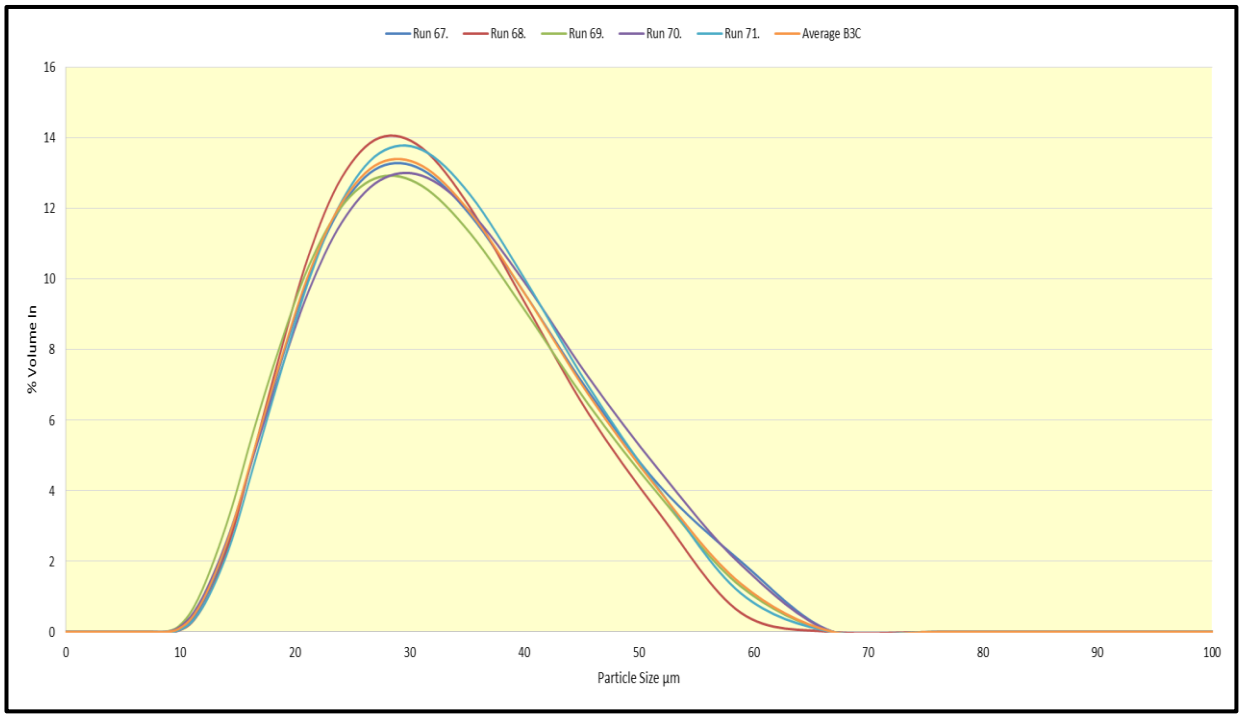

Figure 71 - Graph Showing PSD for B3C Powder Sample

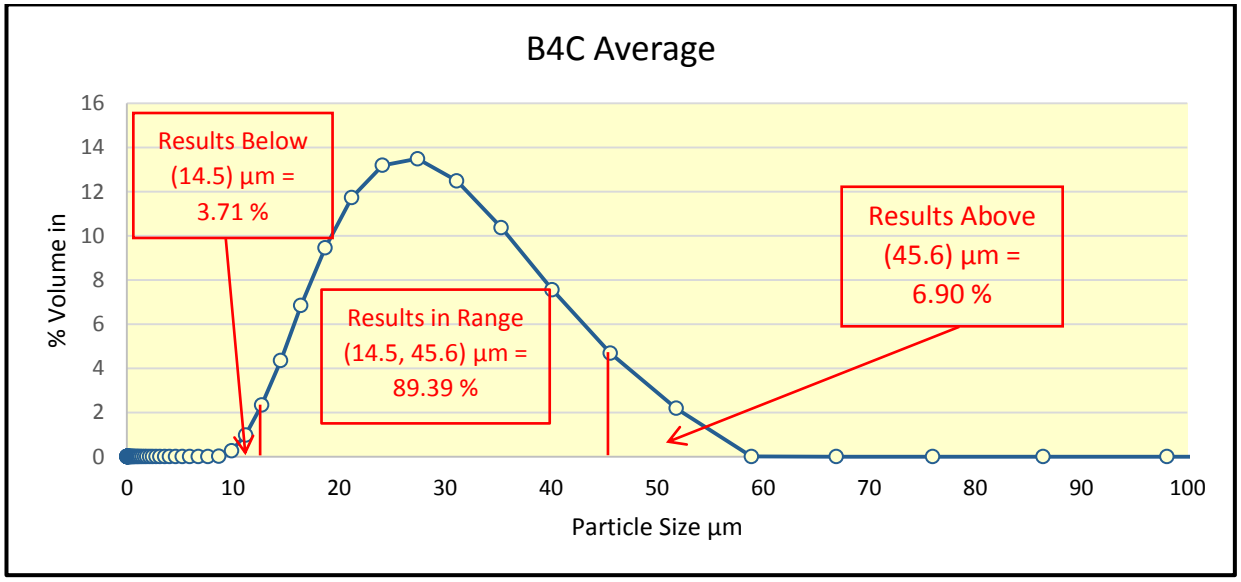

Figure 72 Graph Showing Average PSD for B4C Powder Sample

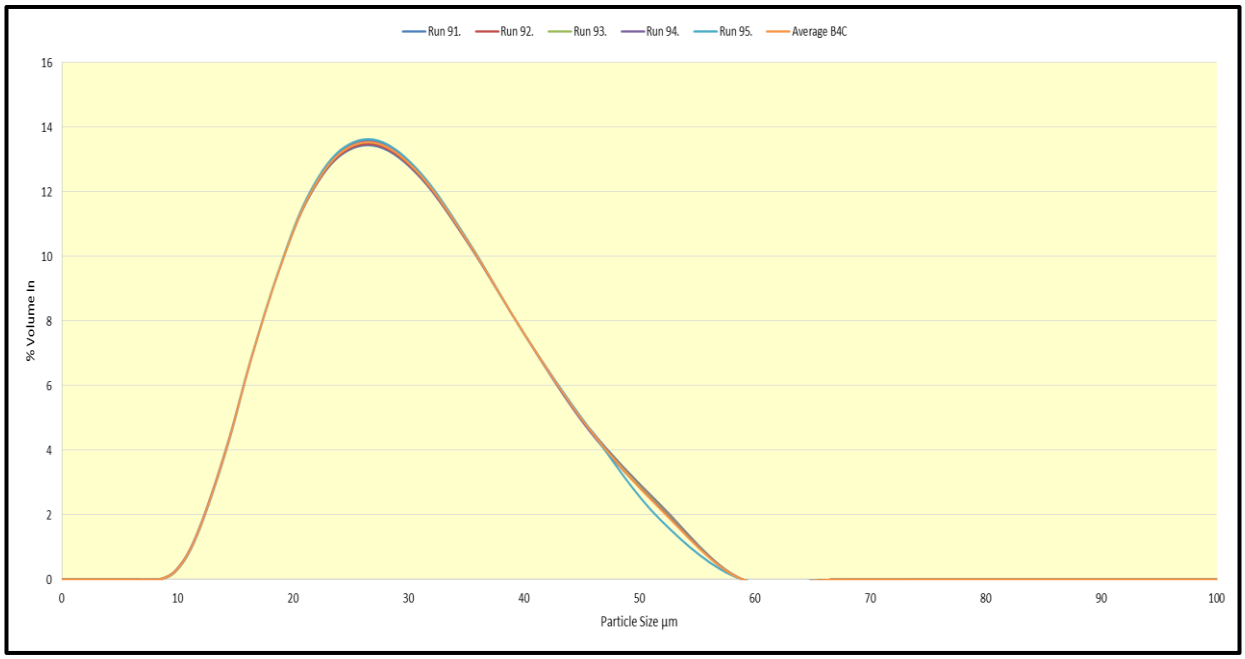

Figure 73 - Graph Showing PSD for B4C Powder Sample

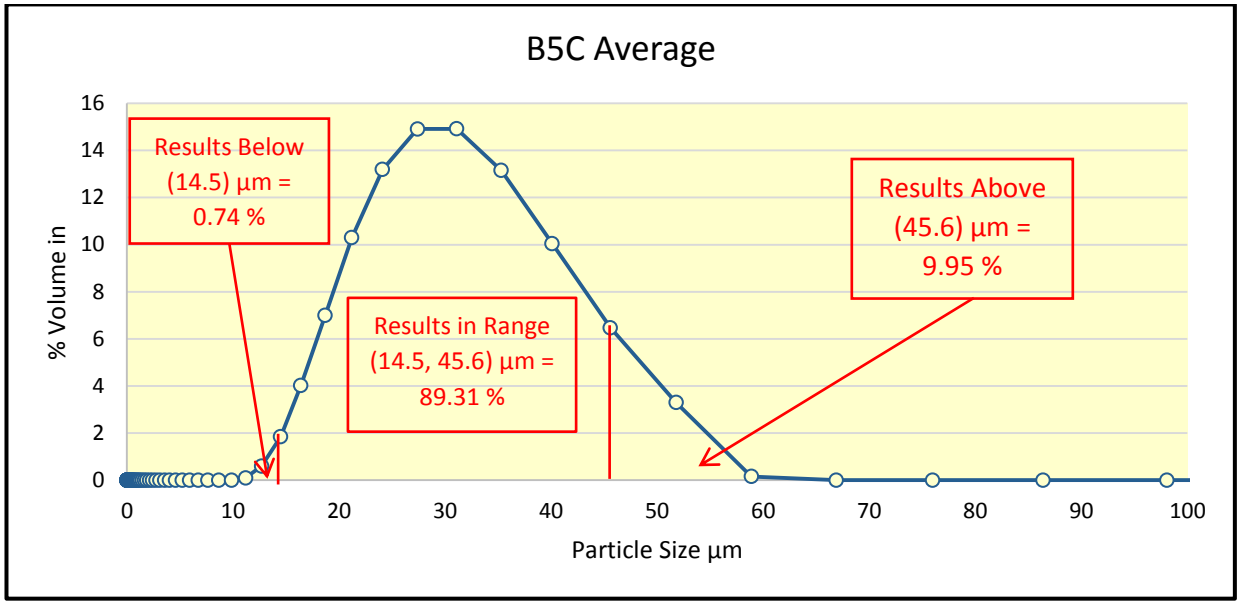

Figure 74 - Graph Showing Average PSD for B5C Powder Sample

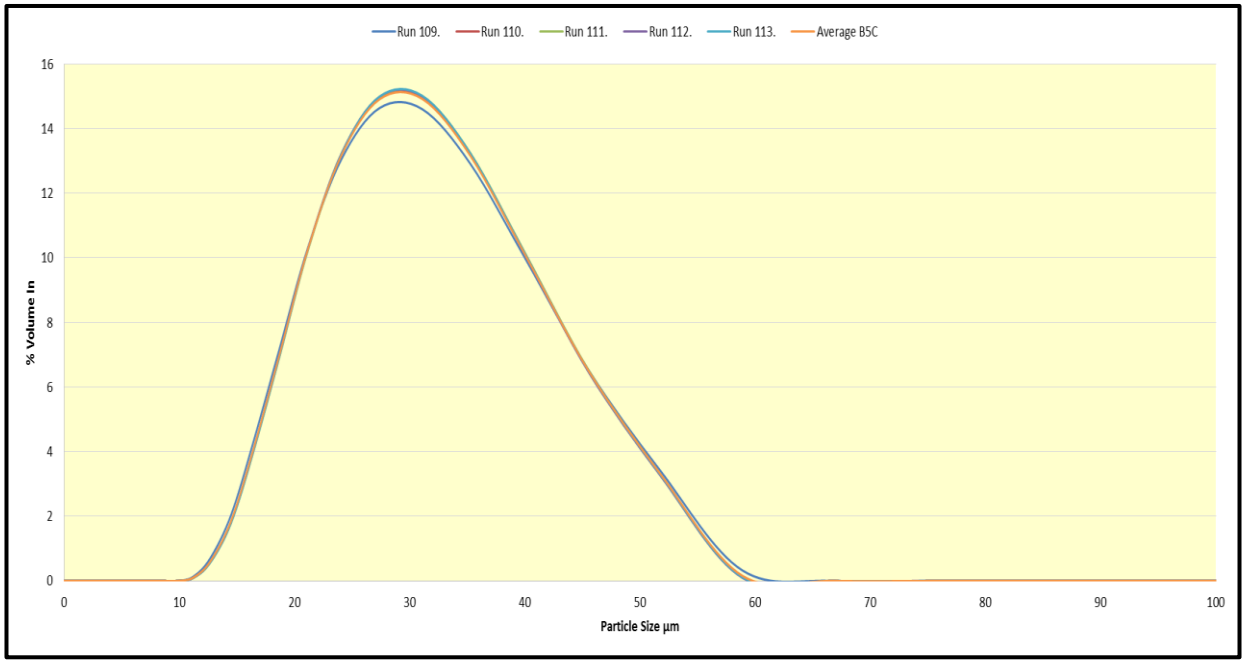

Figure 75 - Graph Showing PSD for B5C Powder Sample

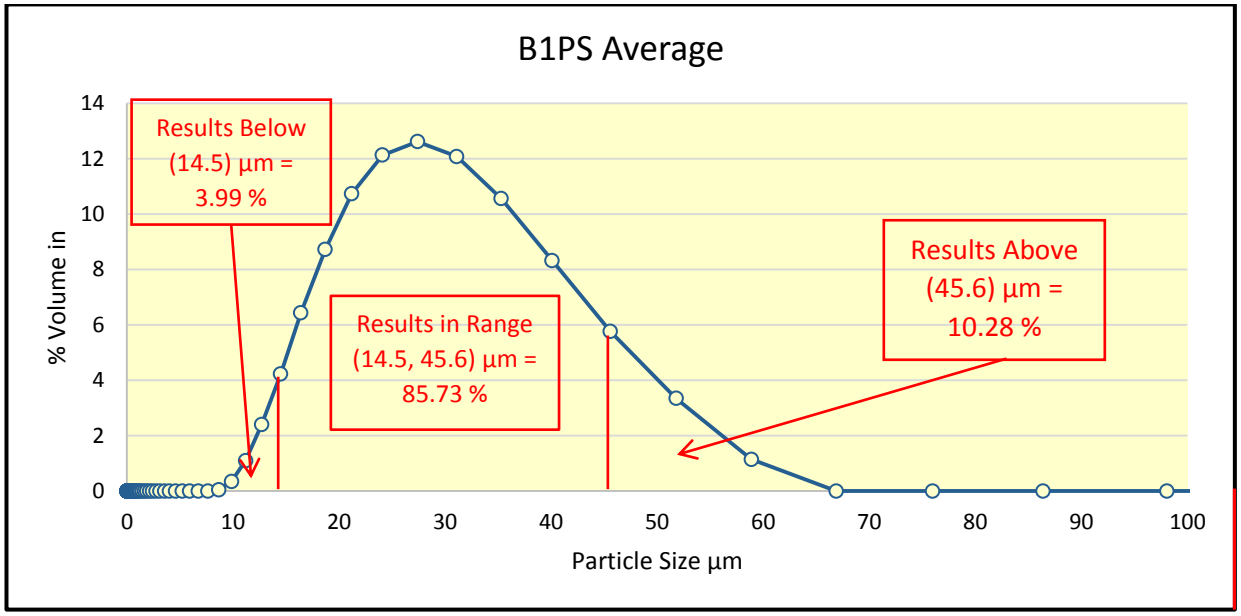

Figure 76- Graph Showing Average PSD for B1PS Powder Sample

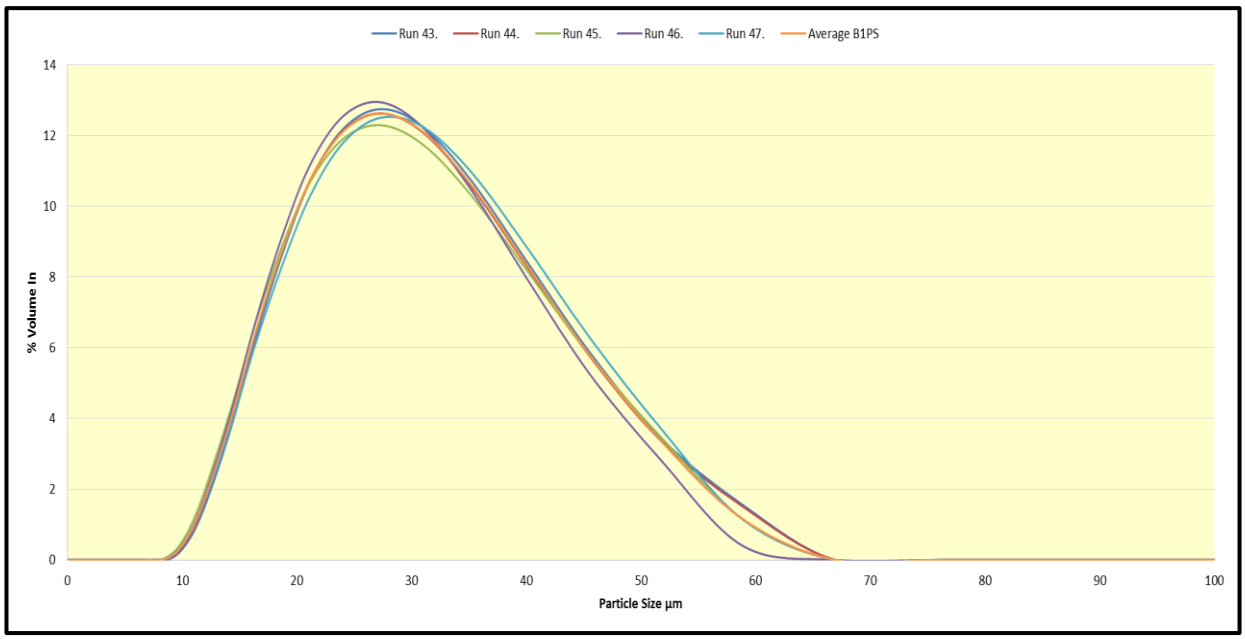

Figure 77 - Graph Showing PSD for B1PS Powder Sample

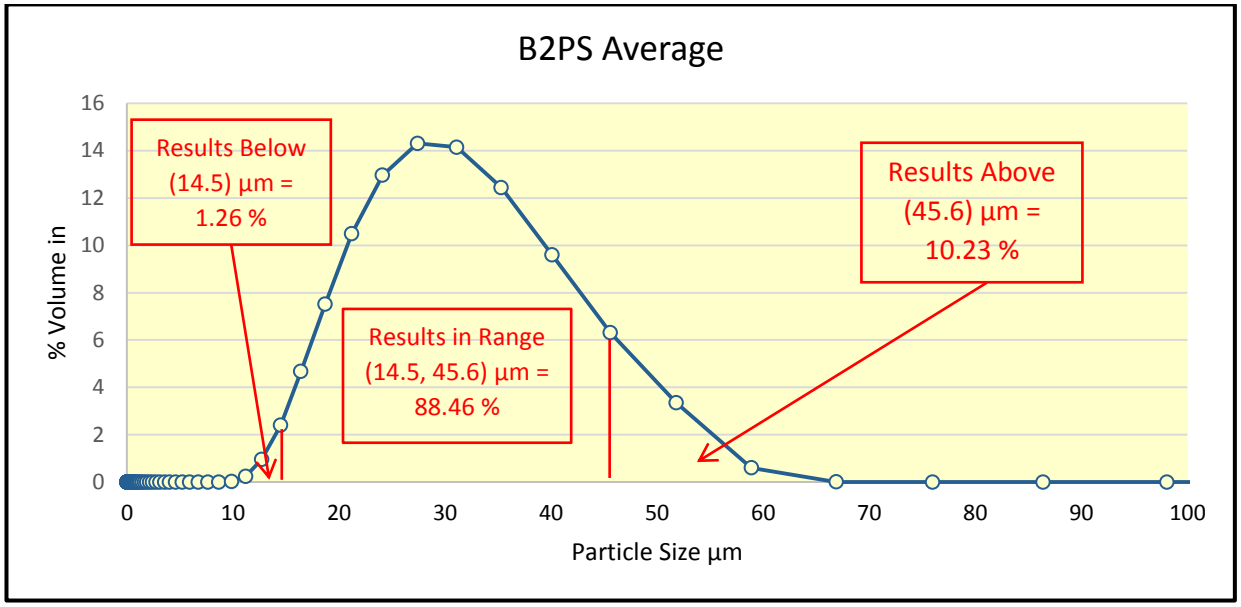

Figure 78- Graph Showing Average PSD for B2PS Powder Sample

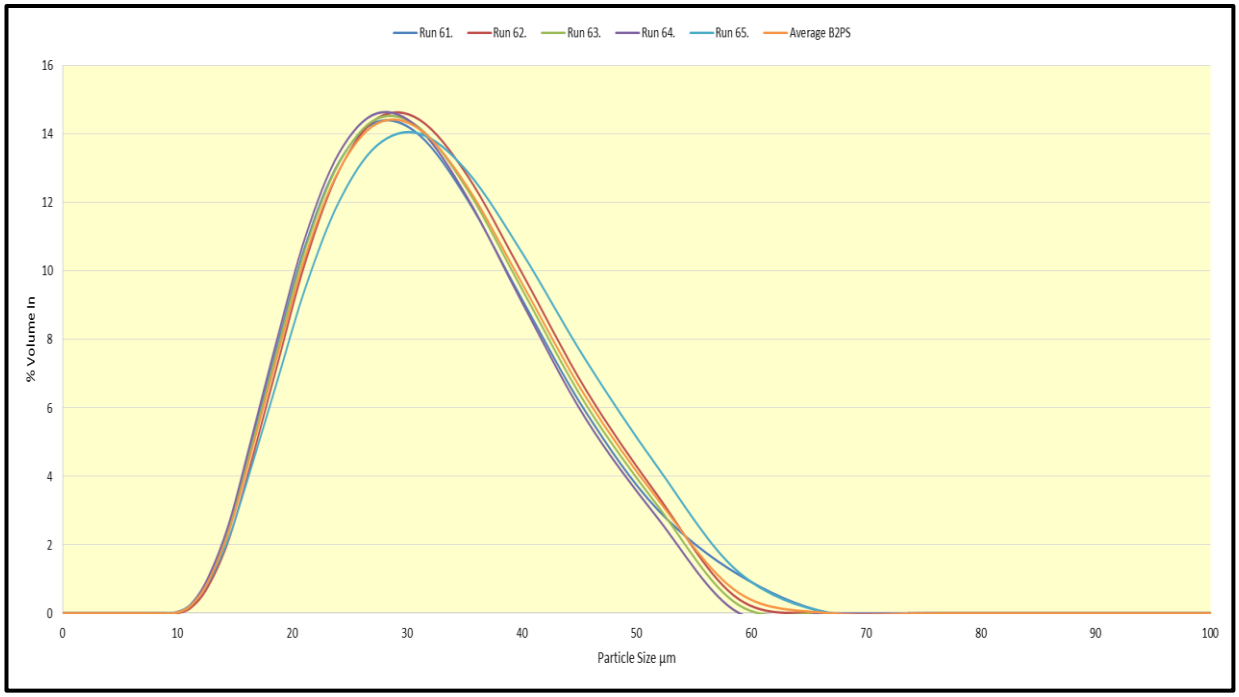

Figure 79 - Graph Showing PSD for B2PS Powder Sample

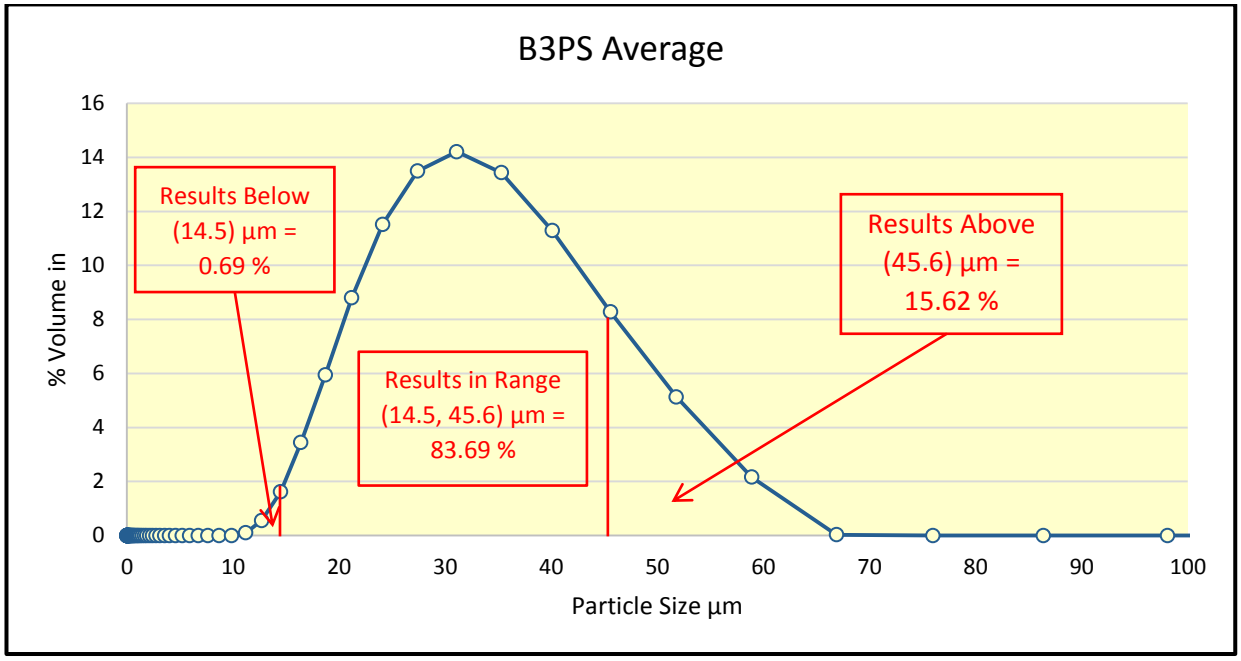

Figure 80- Graph Showing Average PSD for B3PS Powder Sample

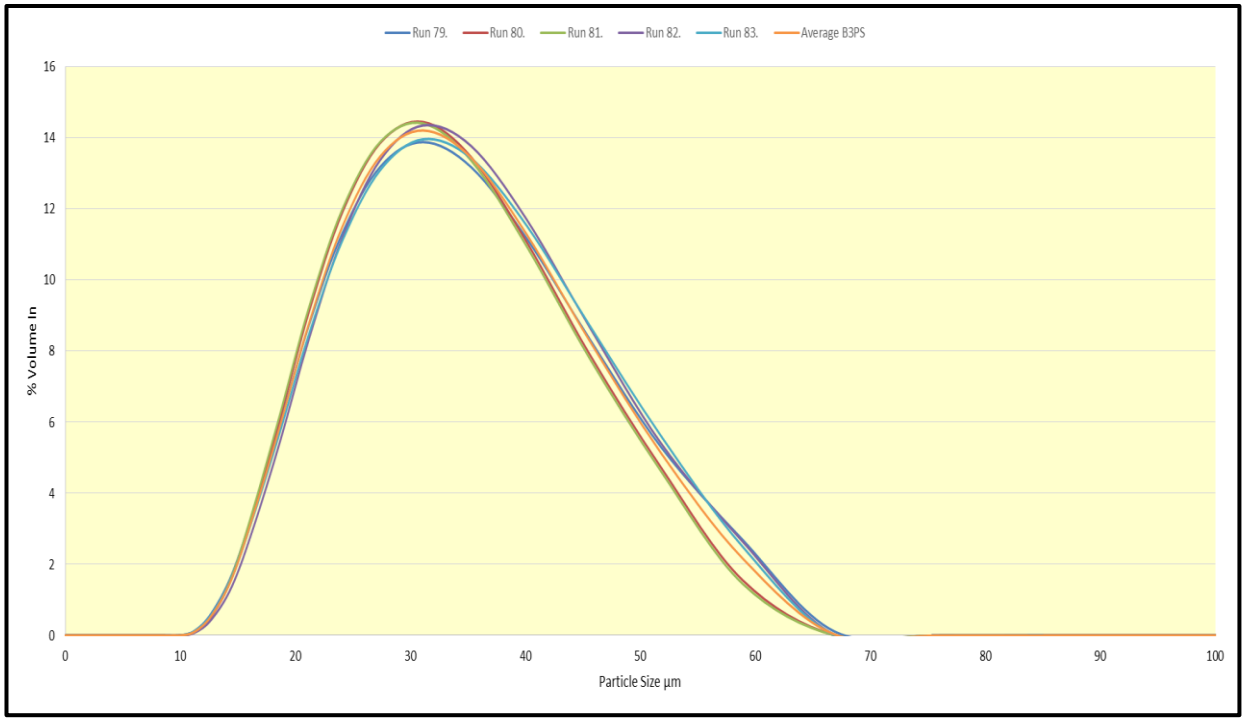

Figure 81 - Graph Showing PSD for B3PS Powder Sample

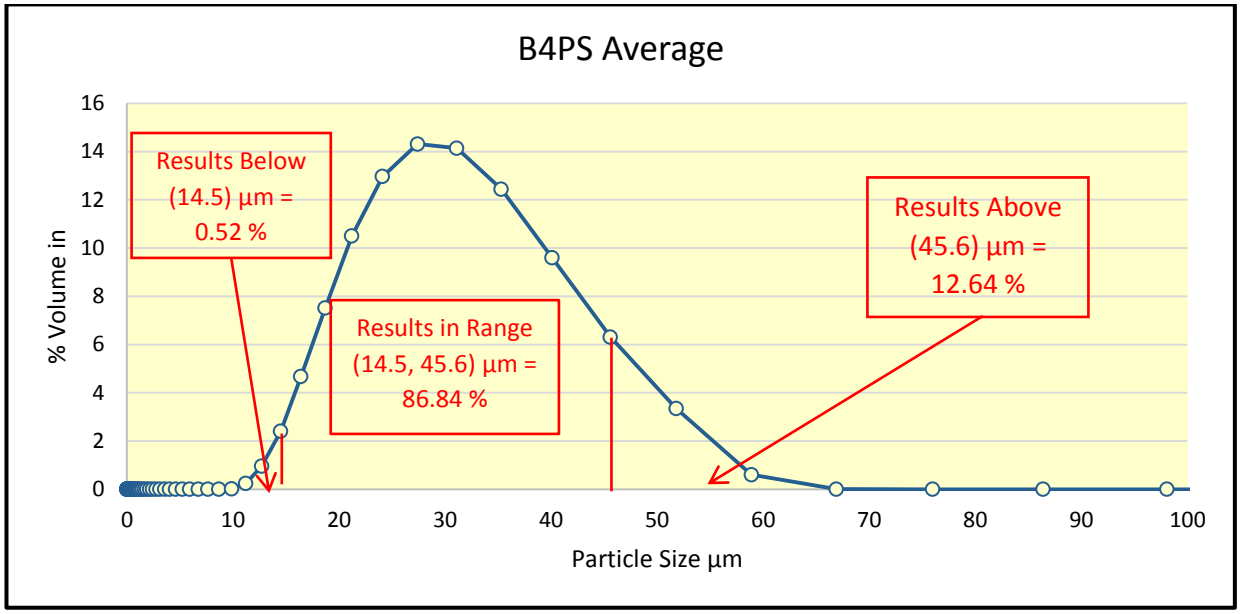

Figure 82- Graph Showing Average PSD for B4PS Powder Sample

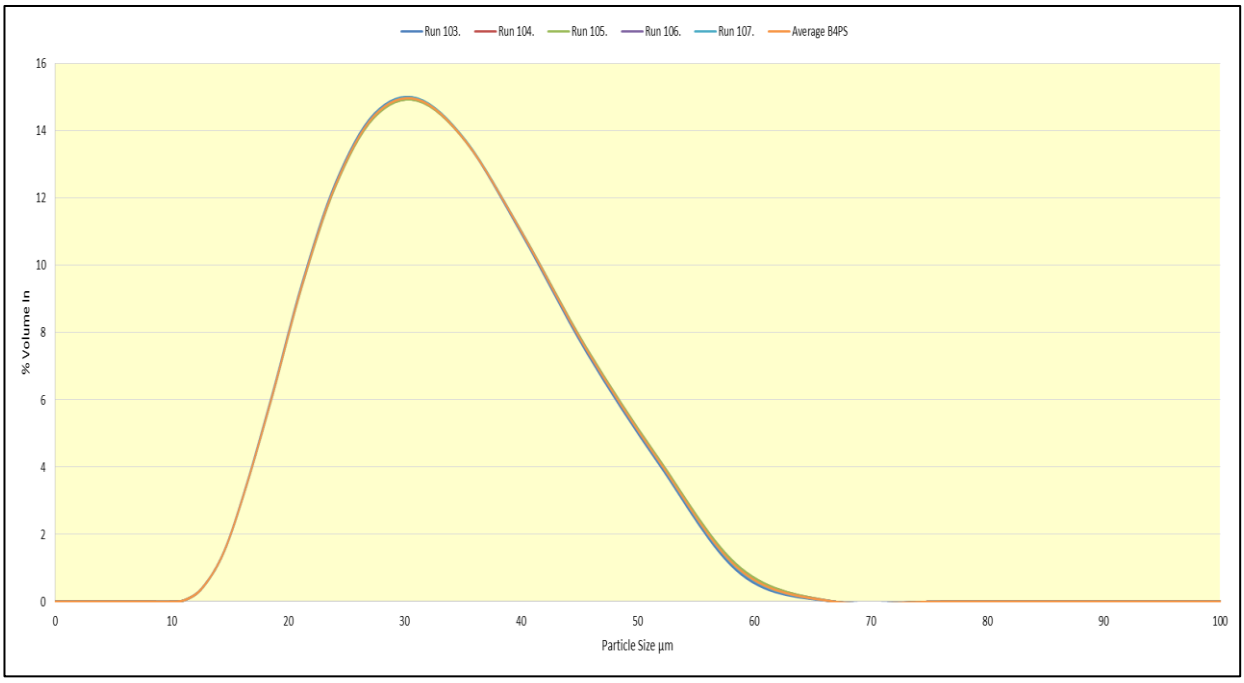

Figure 83 - Graph Showing PSD for B4PS Powder Sample

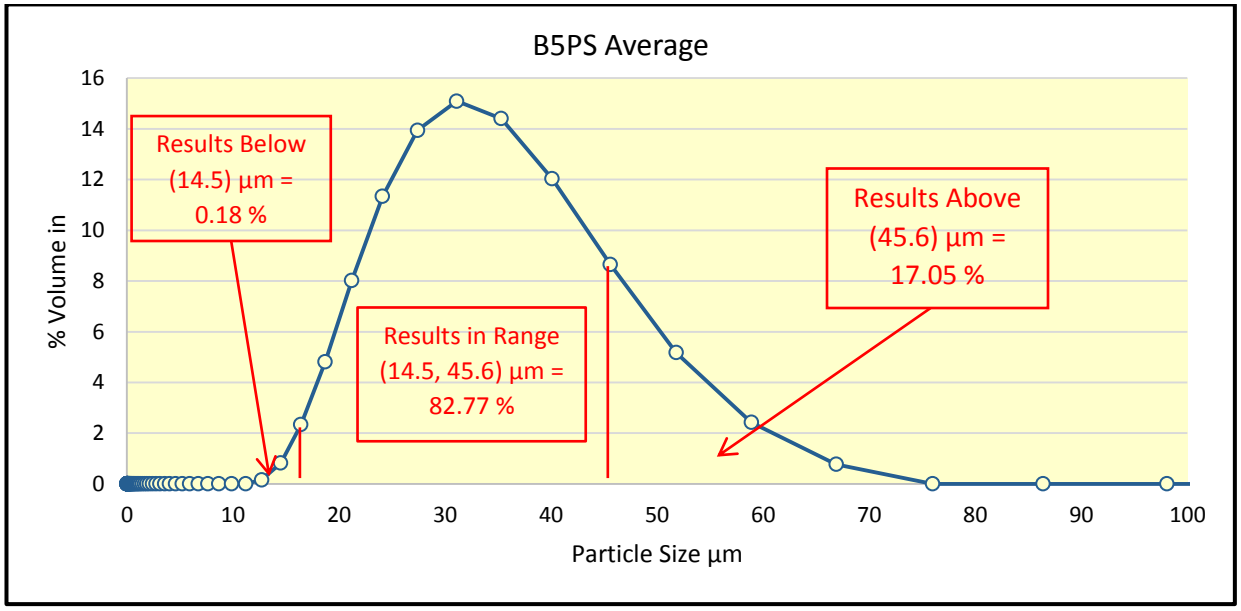

Figure 84 - Graph Showing Average PSD for B5PS Powder Sample

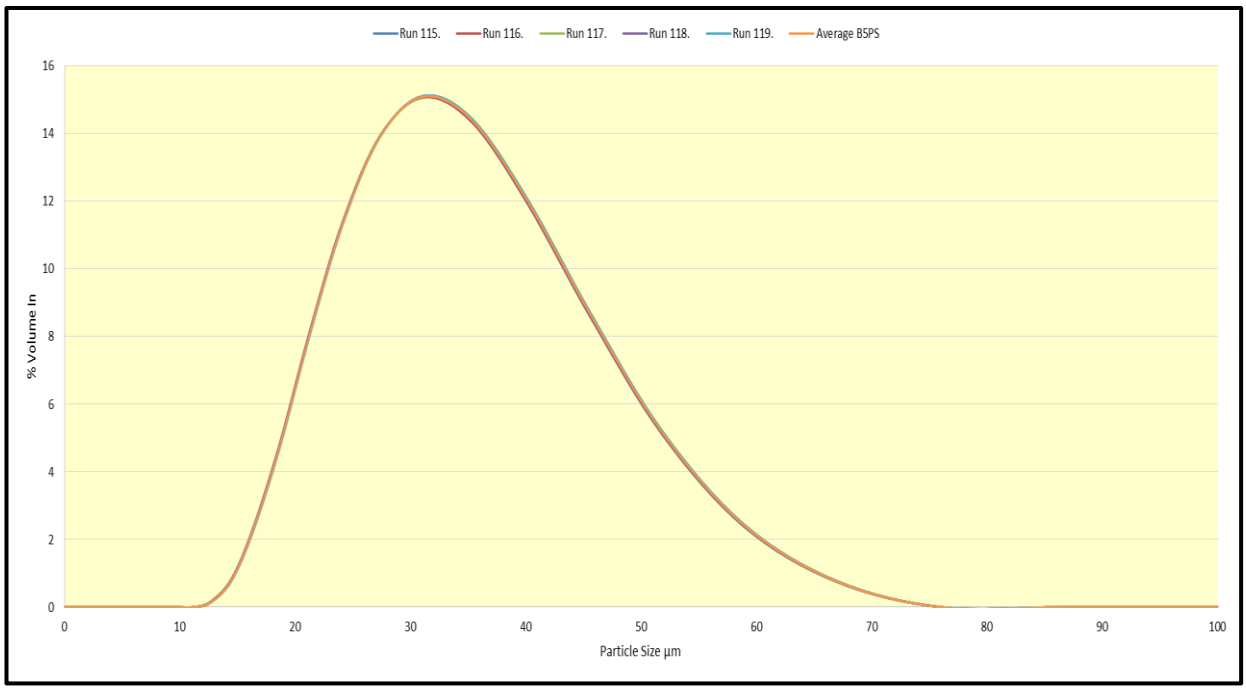

Figure 85 - Graph Showing PSD for B5PS Powder Sample

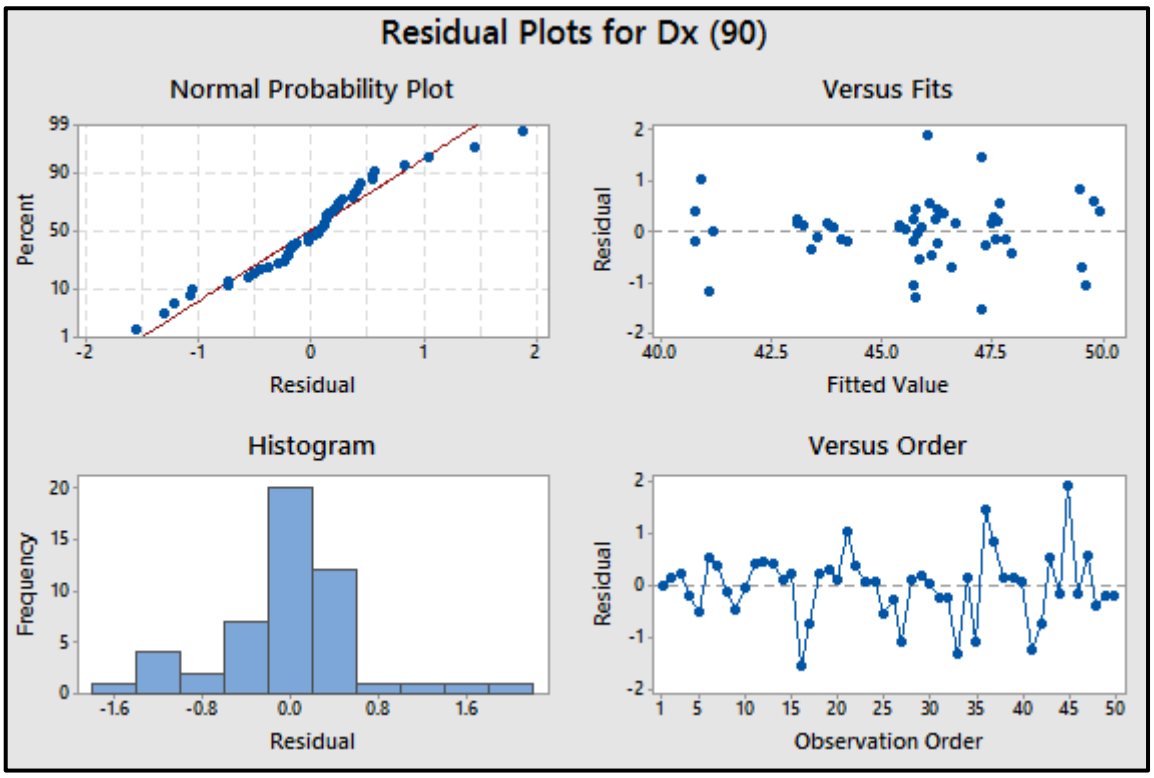

Figure 86 - Residual Plots for Dx(90)

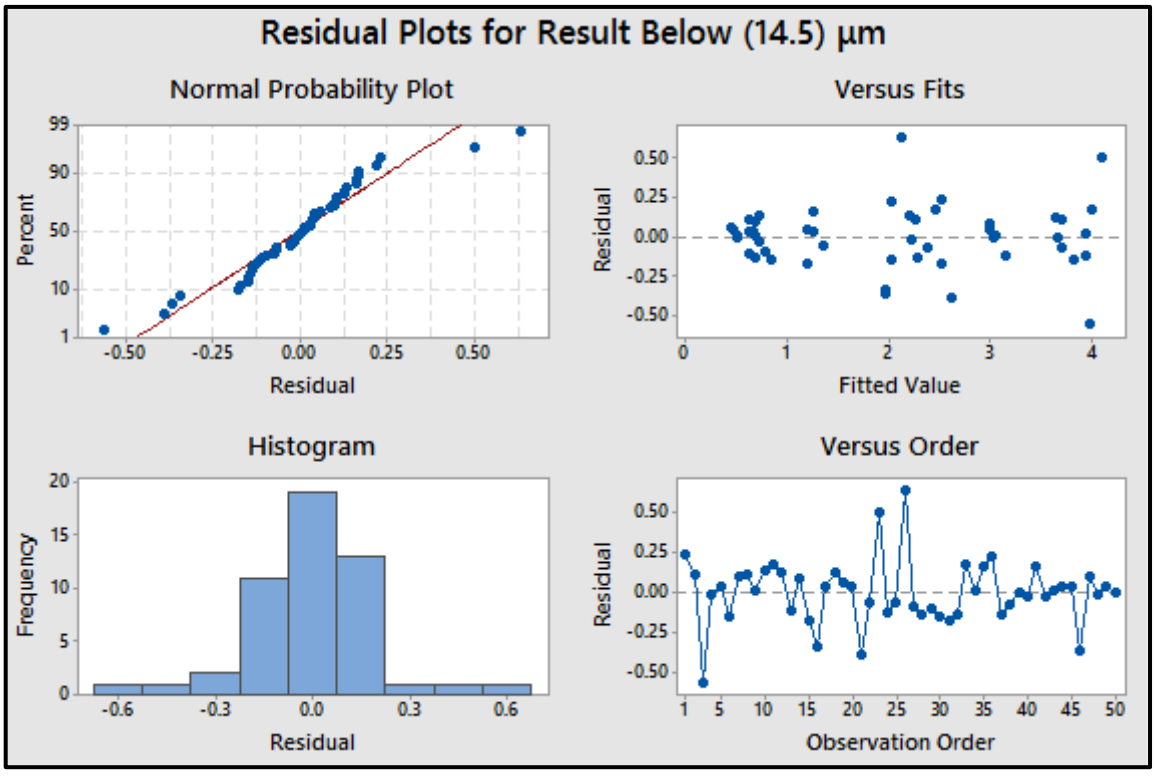

Figure 87 - Residual Plots for Results Below 14.5 µm

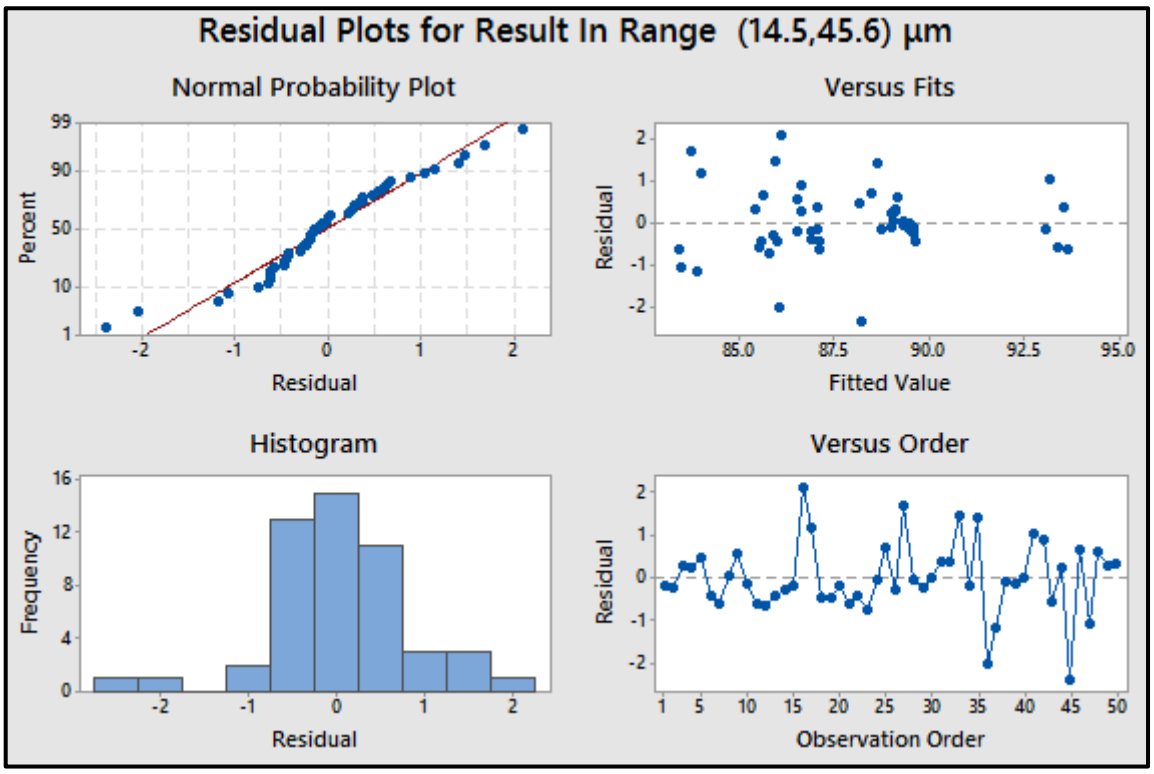

Figure 88 - Residual Plots for Results in Range 14.5 - 45.6 µm

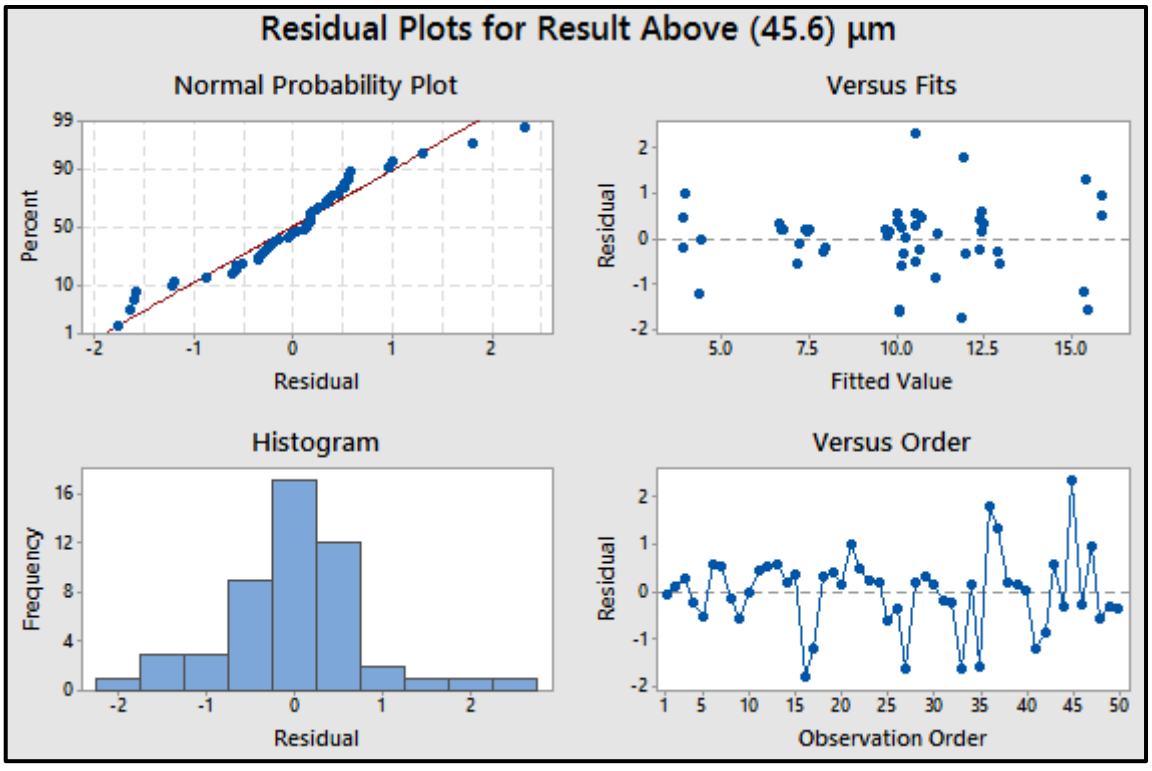

Figure 89 Residual Plots for Results Above 45.6 µm

8.2. Appendix 2 - Nomenclature

Symbol or Abbreviation	Description	Units
UTS	Ultimate Tensile Strength	MPa
-	Yield Strength	MPa
-	Young's Modulus	GPa
-	Elongation	%
PSD	Particle Size Distribution	µm
-	Volume	mm^3
SLM	Selective Laser Melting	N/A
ØDx(10)	Diameter at which 10% of population smaller than	µm
ØDx(50)	Diameter at which 50% of population smaller than	µm
ØDx(90)	Diameter at which 90% of population smaller than	µm
Results below 14.5 µm	% of population with Ø less than 14.5 µm	%
Results below 14.5 – 45.6 µm	% of population with Ø between 14.5 and 45.6 µm	%
Results above 45.6 µm	% of population with Ø greater than 45.6 µm	%
PCB	Powder Collection Box	N/A
ANOVA	Analysis of Variance	N/A
α-value	Predetermined Level of Significance	N/A
p-value	Used to Determine Statistical Significance	N/A
F-Statistic	Ratio of MS Factor to MS Error	N/A
S	Standard Distance from Regression Line	mm
R-Sq	Percentage of Data Points Explained by Model	%
Adj-R-Sq	Above Adjusted for No. of Terms in Model	%
H_0	Null Hypothesis	N/A
H_1	Alternative Hypothesis	N/A
µ	Population Mean	mm
MS	Mean Squares	N/A
ELI	Extra Low Interstitial	N/A
-	Power	W
-	Point Distance	µm
-	Exposure Time	µs
-	Temperature	°C
-	Frequency	Hz
F	Force	kN
Fmax	Maximum Force	kN
OM	Optical Microscope	N/A
-	Porosity	%
HF	Hydrofluoric Acid	N/A
HNO_3	Nitric Acid	N/A
H_2O	Water	N/A
Al_2O_3	Aluminium Oxide	N/A
TiO_2	Titanium Dioxide	N/A

CD	Compact Disk	N/A

References

American Society for Metals. 1972. *Metals Handbook, Vol. 7. Atlas of Microstructures of Industrial Alloys.* 8th Edition. OH. ASM International.

American Society for Metals. 1973. *Metals Handbook, Vol. 8. Metallography, Structures and Phase Diagrams.* 8th Edition. OH. ASM International.

American Society for Testing and Materials. 2011. *ASTM E3-11. Standard Guide for Preparation of Metallographic Specimens.* ASTM International, West Conshohocken, PA, 2011, DOI: 10.1520/E0003-11, www.astm.org.

American Society for Testing and Materials. 2015. *ASTM E8/E8M-15a. Standard Test Methods for Tension Testing of Metallic Materials.* ASTM International, West Conshohocken, PA, 2015, DOI: 10.1520/E0008_E0008M-15A, www.astm.org.

American Society for Testing and Materials. 2007. *ASTM E407-07e1. Standard Practice for Microetching Metals and Alloys.* ASTM International, West Conshohocken, PA, 2007, DOI: 10.1520/E0407-07E01, www.astm.org.

American Society for Testing and Materials. 2007. *ASTM E466-07. Standard Practice for Conducting Force Controlled Constant Amplitude Axial Fatigue Tests of Metallic Materials.* ASTM International, West Conshohocken, PA, 2007, DOI: 10.1520/E0466-07, www.astm.org.

American Society for Testing and Materials. 2013. *ASTM E1409-13. Standard Test Method for Determination of Oxygen and Nitrogen in Titanium and Titanium Alloys by Inert Gas Fusion.* ASTM International, West Conshohocken, PA, 2013, DOI: 10.1520/E1409-13, www.astm.org.

American Society for Testing and Materials. 2013. *ASTM F136-13. Standard Specification for Wrought Titanium-6Aluminum-4Vanadium ELI (Extra Low Interstitial) Alloy for Surgical Implant Applications (UNS R56401).* ASTM International, West Conshohocken, PA, 2013, DOI: 10.1520/F0136-13, www.astm.org.

American Society for Testing and Materials. 2014. *ASTM F1472-14. Standard Specification for Wrought Titanium-6Aluminum-4Vanadium Alloy for Surgical Implant Applications (UNS R56400).* ASTM International, West Conshohocken, PA, 2014, DOI: 10.1520/F1472-14, www.astm.org.

American Society for Testing and Materials. 2014. *ASTM F2924-14. Standard Specification for Additive Manufacturing Titanium-6 Aluminum-4 Vanadium with Powder Bed Fusion.* ASTM International, West Conshohocken, PA, 2014, DOI: 10.1520/F2924-14, www.astm.org.

American Society for Testing and Materials. 2014. *ASTM F3001-14. Standard Specification for Additive Manufacturing Titanium-6 Aluminum-4 Vanadium ELI (Extra Low Interstitial) with Powder Bed Fusion.* ASTM International, West Conshohocken, PA, 2014, DOI: 10.1520/F3001-14, www.astm.org.

Axelsson, S. 2012. *Surface Characterization of Titanium Powders with X-ray Photoelectron Spectroscopy*. Master Programme Dissertation, Chalmers University of Technology.

British Standards Institution. 2009. *BS ISO 13320 2009*: *Particle size analysis. Laser diffraction methods.* London: BSI.

Callister, W. D. 2007. *Materials Science and Engineering: An Introduction.* 7th Edition. London. John Wiley and Sons, Inc.

Donachie, M. J. 2000. *Titanium: A Technical Guide*. 2nd Edition. OH. ASM International.

Facchini, L. Magalini, E. Robotti, P. Molinari, A. Höges, S and Wissenbach, K. (2010) Ductility of a Ti-6Al-4V alloy produced by selective laser melting of prealloyed powders. *Rapid Prototyping Journal*, Vol. 16 Iss: 6, pp.450 – 459.

Joiner, B. L. & Ryan, B. F. 2001. *Minitab Handbook.* 4th Edition. CA: Duxbury Press.

Liu, B. Wildman, R. Tuck, C. Ashcroft, I and Hague, R. 2011. Investigation the effect of particle size distribution on processing parameters optimisation in Selective Laser Melting process. *International solid freeform fabrication symposium: an additive manufacturing conference*. Austin. 2011

Malvern. 2015. *A basic guide to particle characterization.* England: Malvern Instruments.

Minitab. 2015. *Minitab 17.2.1. Statistical* Software – StatsGuide. PA: Minitab, Inc, www.minitab.com.

Moore, D. S. 1999. *The Basic Practice of Statistics.* 2nd Edition. New York: W. H. Freeman and Company.

Oh, J. M. Lee, B. G. Cho, S. W. Lee, S. W. Choi, G. S. Lim, J. W. 2011. Oxygen effects on the mechanical properties and lattice strain of Ti and Ti-6Al-4V. *Metals and Materials International* 17(5), pp. 733 – 736.

Roy, R. K. 2010. *A Primer on the Taguchi Method*. 2nd Edition. Michigan: Society of Manufacturing Engineers.

Russell, A. M. and Lee, K. L. 2005. *Structure-Property Relations in Nonferrous Metals.* London. John Wiley and Sons, Inc.

Seyda, V. Kaufmann, N and Emmelmann, C. 2012. Investigation of Aging Processes of Ti-6Al-4 V Powder Material in Laser Melting. *Physics Procedia* 39, pp. 425 – 431.